# Simplified Core Physics and Fuel Cycle Cost Model for Preliminary Evaluation of LSCR Fueling Options

A Thesis
Presented to
The Academic Faculty

by

Spenser Matthew Lewis

In Partial Fulfillment
of the Requirements for the Degree
Master of Science in the
School of Nuclear Engineering

Georgia Institute of Technology
May 2014

# Simplified Core Physics and Fuel Cycle Cost Model for Preliminary Evaluation of LSCR Fueling Options

Approved by:

Dr. Bojan Petrovic, Advisor
School of Nuclear and Radiological Engineering
*Georgia Institute of Technology*

Dr. Weston M. Stacey, Jr.
School of Nuclear and Radiological Engineering
*Georgia Institute of Technology*

Dr. Glenn E. Sjoden
School of Nuclear and Radiological Engineering
*Georgia Institute of Technology*

Dr. G. Ivan Maldonado
School of Nuclear Engineering
*The University of Tennessee*

Date Approved: December 13, 2013

# ACKNOWLEDGEMENTS

I wish to thank my friends and family for all the support received while in school. I would also like to thank my advisor, Dr. Petrovic, for the exceptional guidance and mentoring he was able to provide throughout my time as a student.

# TABLE OF CONTENTS

# LIST OF TABLES

# LIST OF FIGURES

# LIST OF SYMBOLS

LSCR……..……Liquid Salt Cooled Reactor

FHR……..……Fluoride-Salt High-Temperature Reactor

AHTR…….Advanced High Temperature Reactor

ORNL……..Oak Ridge National Laboratory

FLiBe……...…….Lithium Fluoride and Beryllium Fluoride, $Li_2BeF_4$

FCC……..Fuel Cycle Cost

TRISO…….……Tristructural Isotropic

HTGR……...……High Temperature Gas Reactor

SmAHTR…….Small-Modular Advanced High-Temperature Reactor

MSRE……...……..Molten Salt Reactor Experiment

GIF……...……..Generation IV International Forum

GT-MHR……...……. Gas-Turbine Modular High-Temperature Reactor

CHM……...…….Carbon-to-Heavy Metal

MHC……..…. Molybdenum-Hafnium Carbide

VHTR…….Very High Temperature Gas-Cooled Reactor

RPT……..…….. Reactivity-Equivalent Physical Transformation

IEDS……...…… Iterative Equilibrium Depletion Search

LRM…….……..Linear Reactivity Model

NLRM……...…… Non-Linear Reactivity Model

SWU……Separative Work Unit

# SUMMARY

The Liquid Salt Cooled Reactor (LSCR) provides several potential benefits compared to pressurized water-cooled reactor systems. These include low operating pressure of the liquid salt coolant, the high burnup tolerance of the fuel, and the high operating temperatures which leads to increases in efficiency. However, due to inherently low heavy metal loading, the fuel cycle design presents specific challenges.

In order to study options for optimizing the fuel design and fuel cycle, SCALE6.1 was used to create simplified models of the reactor and look at various parameters. The primary parameters of interest included packing factor and fuel enrichment. An economic analysis was performed on these results by developing a simple fuel cycle cost (FCC) model that could be used to compare the different options from an economic standpoint.

The lithium enrichment of the FLiBe coolant was also investigated. The main focus was to understand the practical limitations associated with the Li-7 enrichment and whether it could be used for beneficial purposes. The main idea was to determine whether a lower-than-equilibrium enrichment could be used at reactor start up so that the Li-6 isotope acts as a burnable absorber. The results for the lithium enrichment study showed that the enrichment converges over time, but the amount of time required to reach steady state is much too long and the FLiBe coolant could not be utilized for reactivity control as a burnable absorber.

The results found through this research provide reasonable guidelines for expected costs and narrow down the types of configurations that should be considered as fuel design options for the LSCR. Additionally, knowledge was gained on methods for modeling the system not only accurately but also efficiently to reduce the required computing power and time.

# CHAPTER 1: INTRODUCTION

The Liquid Salt Cooled Reactor (LSCR), also referred to as Fluoride-salt High-temperature Reactor (FHR) or Advanced High Temperature Reactor (AHTR), is a type of Generation IV reactor. Attractive features of this type of design include the low operating pressure of the liquid salt coolant, the high burnup tolerance of the fuel, and the high operating temperatures which leads to increases in efficiency. However, due to inherently low heavy metal loading, fuel cycle design presents specific challenges and it is the topic of this research.

Since 2000, this reactor design has been in the process of development through the efforts of Oak Ridge National Laboratory for the U.S. Department of Energy, Office of Nuclear Energy's Advanced Reactor Concepts Program. The most recent design specifications have adopted the application of a plank type fuel element and a mixture of lithium fluoride and beryllium fluoride (FLiBe) as the primary coolant [1]. In order to further develop the LSCR design to a commercially competitive level, certain technologies and components require further development.

Since all systems in the reactor must interact with one another, every mechanism is important to the operation of the reactor. The neutronics and reactor physics concepts associated with the fuel design and the liquid salt coolant are included in this list and must be adequately incorporated to create a design that is not only safe but economically competitive with other reactor concepts. There are many parameters that indicate the overall performance of the core including but not limited to the $k_{eff}$, void reactivity coefficient, temperature reactivity coefficient, transient behavior, and fuel burnup.

In order to ensure that the LSCR is a feasible design, many neutronics studies have already been performed to validate different design possibilities and identify possible safety concerns. However, a fully satisfactory solution is yet to be devised and the continuation of this work is therefore necessary to find the optimal design specifications. One of the primary objectives of the LSCR design process is the optimization of the fuel cycle cost (FCC). The LSCR design is challenged by a low heavy metal loading which results in shorter cycle lengths. Additionally, the fabrication of this fuel is expected to be significantly more expensive than $UO_2$ rods used in current light water reactors (LWRs). The improvement of the fuel design and related neutronics is an important aspect of the reactor system to balance cycle length and fuel cost to prevent outage costs from too negatively impacting the overall FCC.

Several different fuel design options have been considered for the LSCR, and they all have implemented the use of tristructural isotropic (TRISO) particles. The initial design mimicked the geometric configuration of high temperature gas reactors (HTGRs) with hexagonal fuel elements and cylindrical fuel compacts, while the most recent design utilizes a plate fuel element. The fuel assemblies are hexagonal and each contains three sections of plank fuel elements. The shift to plate elements occurred with the development of the small-modular advanced high-temperature reactor (SmAHTR). The plank fuel elements are composed of TRISO fuel particles embedded in a graphite matrix [2].

The main focus for this study was to look at preliminary options for optimizing the design of the plank fuel element while constraining the physical dimensions of the plank. The primary variables which were observed include the fuel packing factor and the uranium enrichment. The adjustment of the packing factor changes the amount of graphite available for neutron moderation while changing the uranium enrichment provides either more or less fissile

material. By altering these two variables, substantial changes in both cycle length and discharge burnup were observed. The goal was to find a combination of these variables that is most cost-efficient.

Additionally, a large effort was placed on the neutronics associated with the FLiBe coolant. The coolant plays a role as an additional moderator, but more importantly the lithium portion of the coolant must be highly enriched in lithium-7 to avoid the large absorption cross section of Li-6. Large costs are associated with the necessary enrichment which is on the order of 99.990%, so different options for using lower enrichments would be desirable for reducing the cost of the FLiBe coolant. The option that was evaluated involved taking advantage of the high absorption cross section inherent to Li-6 at reactor start up and using it as a burnable absorber.

In order to perform these parametric studies, SCALE 6.1 was used to model and test the different scenarios. From the resulting data, comparisons were made between the different options by applying a simplified fuel cycle cost model. The FCC model uses both a range of fuel fabrication costs as well as outage costs since an exact figure is unknown. The number of batches was also varied to show the effect of outage costs. Based on these cost comparisons, the most cost effective designs were determined.

The following chapters present the work described above in further detail. Chapter 2 provides an in depth background of the history and development of the LSCR. The methods and models which were used to perform the different studies are described in Chapter 3. The results from these various studies are presented and analyzed in Chapter 4. Finally, Chapter 5 discusses the meaning of the results and what type of conclusions can be drawn from the information.

# CHAPTER 2: BACKGROUND

## 2.1. A Brief History of Liquid Salt Cooled Reactors

The LSCR is the direct descendant of the Molten Salt Reactor Experiment (MSRE) which occurred at ORNL from 1965 to 1969. This project initially developed from the molten fluoride-fueled Aircraft Reactor Experiment, which was an attempt to design a reactor that could be used to power an aircraft. The project occurred at Oak Ridge National Laboratory and in 1954 a prototype was built and operated successfully. However, the project's objective shifted to civilian power in 1956 after recognizing that molten-salt reactors might be an attractive option for power applications. Different design concepts were considered, but it was concluded that a graphite moderated thermal reactor operating on a thorium fuel cycle was best for producing economic power [3].

The MSR relied on the inclusion of uranium fuel directly into the fluoride salt in the form of $UF_4$. Additionally, the project was developed for breeder applications as an objective of the Atomic Energy Commission. Although the project showed promise, it was ultimately terminated in 1973 due to a lack of support and the competition presented by the coinciding fast breeder program [4]. Through the studies done for the MSRE, much knowledge has been gained on the application of fluoride-salts as a coolant for reactors. The effect of salt on other materials is one of many concerns to ensure that failure doesn't occur or at least the reactor can operate for extended periods without need of repair.

By taking advantage of the experience gained from the MSRE and applying these technologies appropriately the LSCR design has become a contender against other Generation IV reactors. The design objectives of Generation IV nuclear energy systems have been specified by

the Generation IV International Forum (GIF) through a set of eight goals encompassing the areas of sustainability, safety and reliability, economics, and proliferation resistance and physical protection. The goals have been outlined below [5].

- Sustainability
    - Provide energy sustainably, and promote long-term availability of nuclear fuel
    - Minimize and manage nuclear waste and reduce the long term stewardship burden
- Safety and Reliability
    - Excel in safety and reliability
    - Have a very low likelihood and degree of reactor core damage
    - Eliminate the need for offsite emergency response
- Economics
    - Have a life-cycle cost advantage over other energy sources
    - Have a level of financial risk comparable to other energy projects
- Proliferation Resistance and Physical Protection
    - Be a very unattractive route for diversion or theft of weapons-usable materials, and provide increased physical protection against acts of terrorism

Current design plans have adopted an economy of scale approach in order to provide a reactor design that produces electric power and industrial process heat at low-cost. The LSCR design from ORNL has been proposed to support an operating power of 3400 $MW_{th}$. The proposed inlet and outlet coolant temperatures are 650$^{o}$C and 700$^{o}$C respectively.

## 2.2. Previous LSCR Research

### 2.2.1. Reactor Benefits

The next generation reactor design needs to demonstrate advanced nuclear reactor technology to produce electricity and hydrogen in an efficient, passively safe, and economical manner. Helium cooled reactors have been the traditional choice for high-temperatures, but liquid-fluoride salt represents another option. The use of a liquid-salt introduces a new set of challenges but comes with several advantages in terms of thermo physical properties and low pressure operation.

The LSCR design is a concept that was initially developed through the collaboration of Oak Ridge National Laboratory, Sandia national Laboratories, and University of California Berkley The LSCR combines attractive features of gas-cooled reactor fuel, liquid-salt reactor coolant, and liquid-metal-cooled reactor design to yield a reactor with exceptional safety and economic features. The coated-particle graphite-matrix fuel developed for the HTGR is used in the LSCR design due to the robustness of the fuel at high temperatures and because it can achieve high fuel performance in terms of burnup and fission gas confinement [6].

By using the experience gained from the Molten Salt Reactor (MSR) program, the liquid salt coolant and related systems could be better chosen. The advantages of implementing a liquid salt coolant involves lower operating pressure, higher power density, better heat removal properties, and reduced shielding requirements for external components. The overall result is improved safety and the potential for a more economical system [7]. The passive safety systems and low pressure operation of liquid-metal-cooled reactors were also adapted to the LSCR. Additionally, the supercritical power conversion cycles developed for fossil fuel plants can be applied to increase efficiency of electricity production [8].

### 2.2.2. Fuel Designs and Materials

The design of the LSCR has gone through a series of development stages. Initially, the pre-conceptual design of the LSCR was heavily based on the prismatic fuel used in helium cooled high-temperature gas reactors (HTGR). At this early phase, the power level was limited to 2400 $MW_{th}$ versus the 3400 $MW_{th}$ design that is currently under consideration by ORNL. In addition, pebble-bed reactor designs for LSCRs have also been heavily studied [9].

Analogous to the HTGR design, TRISO particle fuel was used due to its robustness at high temperatures and high burnup. These TRISO particles were incorporated into graphite matrix fuel compacts which are loaded into a hexagonal graphite matrix fuel block. The design contained a total of 324 columns of fuel blocks arranged into an annular geometry. The blocks filling the interior portion of the annulus and the region between the outer diameter of the core and reactor vessel are non-fueled graphite reflector blocks [9]. Figure 2-1 below shows the arrangement of the fuel assemblies in the reactor core.

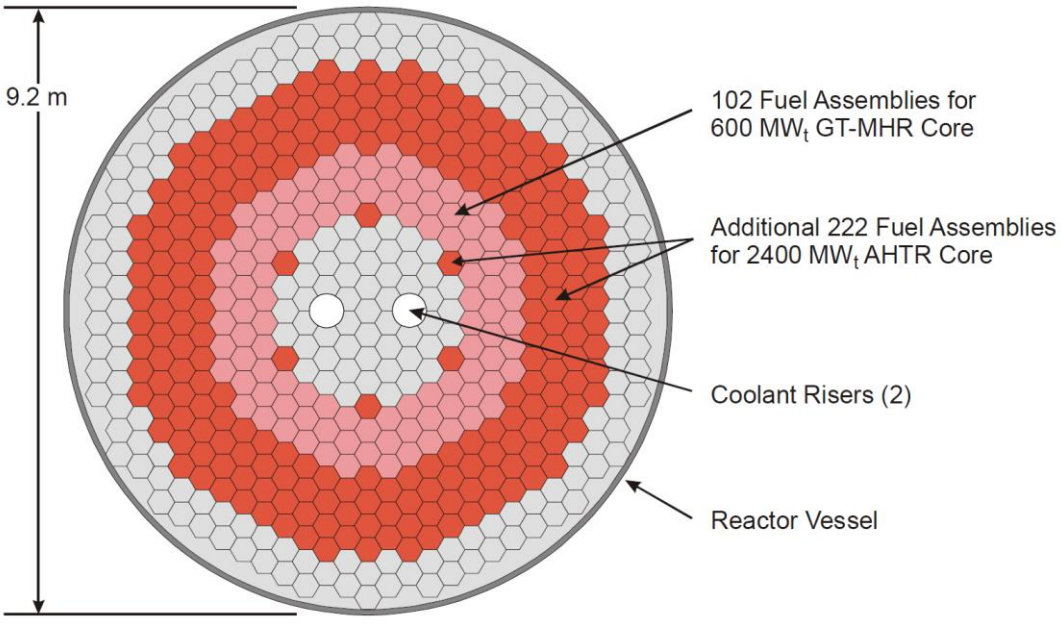


Figure 2-1: Cross sectional view of LSCR core showing columns of fuel assemblies [9]

Table 2.1 shows a list of various design parameters. The study based on these parameters was used to gauge the viability of the LSCR by performing an initial analysis of the reactor core physics performance. The analysis included coolant reactivity effects, fuel burnup, cycle length, and transient behaviors [9].

Table 2.1: LSCR pre-conceptual design parameters [9]

| | | | |
|---|---|---|---|
| Power level | 2400 MW(t) | Electrical output | 1300 MW(e) |
| Core inlet/outlet temperature | 900°C/1000°C | Power cycle | 3-stage multi-reheat Brayton |
| Coolant (alternate) | $Li_2BeF_4$ ($NaF$-$ZrF_4$) | Power cycle working fluid | Nitrogen (helium longer-term option) |
| Mass flow rate | 12,070 kg/s (20% core bypass) | Core inlet pressure outlet pressure | 0.230 MPa 0.101 MPa |
| Volumetric flow rate | 5.54 $m^3/s$ | Pressure drop | 0.129 MPa |
| Channel diameter | 0.95 cm | Core shape | Annular |
| Fraction (core) | 6.56% | Core outer diameter | 7.8 m |
| Velocity | 2.32 m/s (7.6 ft/s) | Core annulus | 2.3 m |
| Fuel kernel | Uranium carbide/oxide | Core height | 7.9 m |
| Enrichment | 10.36 wt % $^{235}U$ | Pumping power | 716 kW |
| Form | Prismatic | Power density | 8.3 $MW/m^3$ |
| Block. diameter | 0.36 m (across flats) | Reflector (outer) | 138 columns |
| Block height | 0.79 m | Reflector (inner) | 55 columns |
| Columns | 324 | Vessel diameter | 9.2 m |
| Mean temperature | 1050°C | Vessel height | 19.5 m |
| Peak temperature | 1168°C | Vessel thickness | 10.0 cm |

The current ORNL configuration is a 3400 $MW_{th}$ fluoride-salt-cooled reactor. The fuel assemblies are hexagonal and each contains three sections of plank fuel elements. The shift to plank elements occurred with the development of the small-modular advanced high-temperature reactor (SmAHTR). The plank fuel elements are composed of tristructural isotropic (TRISO) fuel particles embedded in a graphite matrix [2]. The ORNL design of a reference LSCR reactor core is shown below in Figure 2-2.

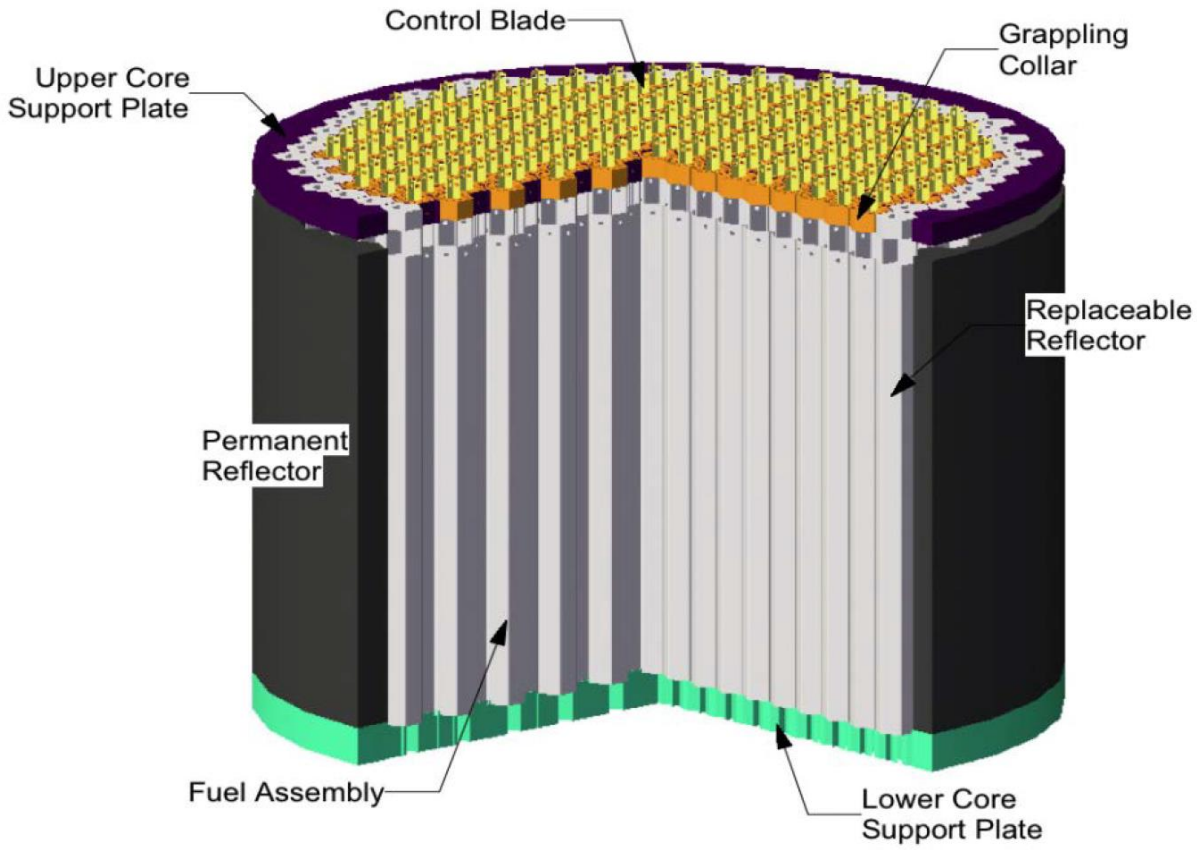


Figure 2-2: 3-D view of the LSCR reactor core [2]

Table 2.2 provides specifications on the main core characteristics for a reference 2.2 year once-through fuel cycle length at a fuel enrichment of 19.75%.

Table 2.2: Main core characteristics of LSCR reference model [2]

| Parameter | Value | Units |
|---|---|---|
| Power (thermal) | 3400 | MW |
| Number of fuel assemblies | 253 | - |
| Assembly lattice type | Hexagonal | - |
| Fuel type | Coated Particle | - |
| Moderator | Graphite | - |
| Reflector | Graphite | - |
| Coolant | FLiBe | - |
| Core height (fuel region) | 5.5 | m |
| Core height (including axial reflector) | 6.0 | m |
| Equivalent core diameter (fueled region) | 7.81 | m |
| Core diameter (including radial reflector) | 9.56 | m |
| Average power per particle | 41 | mW/particle |
| Average power per mass | 103.31 | W/gU |
| Volumetric core power density | 12.9 | $MW/m^3$ |
| Mass of heavy metal | 32.91 | MT |
| Fuel enrichment | 19.75 | $^{235}U/U$ wt % |
| Mass of fissile material | 6.5 | MT |
| Fuel cycle length (once-through) | 2.2 | years |
| Inlet coolant temperature | 650 | $^oC$ |
| Outlet coolant temperature (average) | 700 | $^oC$ |

### 2.2.3. Development of the Current Geometry

The smallest building block of the fuel used in the reactor is the TRISO fuel particles. This type of fuel was developed for HTGRs and has the benefit of performing well at high temperatures and has a higher burnup tolerance than fuel used in light water reactors. Table 2.3 shows possible dimensions of a single TRISO particle. Based on the desired fuel properties, the size of the TRISO particle can be adjusted.

Table 2.3: TRISO particle description for reference LSCR core [10]

| Region | Parameter | Parameter Value (μm) | Material | Density (g/cm³) |
|---|---|---|---|---|
| Kernel | diameter | 427 | Uranium Oxycarbide | 10.90 |
| Buffer | thickness | 100 | Porous Graphite | 1.00 |
| IPyC | thickness | 35 | Pyrolytic Graphite | 1.90 |
| SiC | thickness | 35 | Silicon Carbide | 3.20 |
| OPyC | thickness | 40 | Pyrolytic Graphite | 1.87 |
| Fuel Particle | diameter | 847 | - | - |
| Matrix | pitch | 927 | Carbon Material | 1.59 |

These fuel particles consist of a Uranium Oxycarbide (UCO) kernel surrounded by a buffer consisting of porous graphite, followed by a layer of pyrolitic graphite, silicon carbide, and then an outer layer of pyrolitic graphite. The final step is to embed the TRISO particles into a matrix of carbon [10]. Due to the design of these fuel particles, they have the ability to operate for long periods of time at temperatures up to 1250$^{o}$C [8]. Inherently, this allows for a higher operating temperature in addition to greater resistance to fuel failure.

The plate fuel design was initially developed through studies on the SmAHTR design, which is a concept for a lower-power modular version of the LSCR [11]. The TRISO particles are distributed in two stripes separated by a central carbonaceous material within the slab fuel element. This is where the design diverges from that of the SmAHTR, which distributed TRISO

particles throughout the entire plate. In order to prevent particles from eroding away, a thin (~1 mm thick) sleeve of carbonaceous material separates each fuel stripe from the FLiBe coolant. A cross sectional view of the fuel plank for the ORNL 2.2 year cycle reference design can be seen below in Figure 2-3. The design takes into account both neutronic and thermal hydraulic considerations [2].

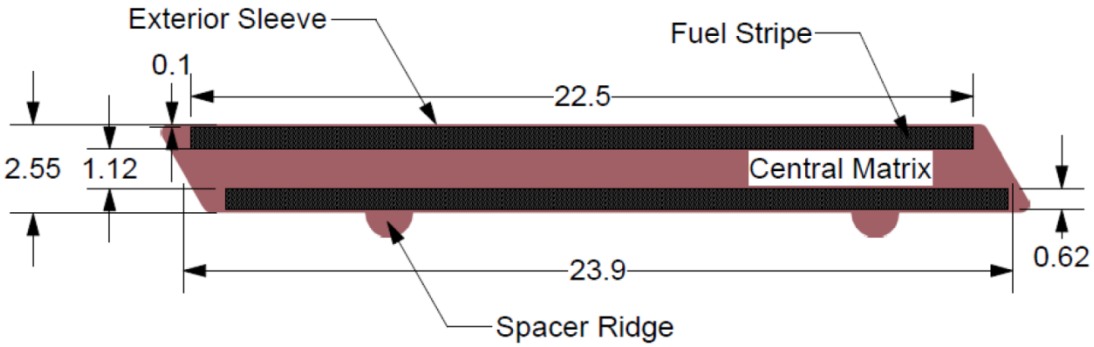


Figure 2-3: Transverse cross section of a fuel plate, dimensions in cm [2]

The fuel assemblies are each 6 m tall hexagonal prismatic boxes with 1 cm thick walls of carbon-carbon (C-C) composite with a density of 1.96 g/cm$^3$. Each box is divided into three symmetric regions by a 4 cm thick Y-shaped structure made of C-C composite. Each of the three regions contains six equidistant fuel plates which are supported by the Y-shaped structure on one end and the full length channel box on the other end. The spacing between fuel plates is filled with the primary coolant, which has been chosen as FLiBe. The channel boxes of adjacent assemblies are separated by 1.7 cm and also filled with coolant. The center of the Y-shaped structure in the fuel assembly serves as the slot for a Y-shaped control blade [2]. Due to the size of the slot, the size of the control blade can be varied slightly. The limiting factor is the thickness of the slot which is 1 cm. The geometric characteristics of the fuel assembly for the reference 2.2 year cycle design are shown below in Table 2.4.

Table 2.4: Geometric characteristics of the fuel assembly for the LSCR reference design [2]

| Characteristic | Value | Units |
|---|---|---|
| Total height | 600 | cm |
| Fueled region height | 550 | cm |
| Fuel assembly pitch | 46.75 | cm |
| Gap between assemblies | 1.7 | cm |
| Outer apothem | 22.5 | cm |
| Channel box wall thickness | 1 | cm |
| Y-shape thickness | 4 | cm |
| Coolant thickness between plates | 7 | mm |
| Coolant thickness between plate and wall | 3.5 | mm |
| Control blade location thickness | 1 | cm |
| Control blade location wing length | 10 | cm |
| Fuel plate thickness | 2.55 | cm |
| Number of fuel plates | 18 | - |

Additionally, a transverse cross section of a group of fuel assemblies is shown in Figure 2-4. The figure shows the Y-shaped structure in the center of the assemblies as well as the FLiBe between fuel plates and adjacent assemblies.

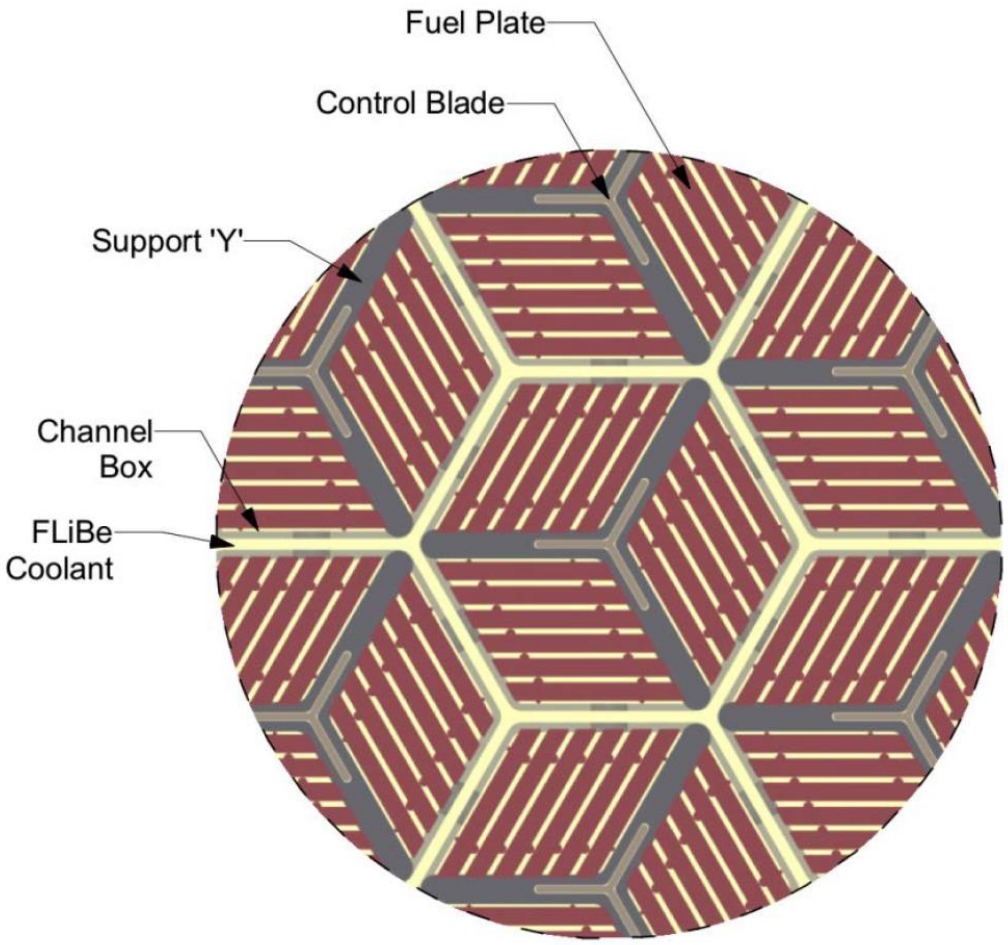


Figure 2-4: Transverse cross section of a group of fuel assemblies [2]

There is one control blade per fuel assembly and the design employs a molybdenum-hafnium carbide alloy (MHC) as the both a neutron absorber and structural material. MHC is a commercial, particle strengthened molybdenum based alloy with 1.2 wt% hafnium and 0.1 wt% carbon. The density of MHC is 10.28 g/cm$^3$. The current dimensions allow for 1 mm of clearance on each side of the control blade when inserted into the assembly. Further studies must be performed on C-C composites to determine if the core level irradiation causes mechanical distortion that could cause jamming of the control blades [2].

In order to supplement the reactivity control provided by the control blades, burnable poison particles can be incorporated into the central matrix of each fuel plate and used to compensate for the large excess reactivity of the initial bare core. The burnable poison of interest is Europium because it burns out at nearly the same rate as the fuel [2].

### 2.2.4. Neutronics and Core Physics

The core design is a key component of the reactor that must operate not only reliably, but also safely. One of the main goals of the LSCR development is to demonstrate the economic competiveness while maintaining full passive safety. There are many factors that contribute to the overall performance of the core including but not limited to the $k_{eff}$, void reactivity coefficient, temperature reactivity coefficient, transient behaviors, and fuel burnup. In order to ensure that the LSCR is a feasible design, many neutronics studies have been performed to validate different design possibilities and identify possible safety concerns.

The initial viability study of the LSCR design was based heavily on the design of the HTGR, which utilizes the TRISO particle to construct fuel elements. Coolant reactivity effects, fuel burnup, cycle length, and transient behaviors were included in the analysis of the core physics performance to identify any issues attributed to the core design [9].

The fuel of this preliminary study is the same TRISO fuel particles used in helium-cooled reactors. The TRISO particles are incorporated into graphite-matrix compacts which are loaded into a hexagonal graphite-matrix fuel block identical to what has been used in previous gas reactors. The primary coolant was chosen to be $Li_2BeF_4$ (FLiBe). The heat capacity of FLiBe is similar to that of water at 4540 $kJ/m^3$, which is about 200 times greater than helium at normal

reactor conditions. There is previous experience with the use of FLiBe as a reactor coolant from the Molten Salt Reactor Experiment (MSRE) [9].

Since the LSCR shares the same fuel and moderator as the very high-temperature gas-cooled reactor (VHTR), the core physics behavior is similar. A key characteristic of this type of reactor is a strong temperature feedback effect due to the Doppler broadening of the uranium and generated plutonium resonances that occur at elevated temperatures [9].

The void coefficient is an important reactor parameter that was scrutinized, because based on the design of the core and choice of coolant the void coefficient can end up being either positive or negative. A variety of different salts were tested to determine their effects on void reactivity and FLiBe was one of the few that had a negative void reactivity. In order to further reduce the void coefficient, the analysis focused on the application of burnable absorbers within the fuel assembly. The analysis demonstrated that this method has the potential to reduce the void coefficient for a fresh core, but would increase fuel cycle costs and allow the void coefficient to increase with burnup due to burnout of the poison [9].

A fuel cycle analysis was performed to determine the burnup of the fuel based on a three-batch equilibrium cycle. Depending on the enrichment of either 10% or 20%, the burnup cycle would be about 330 days and 510 days, respectively [9].

The conclusion of the analysis showed that significant focus needed to be placed on the coolant void coefficient to ensure that it can remain negative throughout the cycle. Additionally, suggestions for future analyses included a new core design, reactivity control system, alternative fuel assembly designs, and optimizing power density and peaking factors [9].

Neutronic studies were also performed by Argonne National Lab on the LSCR using FLiBe as a coolant. The studies were completed using the lattice codes WIMS8 and DRAGON.

The linear reactivity model was used to estimate the reactivity balance and discharge burnup. Once again, a main issue with the design was the void reactivity coefficient which becomes positive in a loss of coolant scenario. The lithium in the coolant was enriched to Li-7 to help mitigate this issue. The other elements of FLiBe only contain one natural isotope. The Li-6 isotope has a high thermal neutron cross section involving an (n, t) reaction, so a secondary reason to remove the Li-6 is to prevent the buildup of $^{3}H$ within the reactor [7].

The design of the reactor under consideration in the study by Argonne National Lab was based on the hexagonal core used for high-temperature gas reactors. The lattice codes WIMS8 and DRAGON were chosen because they can treat the double-heterogeneity effect created by the TRISO particles used to construct the fuel elements [7].

When performing parametric studies for the reactor design, one goal was to determine if the design could meet a cycle length of 18 months and a discharge burnup of 100 GWd/t. The different parameters varied included uranium enrichment, packing factor, and number of batches. Through the variation of these different parameters, it was shown that the desired burnup and cycle length could be theoretically obtained [7].

The coolant void reactivity coefficient was studied to determine the best way to create a negative coefficient over the lifetime of the core. The Li-6 content of the coolant has a large effect on this value so it important to enrich the Li-7 has high as economically feasible. Through the incorporation of burnable poisons and multi-batch fuel schemes, the void coefficient was shown to become more negative at the beginning of the cycle where it was the highest [7].

Similar to other high-temperature reactor designs, a technology challenge exists due to the availability of nuclear qualified materials that can operate at temperatures near $1000^{o}C$. However, compared with a helium coolant, the LSCR will have significantly lower fuel

temperatures (by 150-200°C) for the equivalent temperature of heat delivered for power conversion or hydrogen production [8].

The power level of the design in this ORNL study was 2400 $MW_{th}$ and uses a prismatic fuel design. The prismatic fuel assembly provides more control over the fuel and coolant volume fractions compared to the pebble-bed form. Figure 2-5 represents the schematic for a single hexagonal fuel assembly and Figure 2-1 shows a schematic of the annual core and the placement of the 324 assemblies [8].

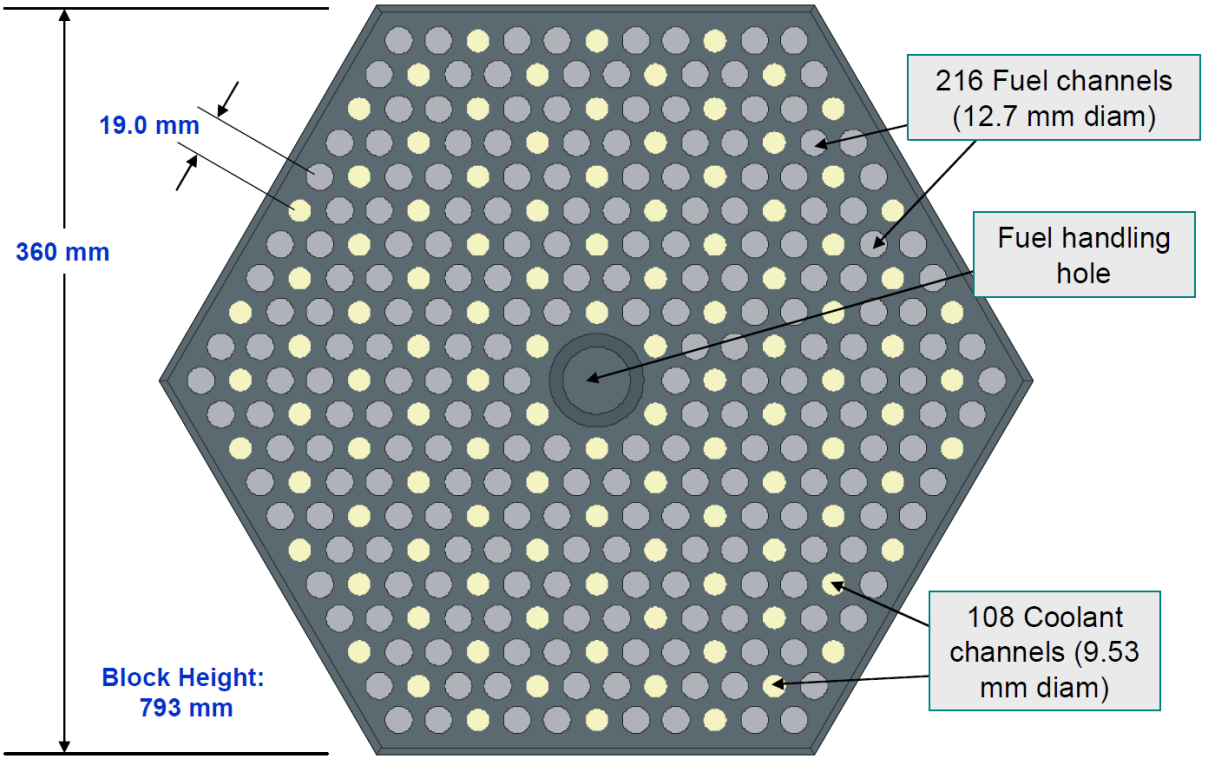


Figure 2-5: Schematic of single hexagonal fuel assembly [8]

The Gas-Turbine Modular High-Temperature Reactor (GT-MHR) has a similarly designed annular core but only has 102 fuel assemblies and a thermal power of 600 MW. An advantage of the LSCR design is the increased power density which allows for a smaller plant footprint. The core design is so similar to the GT-MHR because they share the same types of fuel

and moderator. However, a key difference occurs in neutron cross sections due to the differences in the liquid-salt and helium coolants [8].

It was determined that this type of thermal reactor system has a strong temperature feedback effect due to the Doppler broadening of the uranium resonances that occurs at elevated temperatures. Due to this feature, as the temperature of the fuel increases, the parasitic absorption of neutrons by the fertile component of the fuel increases, reducing the total reactivity of the system and the power level [8].

The coolant void coefficient corresponds to the amount of reactivity that is added or subtracted by the complete removal of the coolant. This LSCR core design can result in this coefficient to be either positive or negative so it was a focus of the physics analysis. The Monte Carlo N-Particle (MCNP-version 4C2) code was used for most of the neutronic analyses.

Table 2.5: Void coefficient of reactivity for different salt compositions (initial SNL model) [8]

| Salt | Total Void Reactivity Effect ($) |
|---|---|
| $BeF_2$ | -1.46 |
| $LiF/BeF_2$ (66/34) | -0.47 |
| $MgF_2/BeF_2$ (50/50) | -0.49 |
| LiF (Li-7) | +0.16 |
| $ZrF_4/BeF_2$ (50/50) | +0.43 |
| $ZrF_4$/LiF (52/48) | +1.25 |
| $NaF/BeF_2$ (57/43) | +1.82 |
| $ZrF_4$ | +1.41 |
| $NaF/ZrF_4$ (25/75) | +1.88 |
| $NaF/ZrF_4$ (50/50) | +2.64 |
| $NaF/ZrF_4$ (75/25) | +3.83 |
| NaF | +7.05 |

As shown above in Table 2.5, the void coefficient is inversely correlated with the neutron absorption cross section of the coolant. The salts containing beryllium are preferred because beryllium has the smallest capture cross section and largest scattering cross section which

correlates to a negative void coefficient for this core design. There are other factors that must be considered so that the void coefficient remains in the desired realm. These include fuel volume fraction and fuel enrichment [8]. Table 2.6 below shows additional information on the properties of FLiBe coolant compared to other common reactor coolants.

Table 2.6: Thermophysical properties of common reactor coolants [8]

| Coolant | $T_{melt}$ ($^oC$) | $T_{boil}$ ($^oC$) | $\rho$ ($kg/m^3$) | $C_p$ ($kJ/kg^oC$) | $\rho C_p$ ($kJ/m^{3o}C$) | k ($W/m^oC$) | $v \cdot 10^6$ ($m^2/s$) |
|---|---|---|---|---|---|---|---|
| **$Li_2BeF_4$ (FLiBe)** | 459 | 1430 | 1940 | 2.34 | 4540 | 1.0 | 2.9 |
| **$0.58NaF\text{-}0.42ZrF_4$** | 500 | 1290 | 3140 | 1.17 | 3670 | ~1 | 0.53 |
| **Sodium** | 97.8 | 883 | 790 | 1.27 | 1000 | 62 | 0.25 |
| **Lead** | 328 | 1750 | 10540 | 0.16 | 1700 | 16 | 0.13 |
| **Helium (7.5 MPa)** | | | 3.8 | 5.2 | 20 | 0.29 | 11.0 |
| **Water (7.5 MPa)** | 0 | 100 | 732 | 5.5 | 4040 | 0.56 | 0.13 |

The main focus of one particular neutronic study performed at Oak Ridge National Laboratory was the optimization of the core design to reach a single-batch fuel length of just over 2 years. Previous core designs have been developed, but the most current is different from a neutronic standpoint due to the application of the plate fuel element. The fuel plates are grouped into three regions of six and spaced equally apart. In order to minimize the activation of the coolant, the primary coolant chosen for the design is FLiBe and it flows from the bottom to the top of the core [1]. However, to reach criticality the Li must be enriched to Li-7 (99.995%) because of the high thermal neutron capture cross section of Li-6.

The calculations were performed using SCALE 6.1. In order to correctly account for self-shielding effects, the Dancoff correction method was applied to the depletion calculations. Since the purpose of the study was to maximize the once through fuel cycle length, the optimum fuel loading was desired. The process of determining this optimum value involved adjusting the

thickness of the central carbonaceous material and varying the fuel loading and carbon-to-heavy metal (CHM) ratio [2].

From the results, a decrease in cycle length occurs as the CHM ratio increases, but there is also a sharp increase in discharge burnup. The varying effects between CHM ratio, cycle length, and discharge burnup are shown in Figure 2-6. The maximum cycle length was determined to be 2.17 years and have a discharge burnup of approximately 80 GWd/MTHM [2].

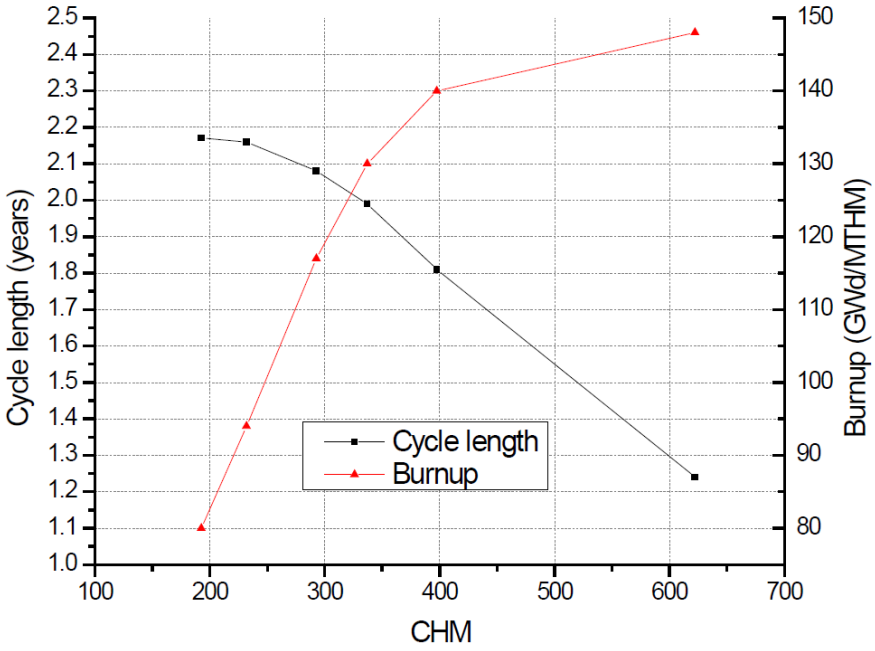


Figure 2-6: LSCR once-through cycle length and discharge burnup as a function of CHM [2]

An important design feature for reactor safety is the isothermal temperature reactivity coefficient. The temperature reactivity coefficient for the LSCR design was evaluated between 800 K and 1850 K and the average was calculated as $(dp/dT)_{iso}$=-3.80 PCM/K for a fresh reference core. The actual coefficient varies over the temperature interval and can be approximated using a linear function. The end of cycle reference core showed that burnup had a beneficial effect on the temperature coefficient which became more negative with an average of

$(dp/dT)_{iso}$=-7.53 PCM/K. The calculations for temperature coefficient of reactivity were performed on an uncontrolled configuration [2].

The void reactivity coefficient is the measured effect on reactivity that occurs when the coolant is removed from the core. The negativity reactivity inserted for this scenario for a fresh core was -2056.3 ± 26.3 PCM which is about -2% Δk/k. The void reactivity coefficient can vary based on the fuel design in question and it has been observed that a high CHM ratio leads to a positive coefficient, which can be seen in Figure 2-7 [2].

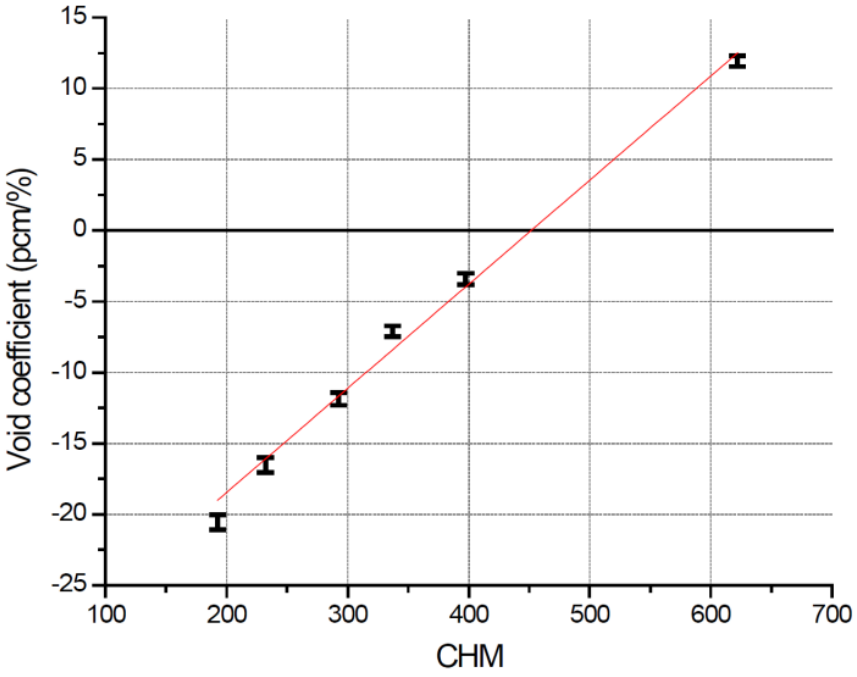


Figure 2-7: Coolant void coefficient as a function of CHM ratio [2]

However, the void coefficient is also related to fission product buildup and change in actinide concentration over the fuel cycle. Compared to the BOC core, the EOC void coefficient is more negative by 18.14 PCM/%.

One method of controlling the reactor involves the application of control rods. The LSCR design uses one control blade per fuel assembly which is composed of molybdenum-hafnium

carbide alloy (MHC) which acts as the neutron absorber in addition to the structural material. Neutron absorption occurs in both the hafnium and molybdenum. The overall reactivity worth of each control blade is low. A normally incident thermal neutron has a 15% absorption probability. When all the blades are inserted, the total negative reactivity is about 10% Δk/k. Due to the limited negative reactivity; the use of burnable poisons must be incorporated into the design of the LSCR core [2].

An option for integrating burnable poisons into the design, involves incorporating them into the central graphite matrix material of each fuel plate. The currently favored burnable poison is Europium because it burns at about the nearly same rate of the fuel. Calculations for a reduced initial activity below 10% Δk/k required a uniform load of about 50 grams of europium per fuel plate [2].

The result of this study proves the feasibility of a single-batch cycle length of 2 years that maintains passive safety features. A main concern is the effect of CHM ratio on the reactivity coefficients, but the results of the study show that CHM values of up to 400 are still able to provide negative reactivity coefficients [2].

### 2.2.5. Modeling of Double Heterogeneity

The double-heterogeneous problem presented by the introduction of TRISO fuel into reactor designs has been an issue due to modeling and computational constraints. A double-heterogeneous system includes heterogeneous fuel particles in a moderator matrix forming the fuel region of the fuel element and the first level of heterogeneity. The fuel elements themselves are heterogeneous with the fuel and moderator or reflector regions and form the second level of heterogeneity [12].

By explicitly modeling each individual particle for a particular design, the required amount of computing power is vastly greater than when traditional homogenization techniques are applied. The application of a simple volume homogenization is unsatisfactory when considering TRISO particles because of the strong resonant self-shielding effect. In order to simplify the model to an equivalent system, different studies have been performed to develop a method that can be applied to the problem. Since the TRISO fuel particle was initially developed for the HTGR, many studies have been focused on HTGR fuels but are relevant to the LSCR.

One particular method that has shown promise for HTGR fuels is the reactivity-equivalent physical transformation (RPT) method. The RPT method can be applied to various different types of codes in order to transform double-heterogeneous fuel problems into single-heterogeneous ones that have an identical reactivity as the initial problem. Testing has proven that the RPT method provides almost identical neutronic parameters at the initial state and is accurate for high fuel burnup [6]. The Korea Atomic Energy Research Institute (KAERI) is developing a strategy based on the HELIOS/MASTER code system for analysis of very high temperature gas-cooled (VHTR) cores. The benchmark results have shown that the code system accurately models both prismatic and pebble-bed reactor cores [13].

The RPT method is designed to accurately represent the resonant self-shielding effect which is inherent in the explicit grain model. The resonant self-shielding effect is significant when fuel is lumped into small particles, as is the case for TRISO particles. If a simple volume-weighted homogenization was performed on the fuel zone with TRISO particles, there would be a significant reduction in resonance self-shielding. Although most lattice codes are unable to handle the double-heterogeneity problem, a few codes such as WIMS, APOLLO, and DRAGON have the ability [13].

The process of performing the transformation from a double-heterogeneous problem to a single-heterogeneous problem, involves moving the fuel particles into a smaller volume to achieve a higher packing factor and then performing a simple homogenization of this region. The unknown variable is the size of the homogenous fuel zone. In order to determine this variable, the neutron multiplication factor of a reference case must correspond to that of the RPT adjusted fuel [6]. After determining the correct RPT dimensions, the calculations are performed using conventional methods [13].

The results of the study using the RPT method in combination with the HELIOS/MASTER code system show that it is a very accurate and practical method for analysis of prismatic and pebble-bed reactor cores [13].

The validity of the RPT method for depletion analysis was investigated for prismatic blocks by adjusting a variety of parameters and comparing the accuracy of the reference case to the RPT case. The RPT method proved to maintain high accuracy for depletion analysis at different temperatures, high fuel enrichment, large kernel diameter, and burnable absorber loaded assemblies [6].

The RPT methodology has been already used to study coated particle fuel for cylindrical and spherical geometries. The proposed fuel design of the LSCR implements plate fuel elements so the RPT method was extended to handle this geometry. In addition to the RPT method, two different techniques were developed to determine maximum discharge burnup. The first technique is an iterative method referred to as Iterative Equilibrium Depletion Search (IEDS). The method is computationally demanding but gives a highly accurate result based on an equilibrium fuel cycle. The second technique is an analytical method known as the Non-Linear Reactivity Model (NLRM). This method was based on the linear reactivity model but includes an arbitrary number of higher order terms. The advantage of this technique is the lower computational requirements since the extrapolation is based on only single batch depletion results [14].

The process for generating an RPT model for the slab geometry is similar to the process for cylindrical and spherical geometries. The fuel particles are initially collected into smaller RPT active slabs and then particles and matrix in the RPT active region are homogenized by volume. The design of the LSCR uses a layered fuel slab which can be represented with an RPT model by a transformation into an equivalent layered slab or a solid slab configuration. The layered slab transformation proves to be more accurate compared to a reference model, but the solid slab has the benefit of reduced computational requirements [14].

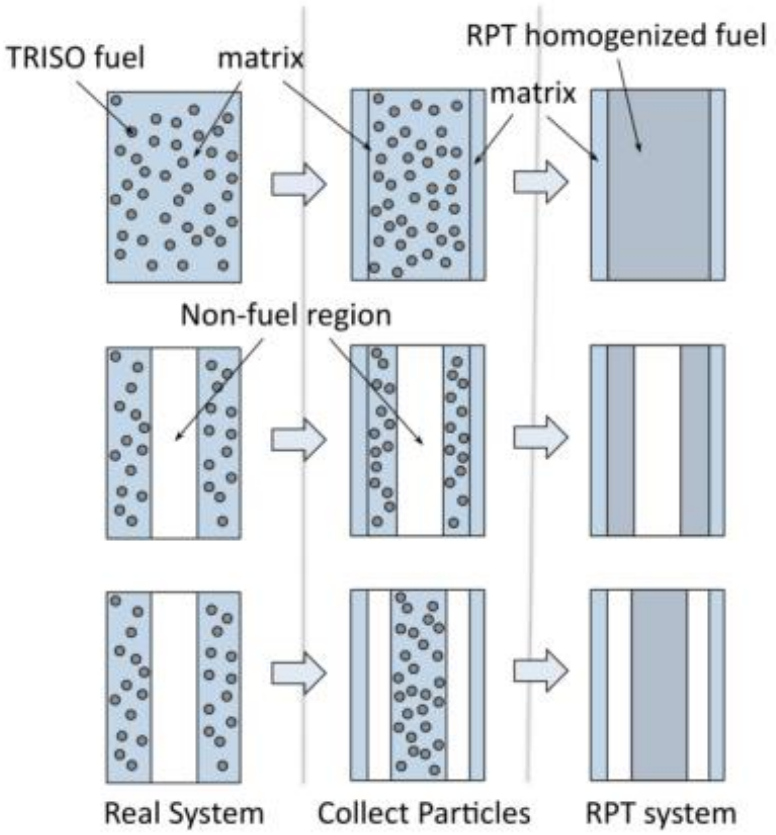


Figure 2-8: Volume homogenizations for RPT method in slab geometries [14]
(Top-solid slab; middle-layered; bottom-solid slab approximation)

The generation of an RPT homogenized composition vector, $N_{RPT}$, for the active region is determined using the following equation.

$$N_{RPT} = \frac{1}{VF_{RPT}} N_{fuel} - \frac{(1 - VF_{RPT})}{VF_{RPT}} N_{matrix}$$

In order to select the volume reduction in the active region, the $VF_{RPT}$ must be calibrated against a high-fidelity continuous-energy explicit grain model of the system. The correct calibration of an RPT model should result in the $k_{eff}$ of the RPT system at the beginning of cycle equivalent to that of the explicit grain model. When determining the correct volume reduction necessary to match the $k_{eff}$ of the reference model, the RPT layered slab transform requires

greater volume reduction than the solid slab transform. The solid slab approximation is able to induce more self-shielding because more of the fuel is grouped together, this enables the solid slab RPT transform to be used for modeling systems with softer neutron spectra where the layered slab RPT transform might fail [14].

The composition evolution of a set of important isotopes was compared for the RPT layered slab and RPT solid slab approximations against the high fidelity explicit grain model. The results of each model match well proving that the RPT method predicts parameters such as burnup and $k_{eff}$ evolution based on the correct physics [14].

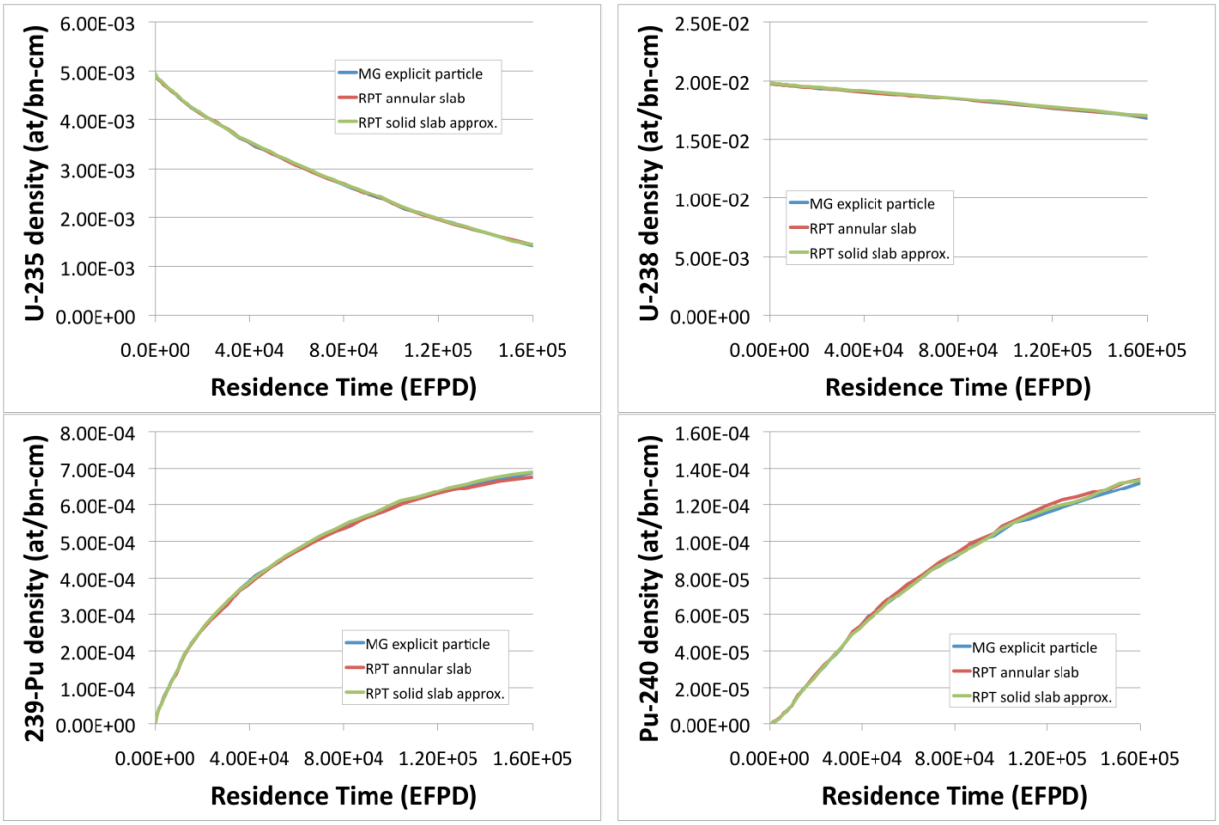


Figure 2-9: Isotopic concentration evolutions in LSCR baseline (central radial and axial position) [14]

A comparison of the computational requirements for the RPT methods (layered slab transform and solid slab approximation transform) relative to the explicit grain reference model showed an increase in the speed of depletion analysis by 10-20 times [14].

The RPT method is the primary method used for handling double-heterogeneous problems, but the Dancoff correction method is a second method that can be used to model TRISO-based fuel in the form used in LSCRs. The Dancoff correction method is used to perform depletion analysis using the TRITON sequence in SCALE. It has been verified by a code-to-code comparison against VESTA. The comparisons indicated good agreement of whole core characteristics such as multiplication factor and the isotopics [15].

The current LSCR design uses TRISO particles embedded in a slab of carbonaceous material. The fuel is concentrated closer to the surface of the slab and a moderating region of carbonaceous material is located in the center. The location of the fuel particles is chosen for better fuel utilization and improved cooling properties. The DOUBLEHET feature available in SCALE6.1 cannot be used for LSCR fuel because it is only applicable to (i.e., implemented for) the cylindrical pins or spherical pebbles of high-temperature gas-cooled reactor designs. The Dancoff correction method takes advantage of the ability of the cross section processing modules to accept a Dancoff factor that is calculated separately as an input parameter [15].

The Dancoff factor represents a correction to the escape probability of a neutron born in a fuel lump in order to account for the shadowing effect from other nearby absorber lumps. In order to calculate the Dancoff factor, the MCDANCOFF module in SCALE can be used or it can be calculated analytically for simple geometries [15].

The method is similar to the RPT method but rather than selecting equivalent dimensions an equivalent Dancoff factor is chosen to force the initial critical state to match the reference case. There are several advantages of using the Dancoff correction method rather than the RPT method. One advantage is that a distribution of Dancoff factors can be calculated for different regions of the reactor to improve the spatial prediction of various quantities. In addition, the

method preserves the real geometry, making the addition of poison particles intermixed with the particles possible. The final advantage is that the Dancoff factor can be used where the RPT method fails to find an equivalent dimension, such as the case in high carbon-to-heavy-metal ratios [15].

The Dancoff correction method was initially tested by comparing it against the DOUBLEHET feature in SCALE and modeling an NGNP prismatic fuel block. The results showed good agreement between the two models [15].

In order to test the validity of the method for the LSCR design, a code-to-code comparison against the VESTA depletion code was performed. VESTA utilizes MCNP5 and ORIGEN 2.2 to perform a depletion analysis. The VESTA case was designed to match the TRITON model as accurately as possible, including the use of a cubic lattice structure to model the randomly distributed TRISO grains. The results were compared for various characteristics to determine the degree of agreement. The results showed that the Dancoff correction method generated an average eigenvalue approximately 275 PCM lower, and thus provides a reasonably accurate, more rapid technique for performing global characteristic analysis [15].

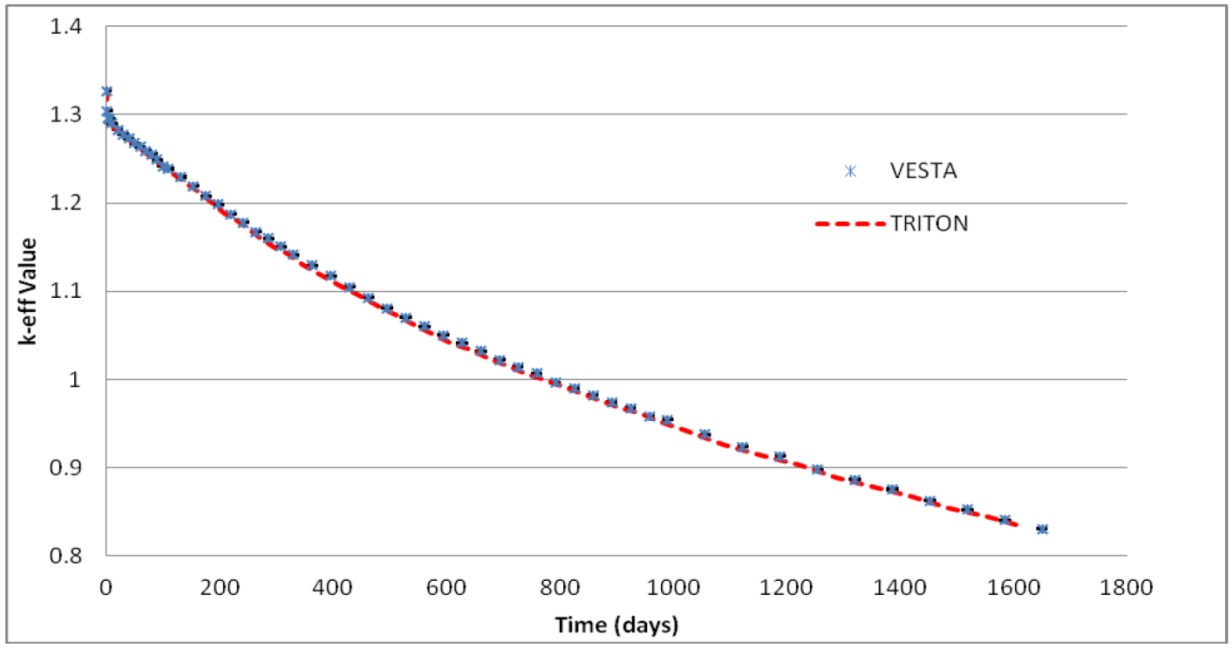


Figure 2-10: Evolution of $k_{eff}$ vs. time for TRITON and VESTA depletion calculations [15]

The Dancoff correction method still has a long computational time but is much more favorable than the VESTA code. Additional studies are necessary to determine whether a distribution of user supplied Dancoff factors will improve the spatial accuracy. The initial findings prove that the method is sufficiently accurate for scoping studies of whole core characteristics [15].

### 2.2.6. Depletion Analysis

In order to correctly determine depletion of the LSCR design, special consideration had to be given to the double-heterogeneous problem presented by the TRISO fuel. Through the application of the RPT methods for slab geometries, a simplified model can be created to accurately model the core. Based on the developed RPT method, a Monte Carlo depletion method was developed to search for the maximum discharge burnup of a multi-batch system. The process works by iteratively estimating the beginning of equilibrium cycle (BOEC) composition and sampling different discharge burnups. This Iterative Equilibrium Depletion Search (IEDS) can define the $k_{eff}$, power, flux, and composition evolutions but is computationally demanding [14].

The IEDS method was implemented using the TRITON module of SCALE. A driver program was developed to iteratively execute TRITON, shuffle EOEC fuel, insert fresh fuel, assess the convergence of the BOEC composition, and pass the EOEC $k_{eff}$ to the next iteration loop once the BOEC composition has converged [14].

A second, analytical method, termed the Non-Linear Reactivity Model (NLRM) was developed through the expansion of the linear reactivity model by including higher order terms. This method allows for the extrapolation of results from single-batch depletion to estimate the maximum discharge burnup and BOEC $k_{eff}$ in systems with multi-batch fuel management schemes. Figure 2-11 shows the NLRM results for different orders compared to the depletion results based on the IEDS method. [14].

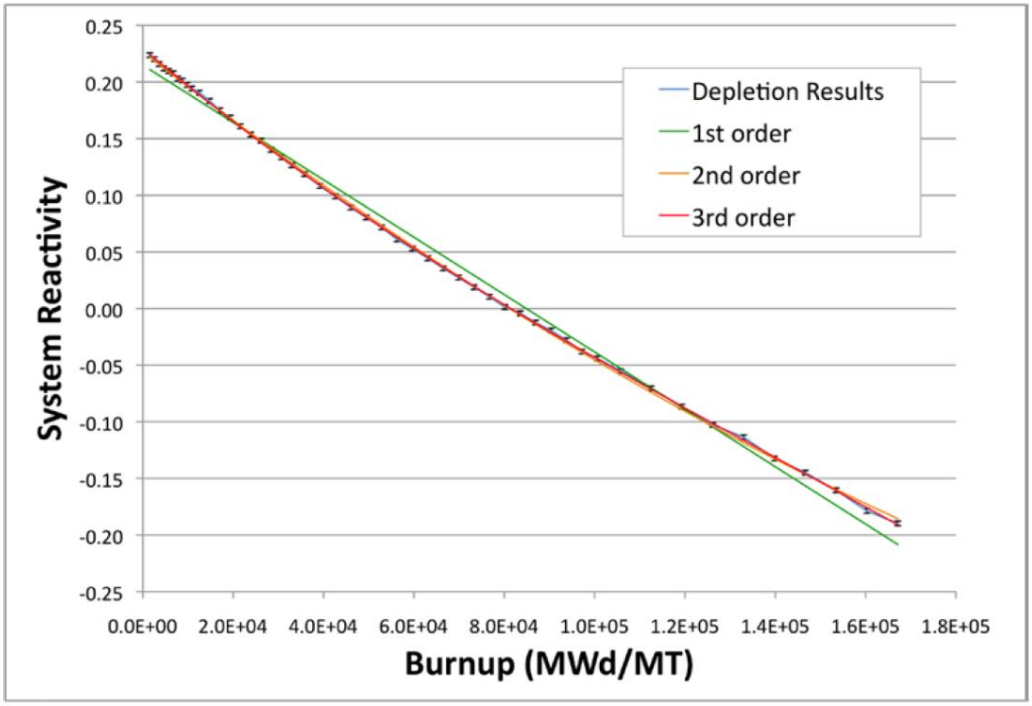


Figure 2-11: Comparison of polynomial expansions of reactivity [14]

The accuracy of the NLRM was also analyzed to insure that the error was acceptable. Additionally, it allows for a comparison to the normally used LRM and shows how the increase in terms effect the error in predicted burnup [14]. By viewing Figure 2-12, the variation between the IEDS method and results from the 1$^{st}$ (normal LRM), 2$^{nd}$, and 3$^{rd}$ orders of the NLRM can be seen. The reloads per fuel cycle refers to the number of batches.

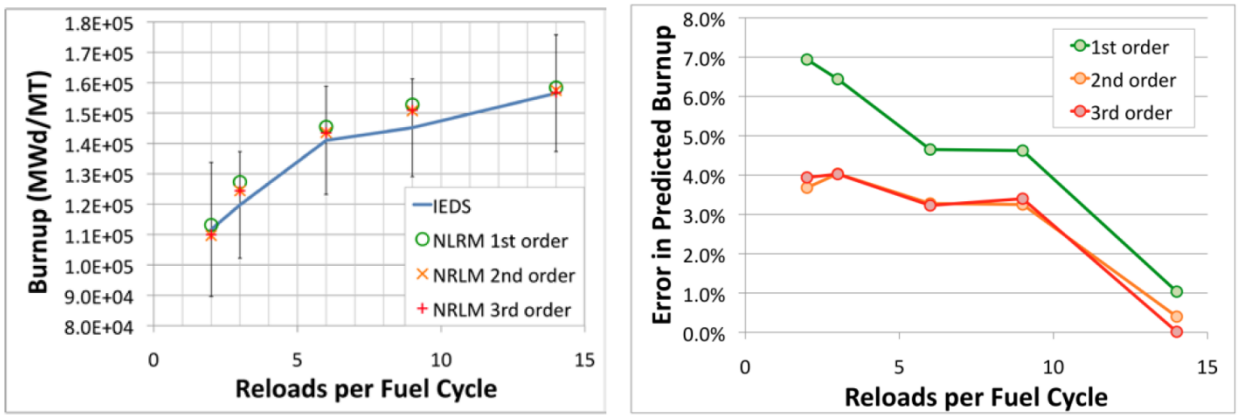


Figure 2-12: Comparison of maximum discharge burnup predicted by IEDS to NRLM [14]

There is a quite a significant computation advantage for using the NLRM over the IEDS methodology which requires iterative calculation of the BOEC composition vector depletion. The NRLM requires only a single depletion calculation to estimate discharge burnup, and the associated error is deemed acceptable. A comparison of the computational requirements of the two methods is shown below in Table 2.7 [14].

Table 2.7: Computational requirements for depletion analysis [14]

| Equilibrium Depletion Method | Batches | Computational Time (days) | Burnup Error (%) |
|---|---|---|---|
| **Iterative Equilibrium Depletion Search** | 2 | 6.9 | - |
| **Iterative Equilibrium Depletion Search** | 6 | 20.7 | - |
| **Non-Linear Reactivity Model** | 2 | 1.0 | 3.7 |
| **Non-Linear Reactivity Model** | 6 | 1.0 | 3.3 |

### 2.2.7. Background Summary

The origins of the LSCR are attributed to a combination of the Molten Salt Reactor program and the HTGR. TRISO fuel particles were first developed as a high temperature fuel to be used in HTGR reactor designs, and the feasibility of a liquid-salt-cooled reactor was shown during the MSR program during the late 1960s. Through the merging of the two technologies, the concept of the LSCR was established. Since the LSCR uses the same fuel as the HTGR, initial design studies were based heavily on the configuration of the HTGR reactors [9]. However, as studies were performed, the design evolved to better handle the neutronic and thermal requirements presented by the liquid-salt coolant.

The current design is most accurately represented by the study documented by Reference 5. This design is based on applying TRISO fuel particles to a plank type fuel element arranged in three symmetric groups of six in a hexagonal fuel assembly, where the reactor core is comprised of 253 fuel assemblies [2]. The plank fuel element was initially developed for the SmAHTR project, which is a design concept for a modular LSCR. TRISO fuel particles have proven to be robust at high temperatures and burnup through the research performed on HTGRs [8].

Each of the fuel assemblies contains a single "Y" shaped control blade that fits in a slot located in the center of the assembly. The control blades are constructed of a molybdenum-hafnium carbide alloy (MHC) which serves as both neutron absorber and structural material. However, the control rods themselves do not provide enough reactivity control, so the central matrix of each fuel plate must also contain burnable poison particles to compensate for the large excess reactivity [2].

The coolant chosen for the LSCR is FLiBe, due to both past experience from the MSR program and its neutronic and thermal hydraulic advantages. It has a volumetric heat capacity

comparable to water, melting temperature of 459$^{o}$C, boiling point of 1430$^{o}$C, and density of 1940 kg/m$^{3}$ [9].

Insuring that a reactor can be economically and safely operated and maintained at a critical state involves the consideration of different properties that influence the overall neutronics of the core. These factors include the $k_{eff}$, void reactivity coefficient, temperature reactivity coefficient, transient behaviors, and fuel burnup.

The preliminary studies used a reactor core design identical to that of the HTGR. One of the focuses of these studies involved the choice of coolant to eliminate a positive void reactivity coefficient at any point during the fuel cycle [9]. In order to alleviate this problem, the lithium content of the FLiBe coolant is enriched to Li-7 because the cross section inherent to Li-6 has a high thermal neutron capture cross section. The other elements in FLiBe only contain one natural isotope. In addition, the removal of Li-6 helps reduce the buildup of $^{3}$H within the reactor as shown by the following reaction [7].

$$^{6}_{3}Li + n \rightarrow {}^{4}_{2}He + {}^{3}_{1}T$$

In general, the advantages of using a liquid-salt coolant include lower operating pressure, higher power density, better heat removal properties, and reduced shielding requirements for external components [7]. The overall result is improved safety and the potential for a more economical system. For this reason the LSCR is a viable competitor against other high temperature reactor concepts, specifically the HTGR.

Another property of this type of thermal reactor system is the strong temperature feedback effect due to the Doppler broadening of the uranium resonances that occurs at elevated temperatures. Due to this feature, as the temperature of the fuel increases, the parasitic

absorption of neutrons by the fertile component of the fuel increases, reducing the total reactivity of the system and the power level [8].

Studies on cycle length have been performed and show that increasing the carbon-to-heavy metal (CHM) ratio leads to a decrease in cycle length. However, the advantage of an increased CHM ratio is a sharp increase in discharge burnup [2].

A key characteristic feature of reactor safety involves the temperature reactivity coefficient. The temperature reactivity coefficient for the LSCR was evaluated in one study between 800 K and 1850 K and the average value is $(dp/dT)_{iso}$=-3.80 PCM/K for a fresh reference core. The actual coefficient varies over the temperature interval and can be approximated using a linear function. Fuel burnup showed a beneficial effect on the temperature reactivity coefficient, which became more negative to an average of $(dp/dT)_{iso}$=-7.53 PCM/K at end of cycle [2].

Modeling and Double-Heterogeneity

The double-heterogeneity presented by the introduction of the TRISO fuel into reactor designs has been an issue due to modeling and computational constraints. By explicitly modeling each individual particle for a particular design, the required amount of computing power is vastly greater than when traditional homogenization techniques are applied. The application of a simple volume homogenization is unsatisfactory when considering TRISO particles because of the strong resonant self-shielding effect. In order to simplify the model to an equivalent system, studies have been performed to develop a method that can be applied to the problem. Since the TRISO fuel particle was initially developed for the HTGR, many studies have been done on HTGR fuels and are relevant to the LSCR.

A popular technique for creating a simplified equivalent model involves the application of the reactivity-equivalent physical transform method. This technique can be applied to various different codes to transform a double-heterogeneous fuel problem into a single heterogeneous one. The RPT method is designed to accurately represent the resonant self-shielding effect which is inherent in the explicit grain model. The resonant self-shielding effect is significant when fuel is lumped into small particles, as is the case for TRISO particles. A simple volume-weighted homogenization would cause a significant reduction in the resonance self-shielding [13].

In order to apply the RPT method, an explicit grain reference model is used to determine the correct size of the homogenized fuel so that an identical self-shielding effect is present in both the double-heterogeneous and single-heterogeneous problems [13]. Based on the reference mode, the correct calibration of an RPT model should result in the $k_{eff}$ of the RPT system at the beginning of cycle equivalent to that of the explicit grain model [14]. After determining the correct RPT dimensions, the calculations are performed using conventional methods.

When performing the transformation for the RPT method on fuel slabs, the equivalent model can be either a layered slab or a solid slab configuration. The layered slab transformation proves to be more accurate compared to a reference model, but the solid slab has the benefit of reduced computational requirements [14].

The RPT method can also be accurately used to predict burnup for single batch and multi-batch fuel cycles. Two methods that have proven effective are the Iterative Equilibrium Depletion Search (IEDS) and Non-Linear Reactivity Model (NLRM). The IEDS technique is computationally demanding but gives a highly accurate result based on an equilibrium cycle. The NLRM method is based on the linear reactivity model but includes a number of higher order terms [14].

The Dancoff correction method is a second technique that can be used to model the TRISO-based fuel in the form used in LSCRs. This method is used to perform depletion analysis using the TRITON sequence in SCALE. A double-heterogeneous feature exists in SCALE but is only applicable to the cylindrical pins or spherical pebbles of HTGR designs. The Dancoff correction method takes advantage of the ability of the cross section processing modules to accept a Dancoff factor that is calculated separately as an input parameter. The Dancoff factor represents a correction to the escape probability of a neutron born in a fuel lump in order to account for the shadowing effect from other nearby absorber lumps [15].

The method is similar to the RPT method but rather than selecting equivalent dimensions an equivalent Dancoff factor is chosen to force the initial critical state to match the reference case. The advantages of Dancoff correction over RPT include improved spatial prediction of various quantities by using a distribution of Dancoff factors, the preservation of the real geometry, and the ability to handle situations with high CHM ratios [15].

In order to correctly determine the depletion of the LSCR design, special consideration had to be given to the double-heterogeneous problem presented by the TRISO fuel. Through the application of the RPT methods for slab geometries, a simplified model can be created to accurately model the core. Based on the developed RPT method a Monte Carlo depletion method was developed to search for the maximum discharge burnup of a multi-batch system. The process works by iteratively estimating the BOEC composition and sampling different discharge burnups. This Iterative Equilibrium Depletion Search (IEDS) can define the $k_{eff}$, power, flux, and composition evolutions but is computationally demanding [14].

A second technique is an analytical method termed the Non-Linear Reactivity Model (NLRM). It was developed through the expansion of the linear reactivity model by including

higher order terms. This method can be used to estimate the maximum discharge burnup and BOEC $k_{eff}$ in systems with multi-batch fuel management schemes by extrapolation of the results from a single-batch depletion. There is a significant computational advantage for using the NLRM over the IEDS methodology and it has an error within an acceptable range when using only a second order term [14].

# CHAPTER 3: MODELS AND METHODOLOGY

## 3.1. Development of SCALE Models

In order to perform the various parametric studies on the LSCR, a series of simplified models were progressively developed so that the reactor system could be modeled accurately and efficiently. The first step was the development of a model to represent a single fuel plate. Based on the plate model, an assembly model was developed and then finally used to create a simple full 3D core model. These models were developed for SCALE6.1 and were primarily run on a computer cluster consisting of 48 nodes. Each node had 8 available processors and either 16 GB or 64 GB of RAM. A personal computer with an Intel i7 2.8 GHz processor and 8 GB of RAM was also used to run models in SCALE.

### 3.1.1. Simple 1D Plate Model

The 1D plate model consists of a section of a fuel plate which has been cut in half along its center axis and has half of the normal coolant between the plates. Since the coolant between the plates is normally 0.7 cm thick, a coolant thickness of 0.35 cm was used for the model. The coolant is a mixture of lithium fluoride and beryllium fluoride termed FLiBe. This fluoride-salt has a temperature dependent density which is roughly 1.940 g/cm$^3$, a melting temperature of 459$^o$C, and a boiling temperature of 1430$^o$C. Additionally, FLiBe has a volumetric heat capacity comparable to water, making it advantageous from a thermal hydraulic perspective [16].

The fuel in the plates is a random distribution of tristructrual isotropic (TRISO) particles placed in stripes on the outside of the fuel plates. Particles are placed into a graphite matrix material to hold them in place. The inner region of the plank is filled with graphite which is

essential as a neutron moderator. The different layers of the TRISO particle are shown in Figure 3-1. The fuel kernel is shown in the middle and is surrounded by a series of different materials.

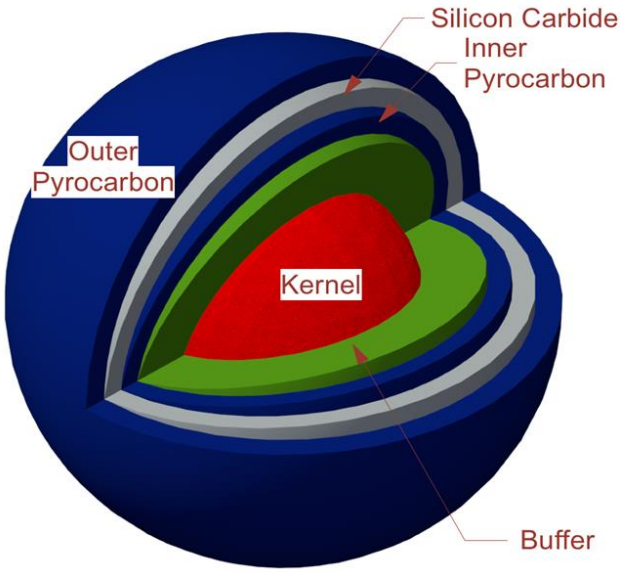


Figure 3-1: AGR-2 fuel particle [10]

The dimensions used for the TRISO particles are those used in the design developed by ORNL [10]. Table 3.1 provides dimensions for the different components of a single TRISO particle and the graphite matrix in which it would be embedded. However, the specific pitch can be varied as a means to adjust packing factor.

Table 3.1: TRISO fuel particle dimensions [10]

| Region | Parameter | Parameter Value (µm) | Material | Density (g/cm³) |
|---|---|---|---|---|
| Kernel | diameter | 427 | Uranium Oxycarbide | 10.90 |
| Buffer | thickness | 100 | Porous Graphite | 1.00 |
| IPyC | thickness | 35 | Pyrolytic Graphite | 1.90 |
| SiC | thickness | 35 | Silicon Carbide | 3.20 |
| OPyC | thickness | 40 | Pyrolytic Graphite | 1.87 |
| Fuel Particle | diameter | 847 | - | - |
| Matrix | pitch | 927 | Carbon Material | 1.59 |

In order to control the packing factor of the TRISO particles in the model, they are placed inside a cuboid of the matrix material. These cuboids are then used to create a regular square array with a pitch of 927 µm between fuel kernels, which corresponds to a base packing factor of 40%. A regular square array is used versus a random distribution to further simplify the model. In the base plate model, the array of fuel kernels consists of 100 particles in the x-direction, 7 particles in the y-direction, and 50 particles in the z-direction. The number of particles in the y-direction was chosen to most closely match the fuel stripe thickness specified by the design developed by ORNL [10]. The section of the plate was made big enough to ensure that the model could appropriately converge in a reasonable amount of time. A smaller section of fuel would actually require a greater amount of run time to simulate the same number of histories (and provide results with an equivalent uncertainty).

The outermost edge of the fuel plate consists of a sleeve/cladding layer which helps prevent fuel particles from eroding [2]. Based on the design developed by ORNL, the sleeve thickness has been modeled as 0.1 cm [10]. Figure 3-2 shows the geometrical configuration of the fuel plate through a cross sectional view of the x-y plane. From top to bottom the figure shows the FLiBe coolant (blue), the fuel sleeve/cladding (yellow), the array of fuel kernels nested in graphite matrix, and the graphite located at the center of the fuel (red). A full width plate would be shown if the image was mirrored on the bottom edge.

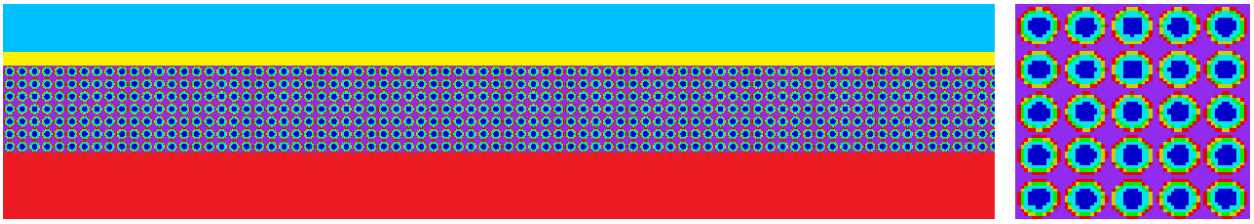

Figure 3-2: Cross sectional view of plate model (with enlarged section)

The dimensions of the half fuel plate model are shown in Table 3.2. All dimensions are based on those specified by ORNL designs but have been slightly altered to fit certain physical constraints. Since the model does not take length and height into consideration those parameters are not included.

Table 3.2: Fuel plate dimensions

| Component | Thickness (cm) |
|---|---|
| Coolant | 0.3500 |
| Sleeve/Cladding | 0.1000 |
| Fuel Stripe | 0.6486 |
| Graphite Meat | 0.5314 |

The material compositions of the TRISO particles, graphite, cladding, and FLiBe were based off those used in the models created by Dan Ilas [10]. However, the materials used by Dan Ilas include boron contamination whereas this model does not. Table 3.3 provides information on the operating temperatures and densities of the different materials used in the model.

Table 3.3: Material temperatures and densities

| Material | Temperature (K) | Density (g/cm$^3$) |
|---|---|---|
| Fuel Kernel (19.75 wt%) | 1200.00 | 10.90 |
| Porous Buffer | 1200.00 | 1.00 |
| Inner Pyrolitic Carbon | 1200.00 | 1.90 |
| Silicon Carbide | 1200.00 | 3.20 |
| Outer Pyrolitic Carbon | 1200.00 | 1.87 |
| Matrix Material | 1200.00 | 1.59 |
| Graphite Meat | 1200.00 | 1.59 |
| Sleeve/Cladding | 1000.00 | 1.59 |
| FLiBe | 948.15 | 1.95 |

Although the specified model of the TRISO particle is exact, it was desirable to perform certain simplifications to reduce the model complexity and decrease the necessary run time. The main source of complexity is from the complicated structure of the TRISO particles. As a

simplification, all the layers of the TRISO particle surrounding the fuel kernel were homogenized with the matrix material. A simple volume homogenization of this type has the potential to drastically decrease run time requirements with little reduction in accuracy because the different components being homogenized are mainly different forms of carbon resulting in limited effect on the neutronics.

The optimum homogenized configuration was determined by performing five different levels of homogenization. The first model used no homogenization by modeling each of the TRISO layers individually and creating an array of the explicitly modeled particles. The next level of homogenization was performed by only homogenizing select layers of the TRISO particle. The layers homogenized were the buffer and inner pyrolitic carbon layers and then the outer pyrolitic carbon layer and matrix material. The silicon carbide layer was left intact because it is significantly different in composition compared to the others. The next model was a homogenization of all the layers of the TRISO particles and the matrix material leaving an array of fuel kernels in one homogenous mixture. The last two models were a homogenization of the entire TRISO particle along with the matrix material. However, the first model continues to use an array for the homogenized mixture while the second uses a solid block of the material, similar to how an RPT (reactivity equivalent physical transform) model would be designed [6]. This was done to determine how the run time is affected by the use of an array. Table 3.4 below shows the results based on the $k_{inf}$ and the required run times.

Table 3.4: Variance of $k_{inf}$ due to homogenization

| | Level of Homogenization | $k_{inf}$ | Uncertainty | Run Time (min) |
|---|---|---|---|---|
| No Homogenization | 1 | 1.15948 | 0.00025 | 1637.75 |
| Partial Layer Homogenization | 2 | 1.15898 | 0.00027 | 1211.22 |
| TRISO Layer Homogenization | 3 | 1.15891 | 0.00023 | 820.95 |
| Complete Homogenization | 4 | 1.11214 | 0.00019 | 744.69 |
| Complete Homogenization (RPT) | 5 | 1.11201 | 0.00023 | 232.84 |

The results show that the $k_{inf}$ for the first three models are very similar. The decrease in run time between the fully explicit model and the homogenization of all layers is around 800 minutes which is about a 50% improvement. This a significant decrease in run time while still showing a high level of agreement based on the $k_{inf}$. The large reduction in time between the last two models is also of interest. This represents that the use of a large array has a significant impact on the run time. Figure 3-3 shows a graphical representation of the data.

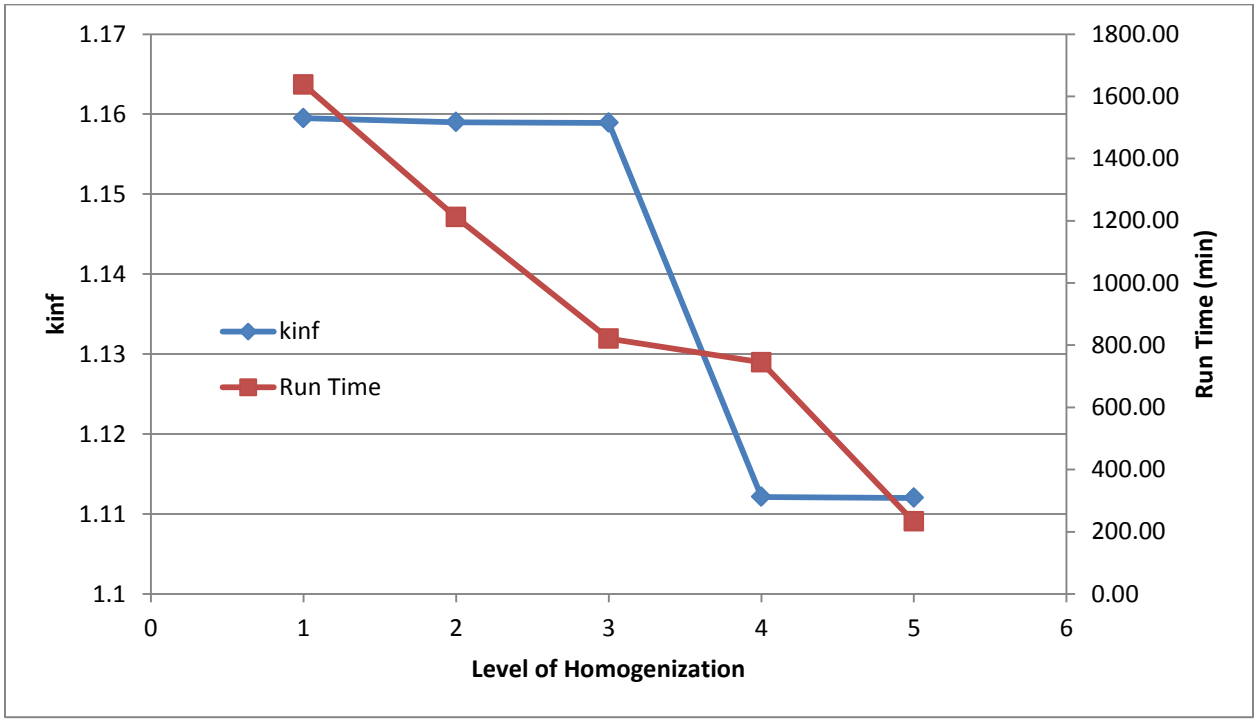


Figure 3-3: Variance of $k_{inf}$ due to homogenization

In order to show a better comparison of the first three levels of homogenizations, Figure 3-4 is shown on the following page and only includes those three points. This figure includes the uncertainty associated with each of the cases and shows how they greatly overlap. Based on the data, the homogenization of the TRISO layers and matrix material is an acceptable simplification that significantly reduces the required run time.

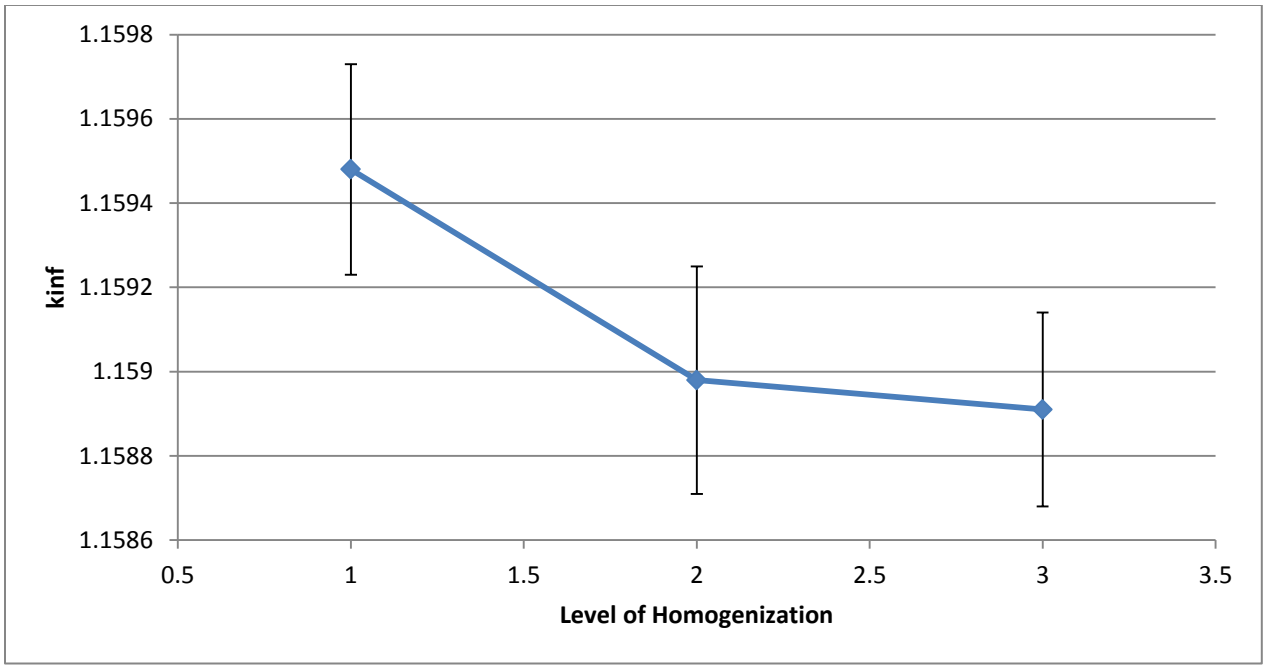


Figure 3-4: Variance of $k_{inf}$ due to homogenization

The finalized plate model applies the homogenization of the TRISO layers and the matrix material as a means to simplify the model and reduce the run time. All other aspects of the model remain the same as what has already been mentioned. Figure 3-5 shows a cross sectional view of the simplified model. It is very similar to Figure 3-2; however, there are no longer multiple layers surrounding the fuel kernel.

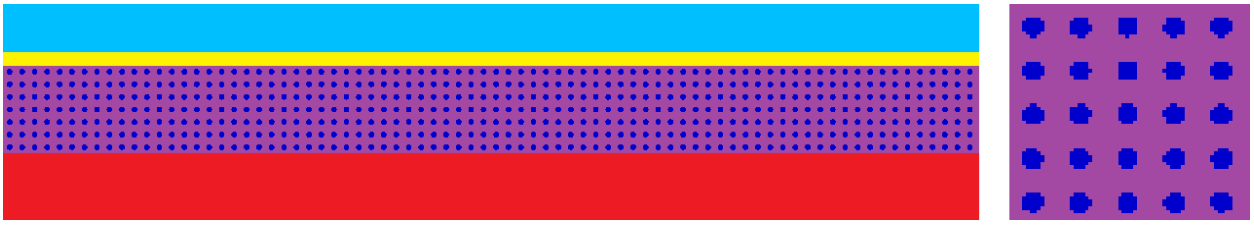

Figure 3-5: Cross sectional view of simplified plate model (with enlarged section)

### 3.1.2. 2D Assembly Model

In order to improve upon the accuracy and relevance of the studies being performed on the LSCR, it was necessary to further develop the models being used to perform the various simulations. A one-dimensional fuel plate model was initially developed to gain a general understanding of the neutronic response due to a variety of parameters. The next step was the development of a two-dimensional assembly model that could be used to generate results that more accurately represent the true response of the system.

Due to the limitations inherent to SCALE, the model is not truly two-dimensional. Since the use of spherical fuel particles cannot be applied to create a true two-dimensional model, the z-dimension is assumed to be unchanging and has been set with reflected boundaries to create the desired effect.

The current LSCR fuel assembly design is a 6 meter tall hexagonal prismatic box with 1 cm thick walls of carbon-carbon composite. Each assembly box is divided into three symmetric regions by a 4 cm thick Y-shaped structure made of carbon-carbon composite. Each of the three regions contains six equidistant fuel plates which are supported by the Y-shaped structure on one end and the full length channel box on the other end. A two dimensional cross section of an assembly is shown in Figure 3-6.

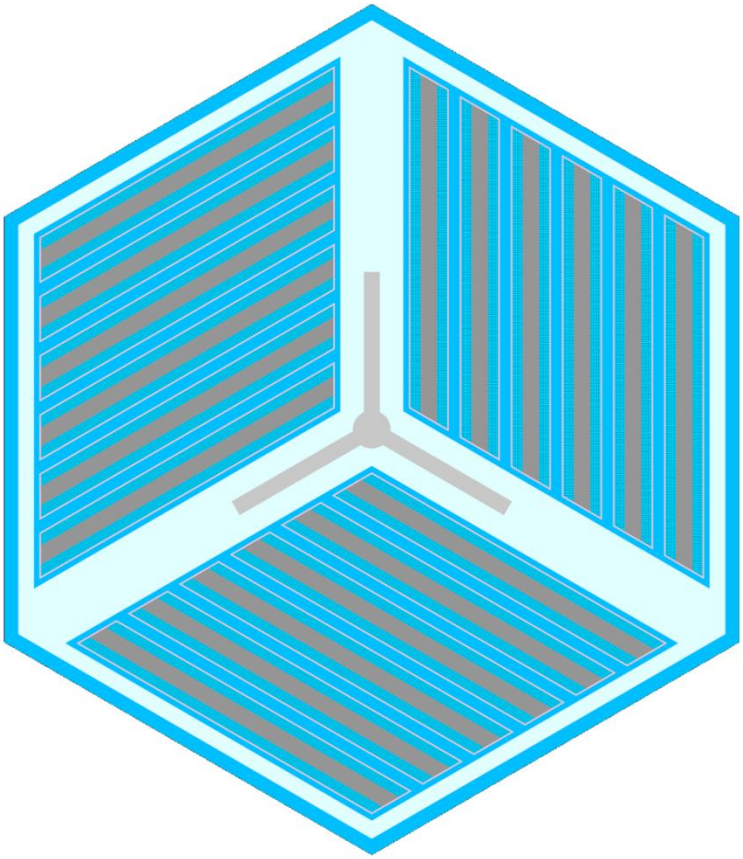

Figure 3-6: Assembly model

The spacing between fuel plates is filled with the primary coolant, which has been chosen as FLiBe. The channel boxes of adjacent assemblies are separated by 1.7 cm and also filled with FLiBe coolant. The center of the Y-shaped structure in the fuel assembly serves as the slot for a Y-shaped control blade, where the slot has a thickness of 1 cm [2]. Table 3.5 provides the geometric characteristics of the fuel assembly.

Table 3.5: Geometric characteristics of fuel assembly [2]

| Characteristic | Value | Units |
|---|---|---|
| Total height | 600 | cm |
| Fueled region height | 550 | cm |
| Fuel assembly pitch | 46.75 | cm |
| Outer apothem | 22.5 | cm |
| Channel box wall thickness | 1 | cm |
| Y-shape thickness | 4 | cm |
| Coolant thickness between pates | 7 | mm |
| Coolant thickness between plate and wall | 3.5 | mm |
| Fuel plate thickness | 2.55 | cm |
| Number of fuel plates | 18 | - |

The model was designed to match the specified characteristics as accurately as possible. However, some simplifications were made to reduce the overall complexity of the model. The main structural simplification occurs from not including the supports (distancing strips) that would be used to hold the individual fuel plates in their correct positions. The inclusion of this feature would add to the complexity of the model while having little effect on the overall neutronics.

The development of this assembly model was also based on some of the simplifying assumptions that were determined through the development of the fuel plate model. A primary assumption is the handling of the TRISO fuel particles and the matrix material in which they are embedded. From the studies performed on the fuel plate model, it was determined that a simple volume homogenization of the layers surrounding the fuel kernel along with the graphite matrix has minimal effect on the neutronics of the system while significantly reducing the required run time. These results are the basis of the simplifying homogenization assumption which has also been utilized in the assembly model

In order to control the packing factor of the TRISO particles, the fuel kernels were placed inside a cuboid of the homogenized matrix material and TRISO layers. These cuboids were then

used to create a regular square array with a pitch of 927 µm between fuel kernels, which corresponds to a base packing factor of 40%. A regular square array was used versus a random distribution to further simplify the model. A thickness of 7 layers of TRISO particles was used to remain consistent with the fuel plate model. The array was then placed on both sides of a parallelepiped composed of the central graphite found between the two layers of fuel. The resulting thickness of the plate was 2.55 cm and the height of the slice represented in the model was chosen to be 100 TRISO particles. Due to the angled edges of the parallelepiped, there is the potential for some fuel particles at the edge of the plate to be partway cut-off. As mentioned previously, the dimensions and sizes described represent a base model from which adjustments were made to vary parameters such as packing factor. For simplicity, no spacer material was used to prevent this from occurring. To ensure that this was an acceptable simplification, both cases were tested and there was a negligible effect on the neutronics whether the particles remain whole or not.

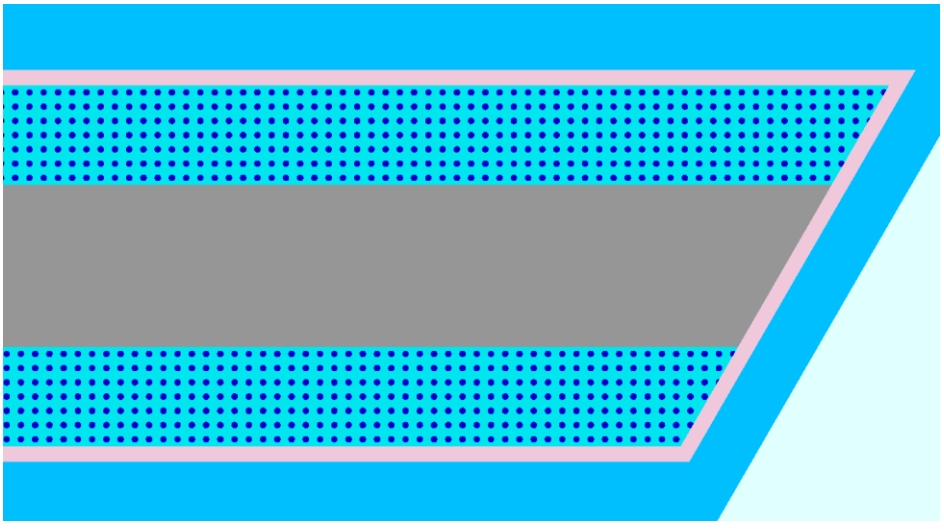

Figure 3-7: Fuel plate from assembly model

A portion of one of the modeled fuel plates can be seen on the preceding page in Figure 3-7. The blue surrounding the plate represents the FLiBe coolant and the outermost edge of the fuel plate consists of the sleeve/cladding layer which helps prevent fuel particles from eroding [2]. The thickness of this sleeve is 0.1 cm all the way around the fuel plate and it is composed of graphite. As mentioned previously, it can be seen that some of the particles at the edge of the plate have been partly cut-off.

After correctly defining a single fuel plate, a group of six plates was created by repeatedly placing the initial fuel plate into a section of coolant. The plates are each 2.55 cm thick and there is 7 mm of coolant between each of the plates. The coolant between the end plates and the wall is 3.5 mm thick. The grouping of six plates is shown below in Figure 3-8.

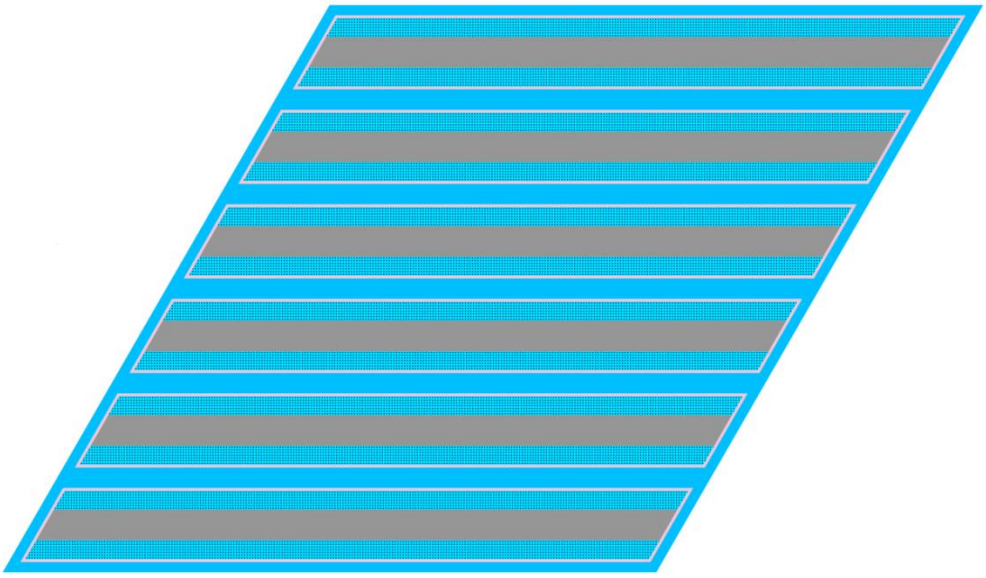

Figure 3-8: Group of six plates from assembly model

The next step in setting up the model involved placing the group of six plates into the three appropriate regions of the hexagonal assembly. The different groups were each oriented differently so they had to be rotated accordingly. In order to complete the model the control

blade slot must be defined and the region surrounding the assembly must be filled with the correct amount of coolant. The resulting geometry of the full assembly was shown previously in Figure 3-6.

The final simplification required for the completion of the model was the application of reflected boundaries on all sides of the hexagonal fuel assembly. Periodic boundaries could also have been used and were tested to show that there is a negligible difference when compared to reflected boundaries. This assumption effectively creates an infinite array of assemblies and results in a situation where there is zero leakage out of the system and the system multiplication is calculated in terms of $k_{inf}$.

The resulting assembly model very closely approximates the reference assembly geometry. Relative to the fuel plate model, this assembly model provides results that are much more representative of a full reactor core.

### 3.1.3. Simplified 2D Full Core Model

The final development stage involved creating a full core model based on the previous plate and assembly models. The application of a full core model allows for the most accurate results for the reactor system, including $k_{eff}$, which can then be used to find leakage and determine the equivalent $k_{inf}$ for a fully reflected 2D assembly model.

The creation of a full core model was a fairly simple process because it only required creating an array of the assembly models previously developed and surrounding the array with a layer of reflector blocks along with the reactor pressure vessel. Similarly to the assembly model, the z-dimensions use reflected boundaries to effectively create a 2D model. However, the radially outer boundary of the reactor utilizes a vacuum boundary to account for leakage.

The core consists of 253 fuel assemblies arranged in a hexagonal lattice, roughly cylindrically shaped [10]. The reflector blocks are arranged around the lattice of assemblies as a means to reduce leakage out of the system. From this point, a reactor vessel surrounds the lattice of reflector blocks and assemblies. The space between the reflector blocks and the outer boundary of the core is filled with the primary coolant, FLiBe. Figure 3-9 shows a cross sectional view of the reactor core.

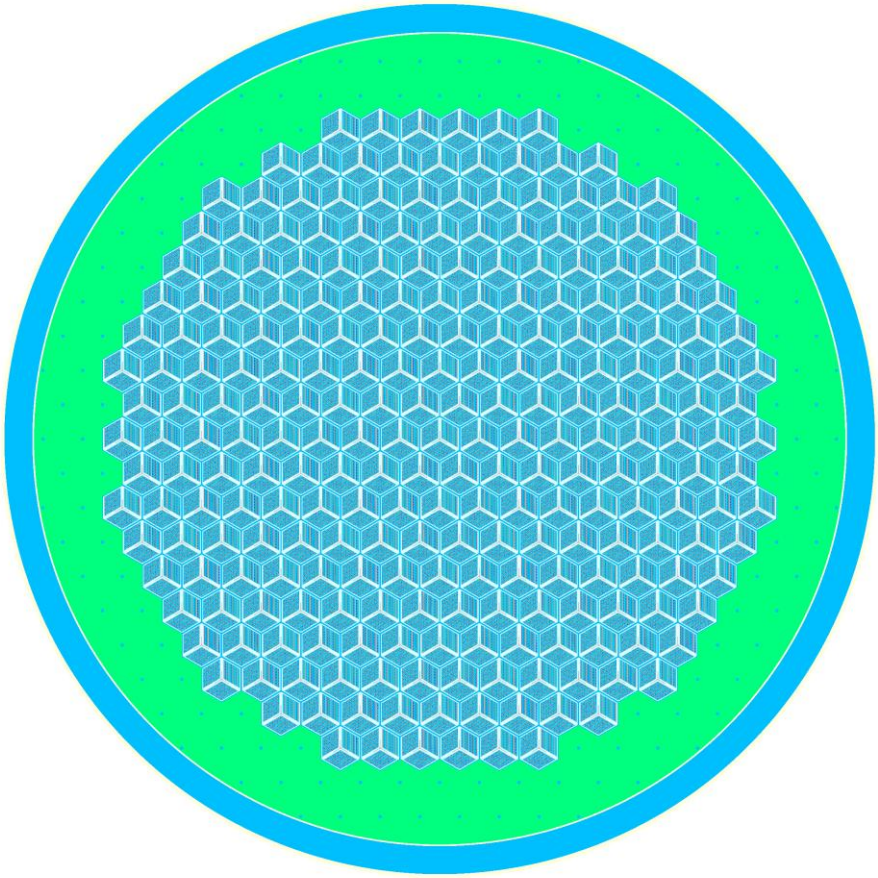

Figure 3-9: Cross sectional view of reactor core

## 3.2. Simplified Fuel Cycle Cost Model

A simplified fuel cycle cost model was developed to determine the costs associated with different packing factors and uranium enrichments and narrow down selections. In order to keep the cost model simplified, certain assumptions were made. The main simplifications involve ignoring the time value of money, ignoring losses, applying the linear reactivity model, and taking outages into account through the application of a fixed cost. By applying the cost model for the different cycle lengths and discharge burnups obtained from the various models, certain bounds can be developed to include the most attractive options for the fuel design.

The first step involved in developing the cost model was determining prices for the cost of $U_3O_8$, the cost of conversion to $UF_6$, and the cost per separative work unit (SWU). These values were obtained from the Ux Consulting Company (UxC) website and are the spot prices for May 27, 2013. Table 3.6 shows the different cost components.

Table 3.6 UxC spot prices for uranium, convesion, and SWUs

| Product | Price |
|---|---|
| **U3O8 (lb)** | $40.50 |
| **U3O8 (kg)** | $89.29 |
| **U3O8 (kgU)** | $105.29 |
| **Conversion (kgU)** | $10.00 |
| **UF6 (kgU)** | $115.29 |
| **SWU Price (SWU)** | $112.00 |

The next step for creating the cost model involved finding the number of SWUs necessary for a particular uranium enrichment. The variable $x_p$ is used to describe the desired uranium enrichment while the variables $x_f$ and $x_w$ describe the weight percent of the feed material and the weight percent of the tails, respectively. A value of 0.711% was used for $x_f$ and corresponds to the natural enrichment of uranium. The value chosen for $x_w$ was 0.2%. Other

important variables include F, P, and W which relate to the feed input rate, product output rate, and tails output rate, respectively. The following two equations show how each of these variable relate to one another [17].

$$F = P + W \tag{3.1}$$

$$x_f F = x_p P + x_w W \tag{3.2}$$

By performing several algebraic manipulations on the previous equations, it is possible to determine ratios for feed to product and tails to product. These ratios can be seen in the two equations below.

$$\frac{F}{P} = \frac{x_p - x_w}{x_f - x_w} \tag{3.3}$$

$$\frac{W}{P} = \frac{F}{P} - 1 \tag{3.4}$$

The two equations from above are required to calculate the number of SWUs required for a particular enrichment. This number is often referred to as the SWU factor and is denoted as S. However, one more quantity is necessary and is referred to as the separation potential, $V(x_i)$. The equation for separation potential is shown below [17].

$$V(x_i) = (2 * x_i - 1) * \ln\left(\frac{x_i}{1 - x_i}\right) \tag{3.5}$$

By appropriately applying the previously explained quantities, the SWU factor can be calculated by using the following equation.

$$S = \frac{SWU}{P * T} = V(x_p) + \frac{W}{P} * V(x_w) - \frac{F}{P} * V(x_f) \tag{3.6}$$

The SWU factor provides the number of SWUs required per kgU (of enriched product) for a particular enrichment. In order to calculate the actual price of enrichment per kgU, the price

per SWU must be multiplied by the SWU factor. Additionally, the price of uranium and price of conversion must be included. The correct formula is shown below where the terms $l_c$ and $l_f$ represent losses associated with conversion and fabrication, respectively. As a simplification losses were assumed to be zero for this model [17].

$$PE = \left[\frac{PU}{(1-l_c)(1-l_f)} + \frac{PC}{(1-l_f)}\right] * \frac{F}{P} + \frac{PS}{(1-l_f)} * S \quad (3.7)$$

The final step for determining the total cost of fuel per kgU, involves including the cost of fabrication. The equation following shows the final required step for determining the total cost [17].

$$FF = PE + PF \quad (3.8)$$

Regrettably, the exact fabrication cost is currently unknown and very uncertain, so several different costs were assumed to cover a range of possibilities. The costs were \$1,300/kgU, \$4,000/kgU, and \$24,000/kgU representing a low, base, and high cost [18]. Table 3.7 provides values for the total cost of fuel for each different fabrication cost as well as enrichments of 5%, 10%, 15%, and 19.75%.

Table 3.7: Total cost of fuel production per kgU

| | | Fuel Fabrication Cost | | |
|---|---|---|---|---|
| Uranium Enrichment | | **$1,300/kgU** | **$4,000/kgU** | **$24,000/kgU** |
| | **5.00%** | $3,374.27 | $6,074.27 | $26,074.27 |
| | **10.00%** | $5,847.78 | $8,547.78 | $28,547.78 |
| | **15.00%** | $8,360.33 | $11,060.33 | $31,060.33 |
| | **19.75%** | $10,764.10 | $13,464.10 | $33,464.10 |

In order to provide some perspective on the costs associated with the different fabrication costs, the fuel cost for an entire core was calculated by finding the correct mass of fuel and multiplying by the corresponding total fuel cost. Table 3.8, Table 3.9, and Table 3.10 show these costs in the order of low, base, and high fabrication costs.

Table 3.8: Whole core fuel cost assuming low fabrication cost

| Packing Factor \ Uranium Enrichment | 5.00% | 10.00% | 15.00% | 19.75% |
|---|---|---|---|---|
| **10%** | $46,512,687.21 | $80,608,807.21 | $115,243,206.29 | $148,378,030.71 |
| **20%** | $73,453,584.98 | $127,298,726.99 | $181,993,928.00 | $234,320,976.53 |
| **30%** | $96,489,107.26 | $167,220,436.21 | $239,068,408.20 | $307,805,559.70 |
| **40%** | $116,820,004.58 | $202,454,895.46 | $289,441,713.51 | $372,662,240.47 |
| **50%** | $135,646,291.16 | $235,081,789.26 | $336,087,086.18 | $432,719,130.25 |

Table 3.9: Whole core fuel cost assuming base fabrication cost

| Packing Factor \ Uranium Enrichment | 5.00% | 10.00% | 15.00% | 19.75% |
|---|---|---|---|---|
| **10%** | $83,730,897.53 | $117,827,017.52 | $152,461,416.60 | $185,596,241.02 |
| **20%** | $132,229,182.32 | $186,074,324.32 | $240,769,525.33 | $293,096,573.87 |
| **30%** | $173,697,114.42 | $244,428,443.37 | $316,276,415.36 | $385,013,566.86 |
| **40%** | $210,296,252.89 | $295,931,143.78 | $382,917,961.83 | $466,138,488.79 |
| **50%** | $244,186,831.30 | $343,622,329.40 | $444,627,626.32 | $541,259,670.39 |

Table 3.10: Whole core fuel cost assuming high fabrication cost

| Packing Factor \ Uranium Enrichment | 5.00% | 10.00% | 15.00% | 19.75% |
|---|---|---|---|---|
| **10%** | $359,421,344.31 | $393,517,464.30 | $428,151,863.39 | $461,286,687.80 |
| **20%** | $567,603,977.38 | $621,449,119.39 | $676,144,320.40 | $728,471,368.93 |
| **30%** | $745,608,278.57 | $816,339,607.52 | $888,187,579.52 | $956,924,731.01 |
| **40%** | $902,712,907.07 | $988,347,797.96 | $1,075,334,616.01 | $1,158,555,142.97 |
| **50%** | $1,048,190,832.32 | $1,147,626,330.42 | $1,248,631,627.34 | $1,345,263,671.41 |

The next step in the process of developing the fuel cycle cost model, involved calculating the cycle length and discharge burnup for a multiple number of batches. The linear reactivity model (LRM) was used to calculate these different quantities. Although, the LRM has been shown to work well when applied to light water reactors, it has previously been discovered that it doesn't perform as well with LSCRs. Instead a non-linear reactivity can be used to better represent the true behavior. However, the LRM was chosen for this particular study in order to

simplify the model. The equations below are used to calculate the discharge burnup and cycle length for a multiple number of batches. The terms $BU_N$ and $T_N$ correspond to discharge burnup and cycle length for N number of batches [17].

$$BU_N = \frac{2*N}{N+1} BU_1 \tag{3.9}$$

$$T_N = \frac{2}{N+1} T_1 \tag{3.10}$$

The costs associated with the reactor can now be calculated in terms of $/MWh$_e$. These units allow an easy comparison between different configurations. The process involves including the costs related to the fuel in addition to the cost relating to outages. The cost relating to outages was considered by using a fixed cost to apply at each refueling. Since an exact outage cost has yet to be determined for the LSCR, two different outage costs of $20 and $50 million were chosen.

In order to find $/MWh$_e$ related to the fuel, it involves dividing the total cost of fuel by the discharge burnup and performing the necessary conversions to reach the correct units. The efficiency of the reactor must also be taken into consideration. An electric conversion efficiency of 45% was used because it is one of the design goals of the ORNL reactor design. The efficiency must be applied to the power produced, so the previously found quantity should be divided by efficiency. The equation below shows the described steps.

$$Fuel\ Cost\ \left(\frac{\$}{MWh_e}\right) = \frac{(Total\ Cost\ of\ Fuel)}{(BU)*(Efficiency)} \tag{3.11}$$

The $/MWh$_e$ for the outage costs is found by dividing the cost of the outage by the total power produced over the course of the cycle length. The electric conversion efficiency must once again be applied to the power to convert to electrical power. The following equation shows the described process.

$$Outage\ Cost\ \left(\frac{\$}{MWh_e}\right) = \frac{(Outage\ Cost)}{(Power)*(Cycle\ Length)*(Efficiency)} \qquad (3.12)$$

The fuel cost and outage cost can be added together to find the cumulative cost in terms of $/MWh$_e$. These steps were completed for each packing factor, uranium enrichment, fuel cost, outage cost, and batch number. The resulting data completes the fuel cycle cost model and can be used to compare different options in order to determine the most economical configurations.

## 3.3. Primary Effects Analyzed

A variety of different parametric/sensitivity studies were performed using the KENOVI and TRITON modules in SCALE. Since the KENOVI module alone is unable to perform burnup calculations, all the studies using this specific module were based on the BOC (beginning of cycle) properties for a LSCR reactor. The TRITON module was used to explore how the system changes over time by applying depletion calculations.

The first step required finding an appropriate simplified model by determining what assumptions could be applied to the model without severely altering the results. This process has already been described and can be seen in the previous section. Related to this subject, a series of different tests were performed to analyze run time versus desired accuracy.

The primary parameters taken into consideration for this study include the packing factor of TRISO particles, the uranium fuel enrichment, and the Lithium-7 enrichment of the coolant. Additionally, a simple fuel cost model was developed and applied to the results to provide a rough estimate on the different costs associated with different types of fuel loadings.

### 3.3.1. Packing Factor and Fuel Enrichment

The primary properties of the fuel include the enrichment of uranium, the amount of fuel, and the amount of available moderator. The amount of fuel and the amount of moderator are directly related with one another because by increasing the amount of one, a decrease in the amount of the other is required. However, this only holds true if the dimensions of the fuel are constrained, which is the case in the particular studies performed.

The amount of fuel in the plate has many effects on the system. These include but are not limited to the $k_{eff}$, achievable burnup, and length of fuel cycle. Since the LSCR is graphite

moderated, the amount of graphite available for the moderation of neutrons largely affects the properties of the system. By varying the amount of fuel in the plates by adjusting the packing factor of TRISO particles in the fuel array, the relationship between fuel and moderator can be observed and any limitations can be discovered.

The packing factor for this situation is defined as a local measurement that represents the volume of a TRISO particle relative to the graphite matrix material which surrounds it. In order to adjust the packing factor, the process involves adjusting the amount of matrix material around a particle which corresponds to altering the pitch.

The packing factor strongly influences moderation in the LSCR because it is graphite moderated system, so a decrease in packing factor leads to a proportional increase in the amount of moderating material available. However, a decrease in packing factor also reduces the total amount of fuel in the assembly. In order to compensate for this decrease in fuel, the fuel enrichment can be varied so that the most optimal design is achieved.

The fuel enrichment is varied by adjusting the amount of U-235 found in the fuel. A study of the effects of fuel enrichment was performed by incrementally adjusting the fuel enrichment between 5 w% and 19.75 w%.

### 3.3.2. Fuel Cycle Cost Model

A simplified fuel cost model was developed as a method to compare the results obtained by varying packing factor and uranium enrichment. The fuel cycle cost model uses the spot prices available from UxC for May 27$^{th}$. In order to keep the cost model simplified, certain assumptions were made. First, the time value of money was neglected. Additionally, while the cost of outages was considered, the costs related to the outage duration were ignored.

### 3.3.3. Lithium Enrichment

The natural isotopic concentrations for lithium are 7.5% Li-6 and 92.5% Li-7. The lithium used in the FLiBe coolant of the LSCR is enriched because of the properties associated with Li-6. A main issue is related to the large absorption cross section inherent to Li-6. The high cross section reduces the neutrons available for fission and greatly affects the system $k_{eff}$. The absorption cross sections for both Li-6 and Li-7 can be seen below in **Error! Reference source not found.**. For the majority of neutron energies, the cross section of Li-6 is about 4 or 5 orders of magnitude larger than Li-7. Based on this information, it is expected that the concentration of Li-6 will significantly affect the neutronics of the system.

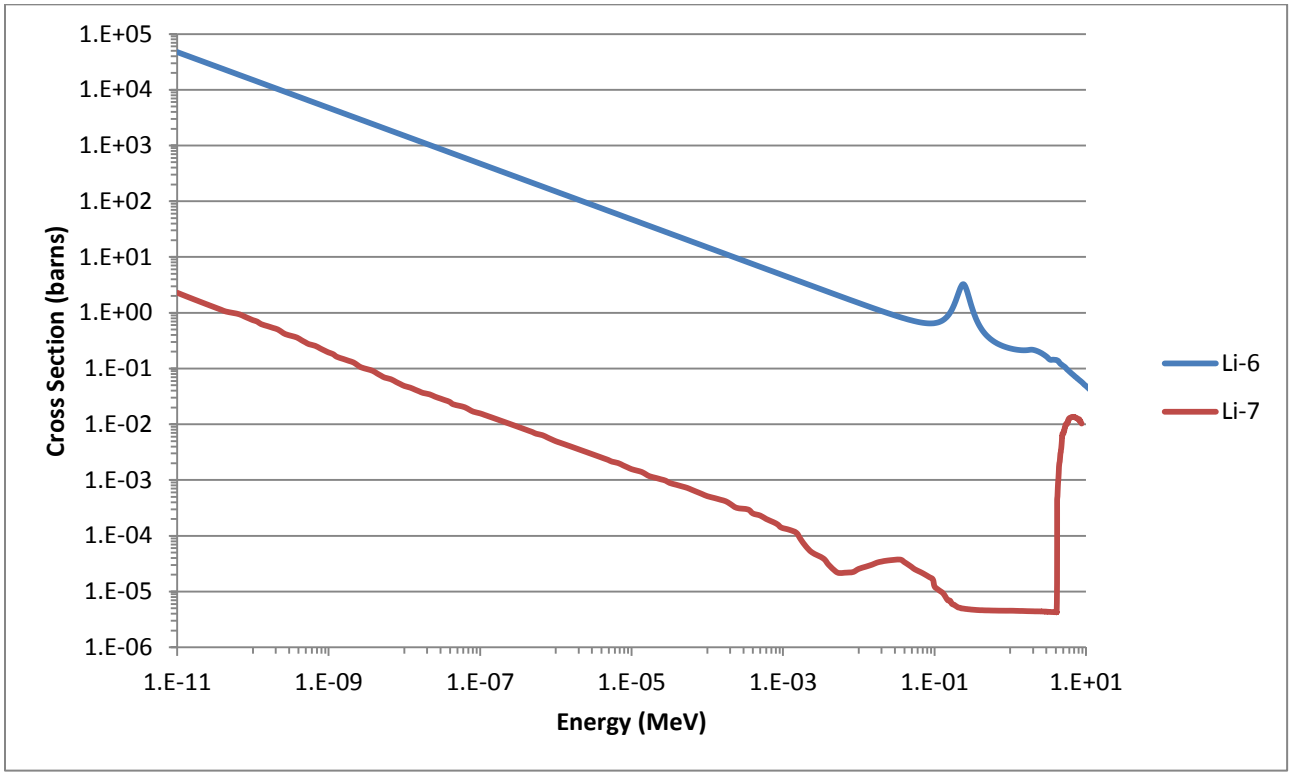


Figure 3-10: Total Absorption Cross Section for Lithium Isotopes

Furthermore, the neutron activation of Li-6 yields tritium which is an undesirable material to be produced within the reactor coolant due to its radioactivity and ability to easily

permeate through materials. The reaction is capable of occurring at all neutron energies, making it an even more difficult problem to handle. Tritium can also be produced through neutron interactions with Li-7 as well, but the neutrons must have high energy which isn't as large of a concern in a thermal reactor. The following equations show the two possible reactions.

$$^{6}_{3}Li + n \rightarrow ^{4}_{2}He + ^{3}_{1}T \quad (3.13)$$

$$^{7}_{3}Li + n \rightarrow ^{4}_{2}He + ^{3}_{1}T + n \quad (3.14)$$

For the study performed, the Li-7 enrichment was varied to include an enrichment of 99.995% which is specified by ORNL, several lower enrichments, and a higher enrichment [10]. The main focus was to understand the practical limitations associated with the Li-7 enrichment and whether it can be used for beneficial purposes. The main idea was to determine whether a lower enrichment can be used at reactor start up so that the Li-6 isotopes act as a burnable absorber. In order for this to work, Li-6 must be depleted sufficiently fast so that Li-7 enrichment would converge to a higher enrichment than what was initially used to start the reactor and the time frame for convergence must be similar to the cycle length. Based on this, the main effort was focused on finding the value that the enrichment converges to and the time frame required for convergence.

# CHAPTER 4: RESULTS AND DISCUSSION

This Chapter presents the results obtained in several studies performed to examine main aspects of LSCR core physics:

- Impact of the finite core geometry and graphite reflector for various core configurations (enrichment and packing fraction) in Sect. 4.1.
- Impact of enrichment and packing fraction on the achievable cycle length and discharge burnup (Sect. 4.2).
- Fuel cycle cost for various combinations of enrichment, packing fraction, and multibatch strategy (Sect. 4.3).
- Impact of lithium enrichment on reactivity and cycle length.

A large amount of data was produced and not all is provided within the text but additional data are is available in the appendices. A sample input code can also be found in the appendices.

Additionally, all of the data contains a certain degree of uncertainty inherent to the Monte Carlo calculations that were performed. In most cases this uncertainty is on the order of a percent or fraction of a percent. However, another source of error can be attributed to not using Dancoff factors to better handle the lumped fuel elements produced by TRISO particles. This error would need to be accounted for and prevented if looking at a design more intensively, but for the type of scoping studies that were performed it should have very little effect on the results.

## 4.1. Full Core Reflector Effects

The most recent LSCR design from ORNL introduces the plate fuel element in order to reach an adequate heavy metal loading and reduce the maximum temperature of the fuel. The modeling of these new fuel elements has proven complex and computationally demanding; so for scoping design and fuel cycle cost studies it is desirable to use a single fuel assembly with reflected boundaries. The use of a single assembly may introduce biases with respect to a full core model which provides the most realistic results. The goal of this particular study was to determine the equivalent $k_{inf}$ values that represent a $k_{eff}$ of one for the corresponding full core models. The term equivalent $k_{inf}$ can be defined as the adjusted multiplication of an infinite assembly model that represents a full core model.

By determining an equivalent $k_{inf}$ for the assembly model that corresponds to a $k_{eff}$ equal to one for a full core model a certain degree of accuracy can be recovered. When making such an adjustment to $k_{inf}$, the physical aspects related to a finite core and the reflectors are taken into account by compensating for leakage. The necessary adjustments to the $k_{inf}$ values of an assembly were found by comparing simulations from multiple full core models and corresponding assembly models. In each case, the results of the full core model were used to calculate the cycle length corresponding to a $k_{eff}$ of one. The equivalent $k_{inf}$ value of the assembly model was then determined corresponding to this cycle length.

The method outlined above was applied to the parametric study varying packing factor and uranium enrichment for the LSCR. Full core models for packing factors of 20%, 30%, and 40%; and uranium enrichments of 5%, 10%, 15%, and 19.75% were simulated and then used to determine the various cycle lengths (assuming specific power of 103.31 W/gU). The core models employed depleted the fuel as a single region to remain consistent with the assembly model as

well as act as a simplification. The cycle lengths were calculated by performing a linear interpolation between the two depletion points containing $k_{eff}$ of above and below one. The cycle lengths were calculated for each of the different scenarios and are shown below in Table 4.1. The table shows that cycle length is much more sensitive to the enrichment than the packing factor. The reason for this is that an increase in enrichment provides proportionally more fissile material while maintaining the amount of moderator, while the increased packing factor provides more fissile material at the expense of moderator. Moreover, due to the geometrical limitations (constant plate width and height), doubling the packing fraction increases the heavy metal materials by a factor of only about 1.60.

Table 4.1: Cycle lengths (days) for full core model

| | | Uranium Enrichment | | | |
|---|---|---|---|---|---|
| | | **5.00%** | **10.00%** | **15.00%** | **19.75%** |
| **Packing Factor** | **20%** | 139.0 | 380.3 | 599.7 | 793.4 |
| | **30%** | 152.2 | 412.8 | 658.6 | 883.6 |
| | **40%** | 153.6 | 423.3 | 693.4 | 949.4 |

The next step involved using the cycle lengths to calculate the equivalent $k_{inf}$ for each of the corresponding assembly models. However, in order to make sure that the results obtained were reasonable, the $\Delta k$ ($k_{eff}$-$k_{inf}$) was found and examined at each depletion step. The importance of looking at the values for $\Delta k$ is to make sure that at no point is there an excessive degree of variance between the two models. Figure 4-1, Figure 4-2, and Figure 4-3 show the values for $\Delta k$ versus time. The primary interval of interest ranges from the beginning of cycle until the point where the k reaches one, so all points with a k approximately less than 0.80 have been omitted from the figures.

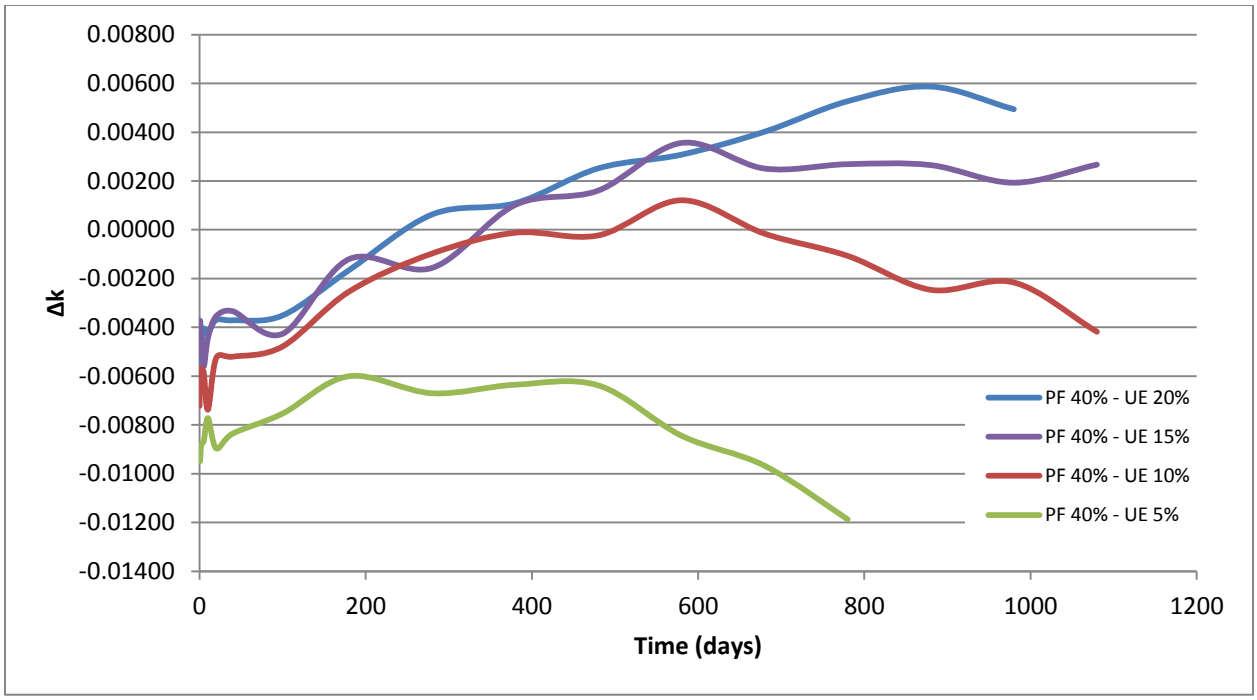


Figure 4-1: Values of Δk for packing factor of 40%

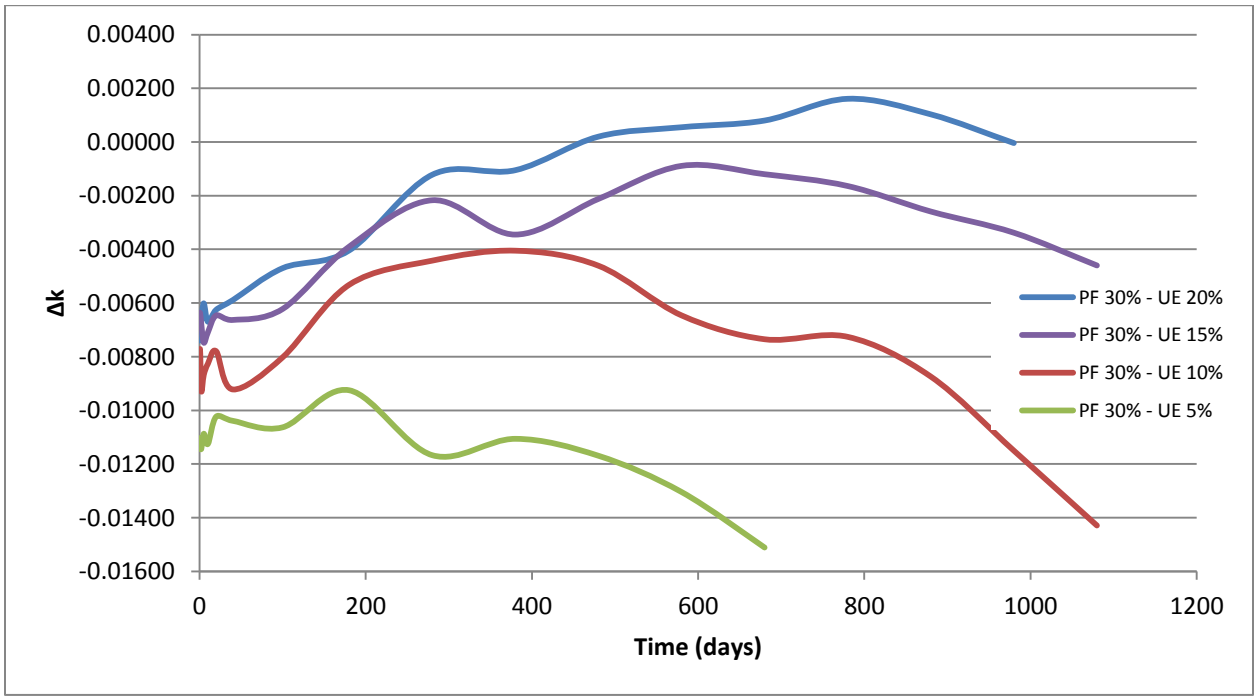


Figure 4-2: Values of Δk for packing factor of 30%

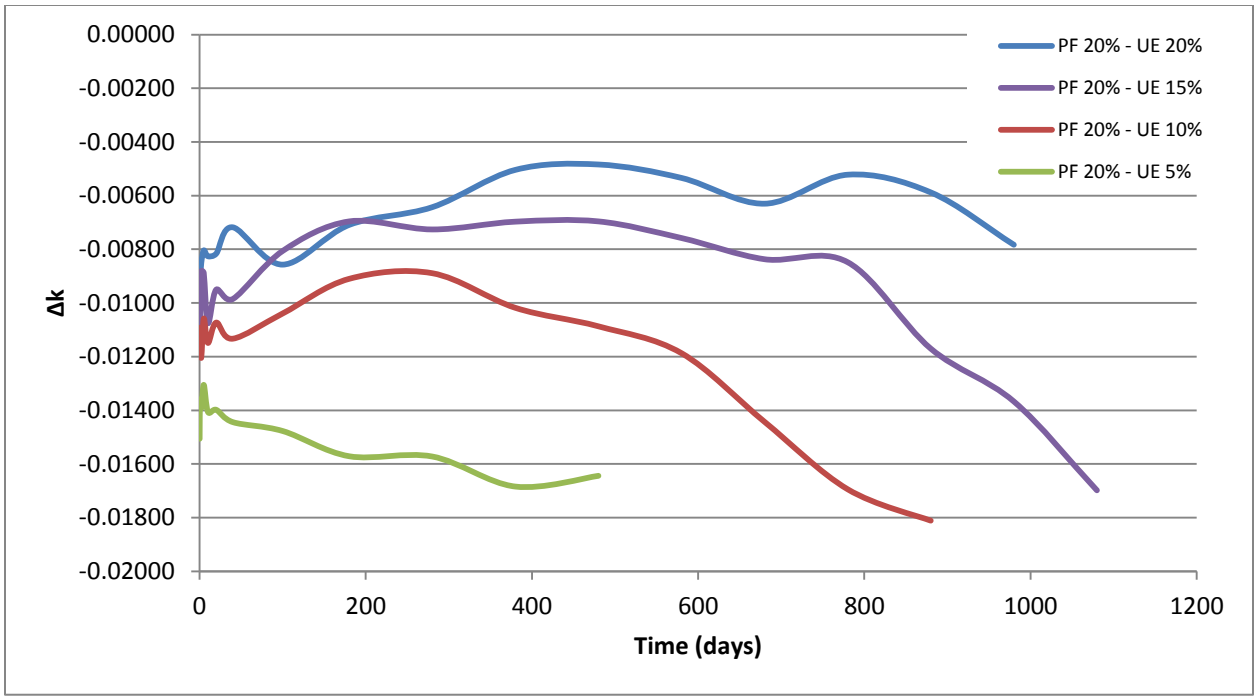


Figure 4-3: Values of Δk for packing factor of 20%

The above figures show that the Δk for the full core and assembly models has a maximum at around 1800 PCM. Additionally, the Δk tends to be mostly negative, which means that in most cases the multiplication of the assembly is larger than the multiplication of the full core. The leakage from a finite core results in a reduction of multiplication so this is consistent with what is expected. Since the values of Δk are not extreme, it is safe to move on and find the equivalent $k_{inf}$ values for each assembly.

Similarly to the cycle length, the equivalent $k_{inf}$ values were calculated using a linear interpolation. The two points used were the depletion points bounding the cycle length found for the full core model. The different equivalent $k_{inf}$ values can be seen in the following table. However, there is a certain level of uncertainty associated with each number which can be attributed to the uncertainty of the SCALE simulations and the linear interpolation which was performed. The different SCALE simulations each resulted in a one-sigma uncertainty of about

45 PCM, thus the combined uncertainty is of the order of 60 PCM, small compared to the [-1000, +500 PCM] Δk range.

Table 4.2: Equivalent $k_{inf}$ values for assembly models

| | | Uranium Enrichment | | | |
|---|---|---|---|---|---|
| | | **5.00%** | **10.00%** | **15.00%** | **19.75%** |
| **Packing Factor** | **20%** | 1.01523 | 1.01018 | 1.00774 | 1.00531 |
| | **30%** | 1.00973 | 1.00423 | 1.00113 | 0.99901 |
| | **40%** | 1.00651 | 1.00017 | 0.99747 | 0.99478 |

Although these values are insightful in regards to the cases that were simulated, there is no information for alternate scenarios. However, the cases that were not included can be estimated by finding an appropriate fit for the known data and then interpolating and (cautiously) extrapolating. Multiple different types of fits were tested to find the one that best represented the data. The first method involved inputting the data into Mathematica and performing a multi-variable linear fit. The following equation was determined by using this method, where uranium enrichment and packing factor are UE and PF, respectively.

$$k_{inf} = 1.028 - 0.0494254 * PF - 0.0714376 * UE \quad (4.1)$$

From this equation, a second table containing the calculated equivalent $k_{inf}$ values was created and can be seen below in Table 4.3. These new values were compared to the originally calculated values to find an average difference of 82 PCM.

Table 4.3: Mathematica linear fit equivalent $k_{inf}$ values

| | | Uranium Enrichment | | | |
|---|---|---|---|---|---|
| | | **5.00%** | **10.00%** | **15.00%** | **19.75%** |
| **Packing Factor** | **20%** | 1.01454 | 1.01097 | 1.00740 | 1.00401 |
| | **30%** | 1.00960 | 1.00603 | 1.00246 | 0.99906 |
| | **40%** | 1.00466 | 1.00109 | 0.99751 | 0.99412 |

The second fitting method also used Mathematica. However, instead a multi-variable second degree polynomial fit was performed. The resulting equation can be seen below.

$$k_{inf} = 1.0414 - 0.11809 * PF + 0.11445 * PF^2 - 0.149901 * UE + 0.3173 * UE^2 \qquad (4.2)$$

After calculating the equivalent $k_{inf}$ values and comparing to the original values an average difference of 36 PCM was found. Although this is quite better than the previous linear fit, it was determined that the fit diverges to quickly once outside the already known data set. As a result, the fit would not work well for extrapolating smaller or larger packing factors.

Another fitting method involved using the linear fit available in Microsoft Excel. Since Excel is unable to fit multiple variables, the different uranium enrichments were fitted individually resulting in a total of four different equations and effectively a piecewise linear fit. After using this method to calculate new equivalent $k_{inf}$ values and compare to the original values, an average difference of 51 PCM was found. While this method shows greater congruence than the multi-variable linear fit, it is limiting in the sense that interpolation between different uranium enrichments is not possible. A table showing the values for this fitting method can be seen below.

Table 4.4: Microsoft Excel piecewise linear fit equivalent $k_{inf}$ values

| | | Uranium Enrichment | | | |
|---|---|---|---|---|---|
| | | **5.00%** | **10.00%** | **15.00%** | **19.75%** |
| **Packing Factor** | **20%** | 1.01485 | 1.00987 | 1.00725 | 1.00497 |
| | **30%** | 1.01049 | 1.00486 | 1.00212 | 0.99970 |
| | **40%** | 1.00613 | 0.99985 | 0.99698 | 0.99443 |

Although fitting the data with one or several equations is common for determining appropriate trends, another option involves finding patterns in the data and determining the trends based on these patterns. By observing the original equivalent $k_{inf}$ values shown in Table

4.2, the beginning of some rough patterns can be seen between different packing factors and enrichments. These patterns show that there is a trend in which the $k_{inf}$ increases by approximately 500 PCM with every 10% increase in packing factor. Additionally, for each doubling of uranium enrichment the $k_{inf}$ increases by approximately 500 PCM as well. The fitting methods already mentioned show additional support to these trends. After determining the different equivalent $k_{inf}$ values based on these trends, the average difference compared to the original data was only 52 PCM. A table showing the values for equivalent $k_{inf}$ based on this method is shown below.

Table 4.5: Visual trends equivlanet $k_{inf}$ values

| | | Uranium Enrichment | | | |
|---|---|---|---|---|---|
| | | **5.00%** | **10.00%** | **15.00%** | **19.75%** |
| **Packing Factor** | **20%** | 1.0150 | 1.0100 | 1.0075 | 1.0050 |
| | **30%** | 1.0100 | 1.0050 | 1.0025 | 1.0000 |
| | **40%** | 1.0050 | 1.0000 | 0.9975 | 0.9950 |

In order to better compare the three different methods used, a set of figures has been created to compare each one to the original set of equivalent $k_{inf}$ values.

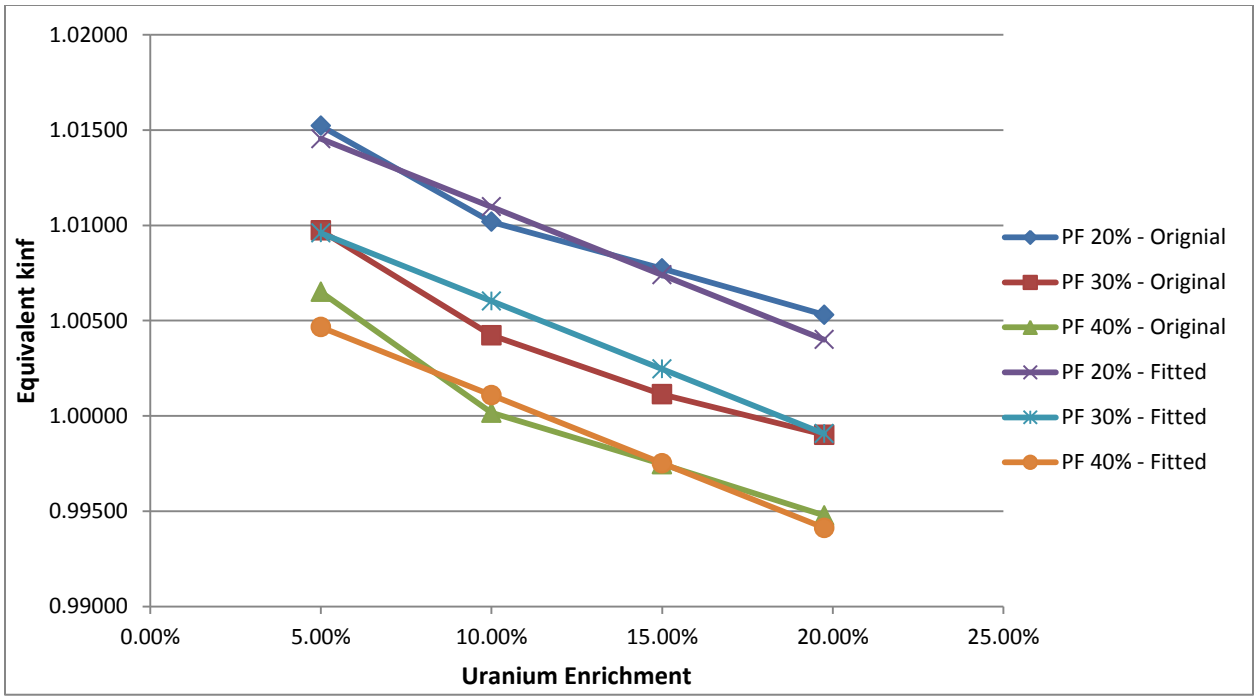


Figure 4-4: Mathematica linear fit equivalent $k_{inf}$ values

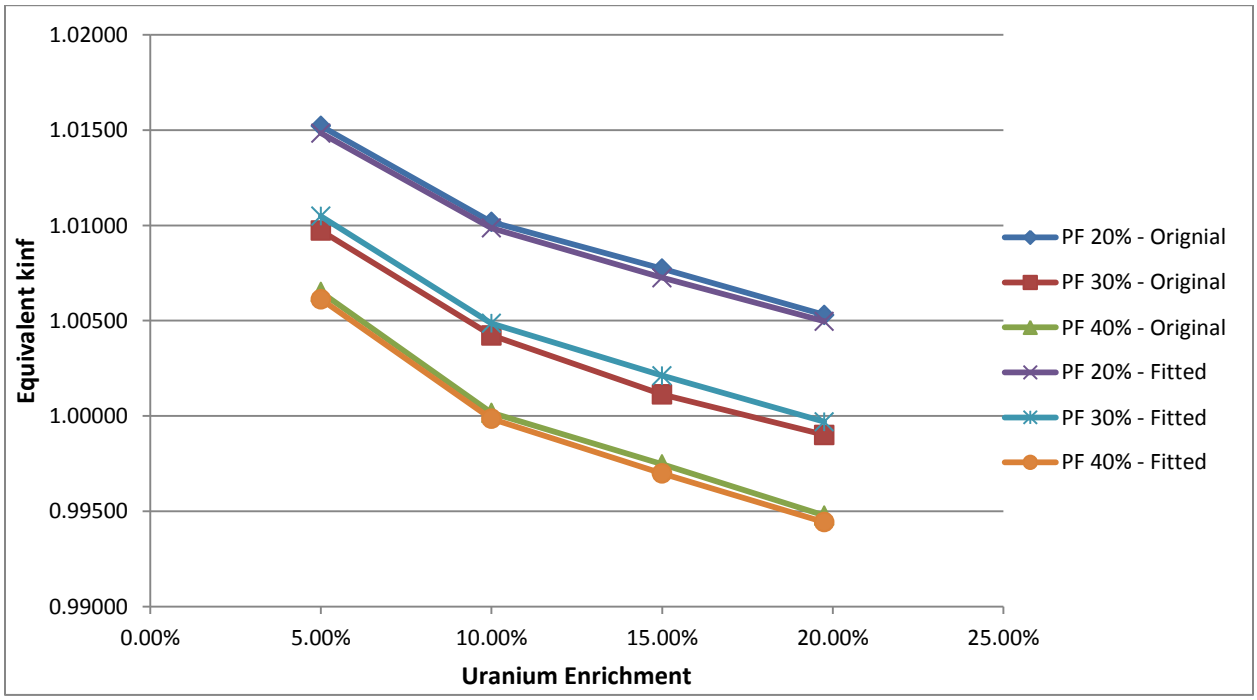


Figure 4-5: Microsoft Excel piecewise linear fit equivalent $k_{inf}$ values

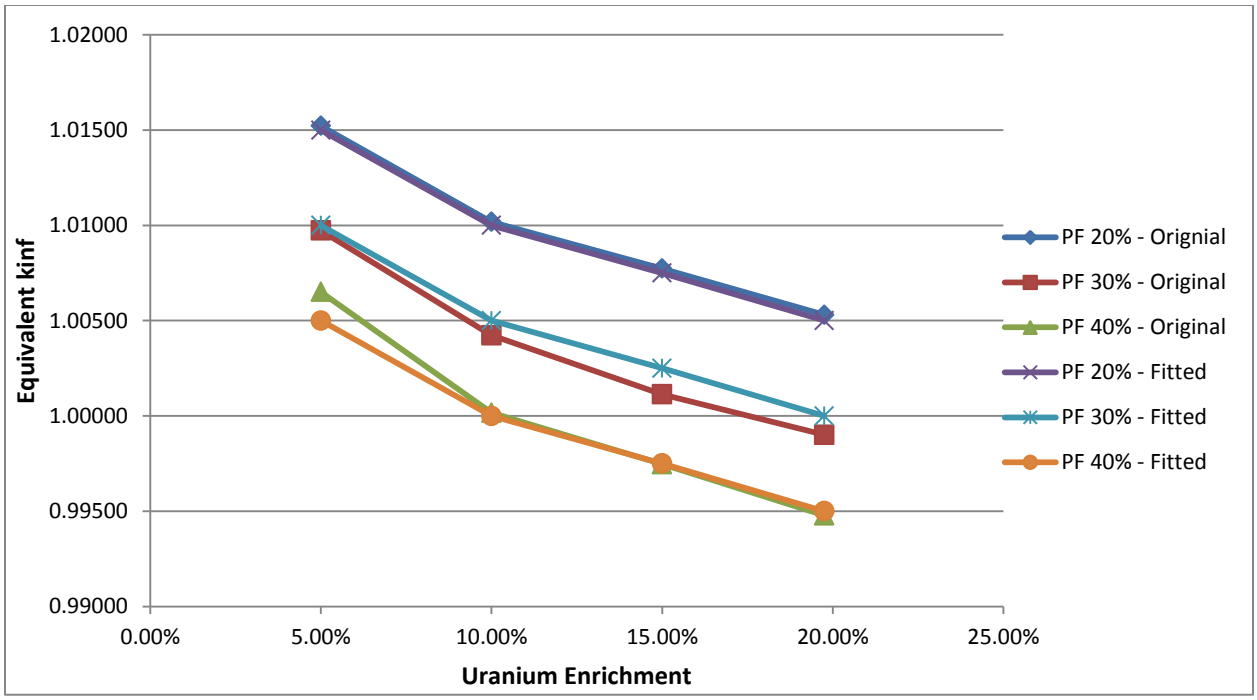


Figure 4-6: Visual trends equivalent $k_{inf}$ values

The previous figures help provide further insight into what method most closely follows the data. It is clear that the multi-variable linear fit found using Mathematica follows the actual data least accurately. The choice between the final two options was based on simplicity. The fit developed based on visual trends is a much simpler model to apply and has a well-defined regularity. It may be possible to determine a more accurate fit but this would require a larger number of simulations in addition to results with lower uncertainties.

From the chosen fitting method, different points outside the range of known data can be extrapolated by following the same trend. Table 4.6 contains the fitted data in addition to extrapolations for packing factors of 10% and 50%. Additionally, a surface plot showing the different values graphically can be seen following the table in Figure 4-7. These values for the equivalent $k_{inf}$ can now be applied to different assembly models to more accurately determine the cycle length of a full core.

Table 4.6: Extrapolated equivalent $k_{inf}$ values based on visual trends

| Packing Factor \ Uranium Enrichment | 5.00% | 10.00% | 15.00% | 19.75% |
|---|---|---|---|---|
| **10%** | 1.0200 | 1.0150 | 1.0125 | 1.0100 |
| **20%** | 1.0150 | 1.0100 | 1.0075 | 1.0050 |
| **30%** | 1.0100 | 1.0050 | 1.0025 | 1.0000 |
| **40%** | 1.0050 | 1.0000 | 0.9975 | 0.9950 |
| **50%** | 1.0000 | 0.9950 | 0.9925 | 0.9900 |

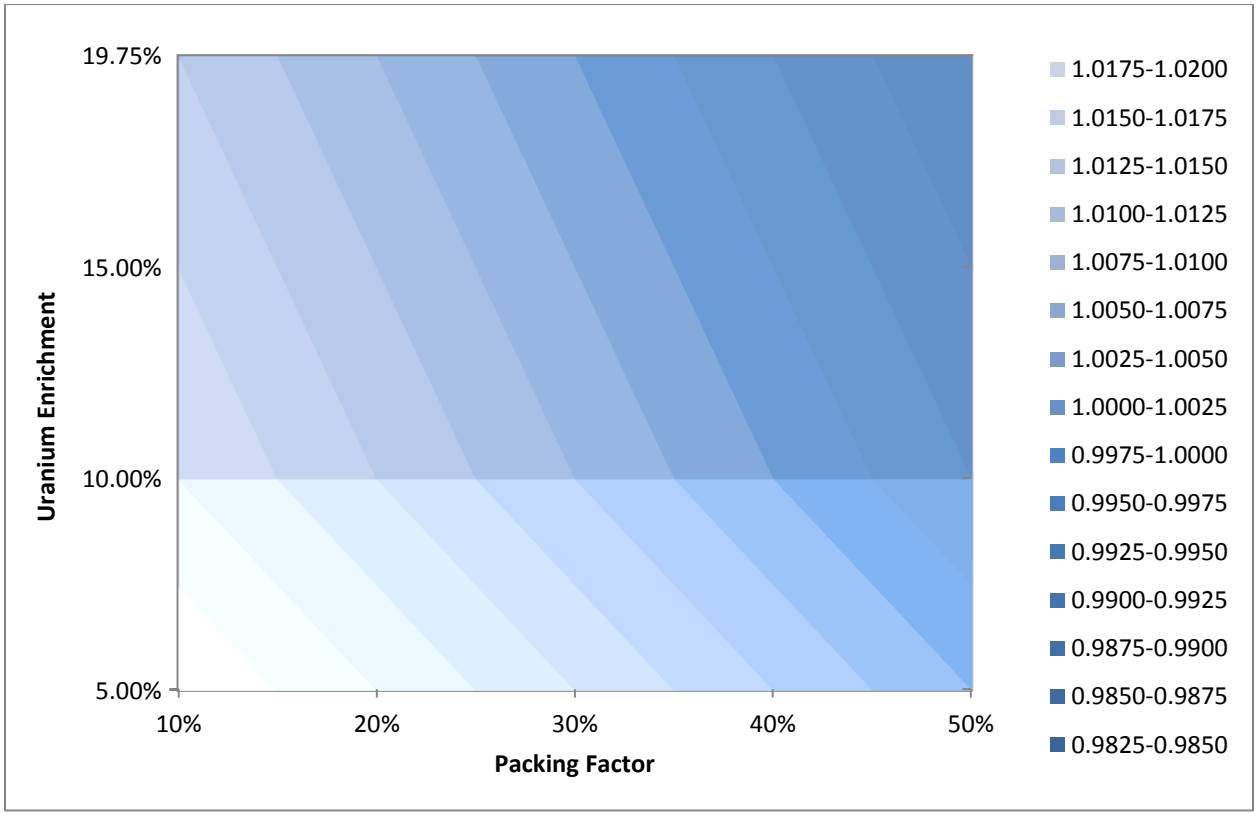


Figure 4-7: Contour plot of fitted equivalent $k_{inf}$ values

From Table 4.6, we should eliminate from considerations at least the two highlighted extreme cases that are not practical: (i) 5% enrichment with 10% packing factor, due to very low heavy metal loading, and (ii) 19.75% enrichment with 50% packing factor, due to severe under-moderation and poor fuel utilization. All the remaining cases fall within the equivalent $k_{inf}$ range of [0.990, 1.015]. That means that the required correction is fairly limited, and even the current

approximate correction which will correct for the main portion of 2D-3D discrepancy (with perhaps up to ~100 PCM residual effect unaccounted for) is fully adequate for the scoping of fuel cycle cost evaluations. This allows effective use of a single-assembly 2D fuel depletion model as a representative of the 3D full core depletion simulation.

The range for equivalent $k_{inf}$ is considerably different for the LSCR compared to the LWR and reveals interesting reactor physics. Due to under-moderation, the reflector is not only reflecting back some of the neutrons, but also thermalizing them and thus improving their thermal utilization, and the overall effect may even be positive, as indicated by the equivalent value being less than unity in some cases. Specifically, the highest value reaches 1.02 (or 1.015 after removing the upper left case) and the lowest value corresponding to a 50% packing factor and 19.75% uranium enrichment is 0.990, indicating that the reflector blocks surrounding the core significantly affect the moderation of the system to the degree that they partly or fully compensate for the leakage.

## 4.2. Packing Factor vs. Uranium Enrichment

Packing factor and uranium fuel enrichment are both important parameters that strongly affect the characteristics of a LSCR, especially the cycle length and discharge burnup. Furthermore, they largely impact the cost related to the production of fuel. The packing factor strongly influences moderation in the LSCR because it is a graphite moderated system, so a decrease in packing factor leads to a proportional increase in the amount of moderating material available. Conversely, a decrease in packing factor also reduces the total amount of fuel in the assembly. The reduction in the amount of fuel has the potential to reduce costs; however, in order to compensate for this decrease in fuel, the fuel enrichment must be varied accordingly. There are larger costs associated with higher enriched uranium, so it is important to find the packing factor and uranium enrichment that proves most economical by applying an appropriate fuel cycle cost model.

When considering the packing factor, it can be described as a local measurement that represents the volume of a TRISO particle relative to the graphite matrix material which surrounds it. In order to adjust the packing factor, the process involves adjusting the amount of matrix material around a particle which corresponds to altering the pitch. The uranium fuel enrichment is the weight percent of U-235, which is the mass of U-235 relative to the cumulative mass of all the uranium isotopes in a particular sample.

A matrix study was performed by varying the fuel enrichment for five different packing factors ranging from 10% to 50%. Four different fuel enrichments were used starting at 5% and ending at 19.75%, resulting in a total of twenty different possible combinations. For each of the different scenarios, a TRITON input code was used to perform a depletion calculation. From the

depletion results, the beginning of cycle (BOC) $k_{inf}$, the cycle length, and the discharge burnup were determined.

The discharge burnup and cycle length were calculated by linear interpolating between two depletion points. An assembly model was used for each of the various simulations; but in order to improve the accuracy of the results, an equivalent $k_{inf}$ was used to correspond to a $k_{eff}$ of one for a full core model. These equivalent $k_{inf}$ values were determined by performing simulations with different full core models and then comparing to the corresponding assembly model. After determining the equivalent $k_{inf}$ for the different scenarios that were tested, a fit was determined so that the correction could easily be applied to alternate cases. The process for calculating the equivalent $k_{inf}$ values is explained in detail in the previous section. Table 4.7 shows the equivalent $k_{inf}$ values used for the different simulations that were performed.

Table 4.7: Equivalent $k_{inf}$ values applied to results

| Packing Factor \ Uranium Enrichment | 5.00% | 10.00% | 15.00% | 19.75% |
|---|---|---|---|---|
| **10%** | 1.0200 | 1.0150 | 1.0125 | 1.0100 |
| **20%** | 1.0150 | 1.0100 | 1.0075 | 1.0050 |
| **30%** | 1.0100 | 1.0050 | 1.0025 | 1.0000 |
| **40%** | 1.0050 | 1.0000 | 0.9975 | 0.9950 |
| **50%** | 1.0000 | 0.9950 | 0.9925 | 0.9900 |

Table 4.8 shows the different values of BOC $k_{inf}$ along with a one-sigma uncertainty. The three figures following the table graphically show how BOC $k_{inf}$, cycle length, and discharge burnup vary relative to both the packing factor and fuel enrichment. The uncertainties for cycle length and discharge burnup should all be within 5% and in most cases much lower.

Table 4.8: BOC $k_{inf}$ variation from packing factor and enrichment

| Packing Factor | Uranium Enrichment 5.00% | 10.00% | 15.00% | 19.75% |
|---|---|---|---|---|
| **10%** | 1.18792 ± 0.00044 | 1.37573 ± 0.00047 | 1.45389 ± 0.00042 | 1.49571 ± 0.00049 |
| **20%** | 1.20785 ± 0.00051 | 1.34907 ± 0.00045 | 1.40739 ± 0.00046 | 1.43971 ± 0.00049 |
| **30%** | 1.19769 ± 0.00052 | 1.32089 ± 0.00053 | 1.37154 ± 0.00053 | 1.40201 ± 0.00047 |
| **40%** | 1.18456 ± 0.00051 | 1.29767 ± 0.00047 | 1.34604 ± 0.00047 | 1.37608 ± 0.00046 |
| **50%** | 1.17314 ± 0.00048 | 1.27812 ± 0.00069 | 1.32499 ± 0.00046 | 1.35450 ± 0.00050 |

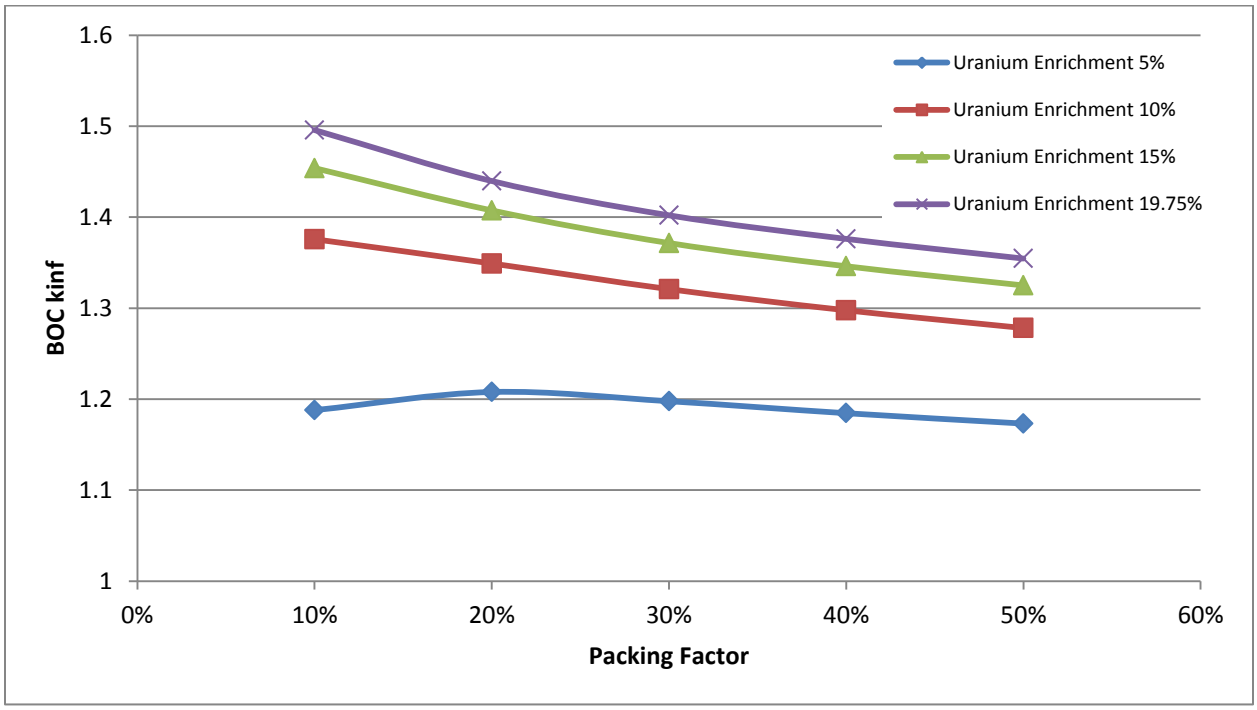


Figure 4-8: BOC $k_{inf}$ relative to packing factor and enrichment

The above plot, Figure 4-8, is helpful in identifying a practical range of fuel enrichments. Error bars have been included to show one standard deviation, however the error is small enough that the bars do not appear in the figure. The highest three enrichments all behave normally and follow a similar trend; however, the fuel enrichment at 5% varies from this trend. The variation occurs at the 10% packing factor and is noticed by the lower BOC $k_{inf}$. Rather than decreasing

from this point, the BOC $k_{inf}$ increases until a 20% packing factor is reached and then decreases from that point onward. This behavior can be attributed to over moderation of the fuel and is undesirable in terms of reactor performance. Besides reducing the $k_{inf}$ of a system, it can also pose an issue in an accident scenario that involves loss of coolant. The loss of coolant would reduce the amount of moderation and cause the system $k_{eff}$ to experience a sudden increase. However, a loss of coolant scenario is not a major concern for this type of reactor design since the FLiBe coolant does not easily boil and has the ability to self-plug leaks. In order to prevent over moderation from occurring, it is important to use either a higher packing factor or higher fuel enrichment. Based on the data, fuel enrichment above 5% would be most practical especially when considering the overall low BOC $k_{inf}$ associated with an enrichment of 5%.

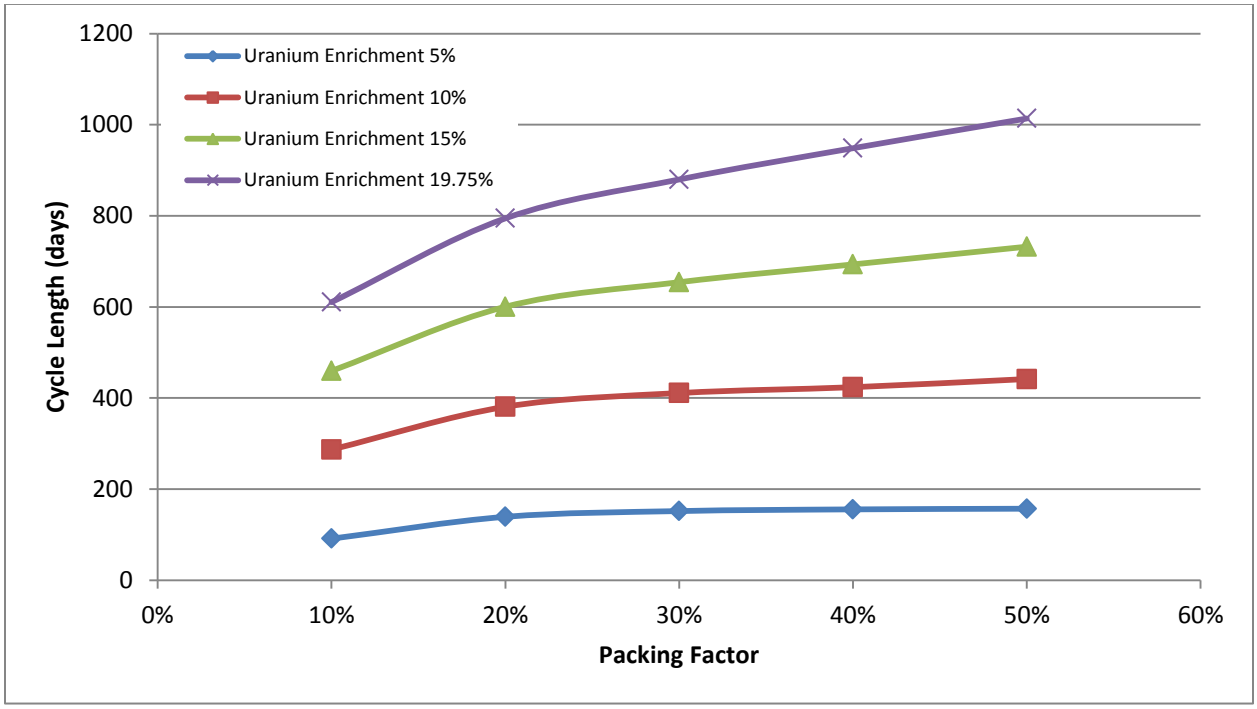


Figure 4-9: Cycle length relative to packing factor and enrichment

From Figure 4-9, the degree to which cycle length changes is strongly influenced by packing factor but only at the highest fuel enrichments. At the 5% and 10% fuel enrichments, the

cycle length remains fairly constant after reaching a 20% packing factor. As a result, there is little incentive to increase the packing factor for lower enrichments because doing so would only require more fuel. Contrary to this, the higher enrichments continue to grow in cycle length as packing factor is increased, with the biggest jump occurring between packing factors of 10% and 20%.

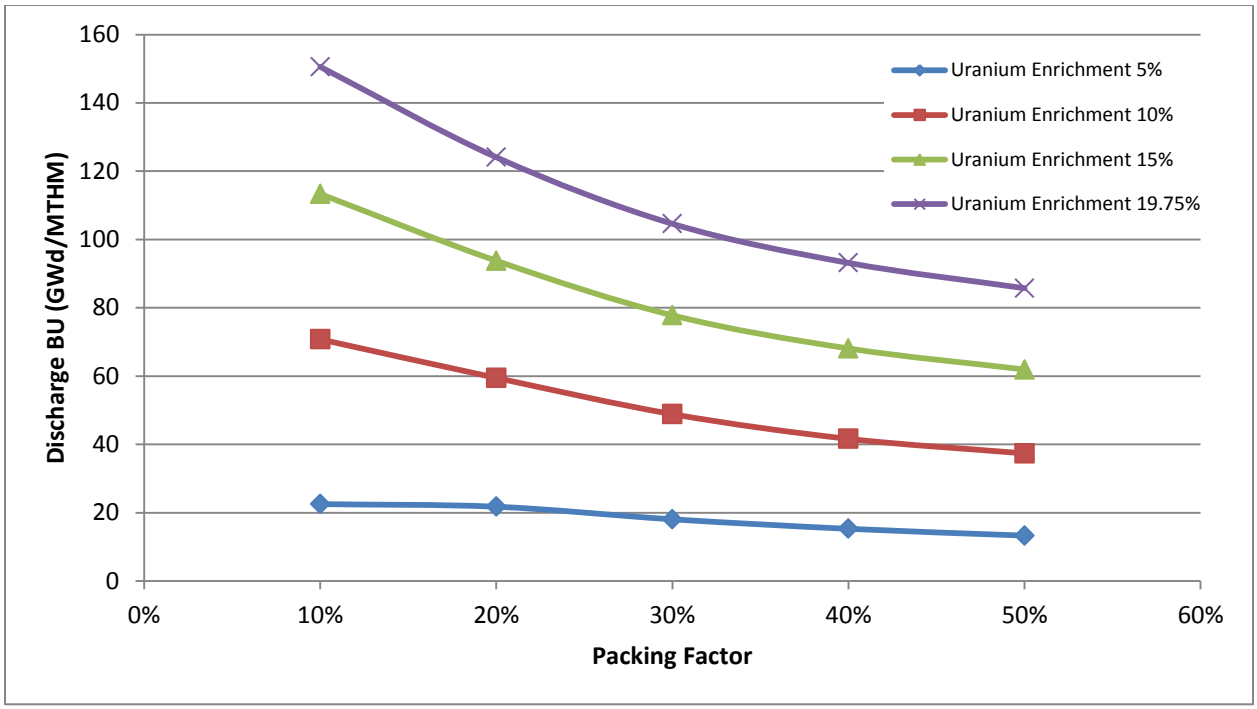


Figure 4-10: Discharge BU relative to packing factor and enrichment

The discharge burnup for each of the different packing factors and fuel enrichments show qualitatively the expected trend. However, the discharge burnup is low for the 5% enrichment, compared to what is achievable in other options, providing further evidence for the impracticality of using this or lower enrichments.

## 4.3. Simplified Fuel Cycle Cost Model

A simplified fuel cycle cost model was developed to determine the costs associated with different packing factors and uranium enrichments. The cost model was described previously in Chapter 3 and uses the spot prices available from UxC for May 27, 2013. In order to keep the cost model simplified, certain assumptions were made. The main simplifications involve ignoring the time value of money, ignoring losses, applying the linear reactivity model, and taking outages into account through the application of a fixed cost. By applying the cost model for the different cycle lengths and discharge burnups obtained from the various models, certain bounds can be developed to include the most attractive options for the fuel design.

Based on the linear reactivity model and single batch data, the cycle lengths and discharge burnups were calculated for fuel cycles ranging from 1-batch to 6-batch refueling schemes. These values can be seen in Table 4.9 and Table 4.10. The numbers shown in these tables are subject to uncertainty from modeling and inaccuracies inherent to using the linear reactivity model. However, these uncertainties should be no greater than 5% or 10% and in most cases much lower. Also due to the uncertainty of fuel fabrication and outage costs this should have little to no effect on the conclusions drawn from the results.

Table 4.9: Cycle length and discharge burnup for 1 to 3 batches

| | | 1 Batch | | 2 Batch | | 3 Batch | |
|---|---|---|---|---|---|---|---|
| **Uranium Enrichment** | **Packing Factor** | **Cycle Length (days)** | **Discharge BU (GWd/MTU)** | **Cycle Length (days)** | **Discharge BU (GWd/MTU)** | **Cycle Length (days)** | **Discharge BU (GWd/MTU)** |
| **5.00%** | **10%** | 91.3 | 22.51 | 60.8 | 30.01 | 45.6 | 33.76 |
| **5.00%** | **20%** | 139.2 | 21.74 | 92.8 | 28.99 | 69.6 | 32.62 |
| **5.00%** | **30%** | 151.8 | 18.05 | 101.2 | 24.07 | 75.9 | 27.08 |
| **5.00%** | **40%** | 155.5 | 15.28 | 103.7 | 20.37 | 77.8 | 22.91 |
| **5.00%** | **50%** | 157.0 | 13.28 | 104.7 | 17.71 | 78.5 | 19.92 |
| **10.00%** | **10%** | 286.9 | 70.77 | 191.3 | 94.36 | 143.5 | 106.15 |
| **10.00%** | **20%** | 380.7 | 59.47 | 253.8 | 79.29 | 190.4 | 89.20 |
| **10.00%** | **30%** | 410.9 | 48.85 | 273.9 | 65.14 | 205.4 | 73.28 |
| **10.00%** | **40%** | 423.8 | 41.62 | 282.5 | 55.49 | 211.9 | 62.42 |
| **10.00%** | **50%** | 441.7 | 37.36 | 294.5 | 49.81 | 220.8 | 56.03 |
| **15.00%** | **10%** | 459.5 | 113.33 | 306.3 | 151.11 | 229.7 | 170.00 |
| **15.00%** | **20%** | 600.3 | 93.77 | 400.2 | 125.02 | 300.2 | 140.65 |
| **15.00%** | **30%** | 654.3 | 77.79 | 436.2 | 103.72 | 327.1 | 116.69 |
| **15.00%** | **40%** | 693.3 | 68.09 | 462.2 | 90.78 | 346.6 | 102.13 |
| **15.00%** | **50%** | 732.2 | 61.93 | 488.2 | 82.57 | 366.1 | 92.90 |
| **19.75%** | **10%** | 610.5 | 150.57 | 407.0 | 200.76 | 305.2 | 225.86 |
| **19.75%** | **20%** | 794.4 | 124.08 | 529.6 | 165.44 | 397.2 | 186.12 |
| **19.75%** | **30%** | 879.7 | 104.60 | 586.5 | 139.47 | 439.9 | 156.90 |
| **19.75%** | **40%** | 948.4 | 93.14 | 632.3 | 124.19 | 474.2 | 139.72 |
| **19.75%** | **50%** | 1013.6 | 85.73 | 675.7 | 114.30 | 506.8 | 128.59 |

Table 4.10: Cycle length and discharge burnup for 4 to 6 batches

| | | 4 Batch | | 5 Batch | | 6 Batch | |
|---|---|---|---|---|---|---|---|
| **Uranium Enrichment** | **Packing Factor** | **Cycle Length (days)** | **Discharge BU (GWd/MTU)** | **Cycle Length (days)** | **Discharge BU (GWd/MTU)** | **Cycle Length (days)** | **Discharge BU (GWd/MTU)** |
| **5.00%** | **10%** | 36.5 | 36.01 | 30.4 | 37.51 | 26.1 | 38.58 |
| **5.00%** | **20%** | 55.7 | 34.79 | 46.4 | 36.24 | 39.8 | 37.28 |
| **5.00%** | **30%** | 60.7 | 28.89 | 50.6 | 30.09 | 43.4 | 30.95 |
| **5.00%** | **40%** | 62.2 | 24.44 | 51.8 | 25.46 | 44.4 | 26.19 |
| **5.00%** | **50%** | 62.8 | 21.25 | 52.3 | 22.14 | 44.9 | 22.77 |
| **10.00%** | **10%** | 114.8 | 113.23 | 95.6 | 117.95 | 82.0 | 121.32 |
| **10.00%** | **20%** | 152.3 | 95.15 | 126.9 | 99.11 | 108.8 | 101.94 |
| **10.00%** | **30%** | 164.4 | 78.17 | 137.0 | 81.42 | 117.4 | 83.75 |
| **10.00%** | **40%** | 169.5 | 66.59 | 141.3 | 69.36 | 121.1 | 71.34 |
| **10.00%** | **50%** | 176.7 | 59.77 | 147.2 | 62.26 | 126.2 | 64.04 |
| **15.00%** | **10%** | 183.8 | 181.33 | 153.2 | 188.88 | 131.3 | 194.28 |
| **15.00%** | **20%** | 240.1 | 150.02 | 200.1 | 156.28 | 171.5 | 160.74 |
| **15.00%** | **30%** | 261.7 | 124.47 | 218.1 | 129.66 | 186.9 | 133.36 |
| **15.00%** | **40%** | 277.3 | 108.94 | 231.1 | 113.48 | 198.1 | 116.72 |
| **15.00%** | **50%** | 292.9 | 99.09 | 244.1 | 103.22 | 209.2 | 106.17 |
| **19.75%** | **10%** | 244.2 | 240.91 | 203.5 | 250.95 | 174.4 | 258.12 |
| **19.75%** | **20%** | 317.8 | 198.52 | 264.8 | 206.80 | 227.0 | 212.70 |
| **19.75%** | **30%** | 351.9 | 167.36 | 293.2 | 174.33 | 251.4 | 179.32 |
| **19.75%** | **40%** | 379.4 | 149.03 | 316.1 | 155.24 | 271.0 | 159.67 |
| **19.75%** | **50%** | 405.4 | 137.16 | 337.9 | 142.88 | 289.6 | 146.96 |

The costs associated with the reactor can now be calculated in terms of $/MWh$_e$. These units allow an easy comparison between different configurations. The process involves including the costs related to the fuel in addition to the cost relating to outages. The portion of cost relating to outages was considered by using a fixed cost to apply at each refueling. Since an exact outage cost has yet to be determined for the LSCR, two different outage costs of $20 and $50 million were chosen. Additionally, the three different fuel fabrication costs were used to represent the low ($1,300/kgU), base ($4,000/kgU), and high ($24,000/kgU) costs that were predicted [18].

Table 4.11: Fuel and outage costs ($/MWhe) for low fuel fabrication cost

| | Outage Cost - $20 million | | | | | | Outage Cost - $50 million | | | | | |
|---|---|---|---|---|---|---|---|---|---|---|---|---|
| **Uranium Enrichment** | **Number of Batches** | | | | | | **Number of Batches** | | | | | |
| | **1** | **2** | **3** | **4** | **5** | **6** | **1** | **2** | **3** | **4** | **5** | **6** |
| | *Packing Factor 10%* | | | | | | *Packing Factor 10%* | | | | | |
| **5.00%** | 19.85 | 19.36 | 21.19 | 23.60 | 26.23 | 28.99 | 28.80 | 32.79 | 39.10 | 45.98 | 53.09 | 60.32 |
| **10.00%** | 9.55 | 8.59 | 8.90 | 9.53 | 10.29 | 11.11 | 12.40 | 12.86 | 14.59 | 16.65 | 18.83 | 21.07 |
| **15.00%** | 8.02 | 6.90 | 6.92 | 7.23 | 7.65 | 8.13 | 9.79 | 9.57 | 10.48 | 11.68 | 12.99 | 14.36 |
| **19.75%** | 7.51 | 6.30 | 6.20 | 6.37 | 6.65 | 6.98 | 8.85 | 8.31 | 8.87 | 9.71 | 10.66 | 11.67 |
| | *Packing Factor 20%* | | | | | | *Packing Factor 20%* | | | | | |
| **5.00%** | 18.28 | 16.64 | 17.40 | 18.76 | 20.36 | 22.07 | 24.15 | 25.45 | 29.14 | 33.43 | 37.96 | 42.61 |
| **10.00%** | 10.54 | 8.97 | 8.93 | 9.27 | 9.75 | 10.32 | 12.68 | 12.19 | 13.22 | 14.63 | 16.19 | 17.83 |
| **15.00%** | 9.16 | 7.55 | 7.32 | 7.43 | 7.68 | 7.99 | 10.52 | 9.59 | 10.04 | 10.83 | 11.76 | 12.75 |
| **19.75%** | 8.72 | 7.05 | 6.73 | 6.73 | 6.88 | 7.09 | 9.75 | 8.60 | 8.78 | 9.31 | 9.96 | 10.68 |
| | *Packing Factor 30%* | | | | | | *Packing Factor 30%* | | | | | |
| **5.00%** | 20.89 | 18.36 | 18.71 | 19.78 | 21.15 | 22.65 | 26.27 | 26.43 | 29.47 | 33.24 | 37.29 | 41.48 |
| **10.00%** | 12.41 | 10.30 | 10.04 | 10.24 | 10.63 | 11.10 | 14.40 | 13.28 | 14.02 | 15.21 | 16.59 | 18.06 |
| **15.00%** | 10.78 | 8.71 | 8.30 | 8.30 | 8.47 | 8.72 | 12.03 | 10.58 | 10.80 | 11.42 | 12.21 | 13.09 |
| **19.75%** | 10.15 | 8.07 | 7.59 | 7.50 | 7.57 | 7.73 | 11.08 | 9.47 | 9.45 | 9.82 | 10.36 | 10.98 |
| | *Packing Factor 40%* | | | | | | *Packing Factor 40%* | | | | | |
| **5.00%** | 23.95 | 20.59 | 20.64 | 21.54 | 22.78 | 24.19 | 29.21 | 28.47 | 31.14 | 34.67 | 38.53 | 42.57 |
| **10.00%** | 14.30 | 11.69 | 11.24 | 11.34 | 11.66 | 12.09 | 16.22 | 14.58 | 15.10 | 16.16 | 17.45 | 18.84 |
| **15.00%** | 12.16 | 9.71 | 9.15 | 9.07 | 9.18 | 9.38 | 13.33 | 11.47 | 11.51 | 12.02 | 12.71 | 13.51 |
| **19.75%** | 11.27 | 8.89 | 8.28 | 8.12 | 8.14 | 8.25 | 12.14 | 10.18 | 10.00 | 10.28 | 10.73 | 11.27 |
| | *Packing Factor 50%* | | | | | | *Packing Factor 50%* | | | | | |
| **5.00%** | 26.99 | 22.84 | 22.62 | 23.37 | 24.52 | 25.86 | 32.19 | 30.65 | 33.02 | 36.38 | 40.12 | 44.07 |
| **10.00%** | 15.73 | 12.72 | 12.13 | 12.14 | 12.40 | 12.77 | 17.58 | 15.50 | 15.83 | 16.77 | 17.95 | 19.25 |
| **15.00%** | 13.24 | 10.49 | 9.82 | 9.67 | 9.73 | 9.89 | 14.36 | 12.16 | 12.05 | 12.46 | 13.08 | 13.80 |
| **19.75%** | 12.16 | 9.53 | 8.83 | 8.61 | 8.59 | 8.66 | 12.97 | 10.73 | 10.44 | 10.62 | 11.01 | 11.48 |

Table 4.12: Fuel and outage costs ($/MWhe) for base fuel fabrication cost

| Uranium Enrichment | Outage Cost - $20 million | | | | | | Outage Cost - $50 million | | | | | |
|---|---|---|---|---|---|---|---|---|---|---|---|---|
| | Number of Batches | | | | | | Number of Batches | | | | | |
| | 1 | 2 | 3 | 4 | 5 | 6 | 1 | 2 | 3 | 4 | 5 | 6 |
| | *Packing Factor 10%* | | | | | | *Packing Factor 10%* | | | | | |
| **5.00%** | 30.96 | 27.69 | 28.60 | 30.54 | 32.90 | 35.47 | 39.91 | 41.12 | 46.50 | 52.92 | 59.76 | 66.80 |
| **10.00%** | 13.08 | 11.24 | 11.25 | 11.74 | 12.41 | 13.17 | 15.93 | 15.51 | 16.95 | 18.85 | 20.95 | 23.13 |
| **15.00%** | 10.22 | 8.56 | 8.40 | 8.61 | 8.98 | 9.42 | 12.00 | 11.22 | 11.95 | 13.06 | 14.31 | 15.64 |
| **19.75%** | 9.17 | 7.55 | 7.30 | 7.41 | 7.64 | 7.95 | 10.51 | 9.56 | 9.98 | 10.75 | 11.66 | 12.64 |
| | *Packing Factor 20%* | | | | | | *Packing Factor 20%* | | | | | |
| **5.00%** | 29.78 | 25.27 | 25.07 | 25.95 | 27.26 | 28.78 | 35.65 | 34.07 | 36.81 | 40.62 | 44.86 | 49.32 |
| **10.00%** | 14.74 | 12.13 | 11.73 | 11.89 | 12.28 | 12.77 | 16.89 | 15.35 | 16.03 | 17.26 | 18.71 | 20.28 |
| **15.00%** | 11.83 | 9.55 | 9.10 | 9.09 | 9.27 | 9.55 | 13.19 | 11.59 | 11.82 | 12.50 | 13.36 | 14.31 |
| **19.75%** | 10.73 | 8.56 | 8.07 | 7.99 | 8.09 | 8.26 | 11.76 | 10.11 | 10.13 | 10.56 | 11.17 | 11.86 |
| | *Packing Factor 30%* | | | | | | *Packing Factor 30%* | | | | | |
| **5.00%** | 34.74 | 28.75 | 27.94 | 28.44 | 29.45 | 30.73 | 40.12 | 36.82 | 38.70 | 41.89 | 45.60 | 49.56 |
| **10.00%** | 17.53 | 14.14 | 13.45 | 13.44 | 13.70 | 14.09 | 19.51 | 17.12 | 17.43 | 18.41 | 19.66 | 21.05 |
| **15.00%** | 14.00 | 11.12 | 10.44 | 10.31 | 10.40 | 10.59 | 15.25 | 13.00 | 12.94 | 13.43 | 14.14 | 14.96 |
| **19.75%** | 12.54 | 9.87 | 9.18 | 9.00 | 9.01 | 9.12 | 13.47 | 11.26 | 11.04 | 11.32 | 11.79 | 12.37 |
| | *Packing Factor 40%* | | | | | | *Packing Factor 40%* | | | | | |
| **5.00%** | 40.32 | 32.87 | 31.55 | 31.77 | 32.60 | 33.73 | 45.57 | 40.75 | 42.05 | 44.90 | 48.35 | 52.12 |
| **10.00%** | 20.30 | 16.19 | 15.25 | 15.10 | 15.27 | 15.59 | 22.23 | 19.08 | 19.11 | 19.92 | 21.05 | 22.34 |
| **15.00%** | 15.83 | 12.46 | 11.60 | 11.36 | 11.38 | 11.52 | 17.01 | 14.23 | 13.96 | 14.31 | 14.92 | 15.65 |
| **19.75%** | 13.96 | 10.90 | 10.07 | 9.80 | 9.75 | 9.82 | 14.82 | 12.19 | 11.79 | 11.95 | 12.34 | 12.83 |
| | *Packing Factor 50%* | | | | | | *Packing Factor 50%* | | | | | |
| **5.00%** | 45.81 | 36.96 | 35.17 | 35.14 | 35.81 | 36.84 | 51.01 | 44.76 | 45.57 | 48.14 | 51.42 | 55.05 |
| **10.00%** | 22.42 | 17.74 | 16.59 | 16.32 | 16.41 | 16.67 | 24.27 | 20.51 | 20.29 | 20.95 | 21.96 | 23.15 |
| **15.00%** | 17.28 | 13.52 | 12.51 | 12.19 | 12.15 | 12.25 | 18.40 | 15.19 | 14.74 | 14.98 | 15.50 | 16.15 |
| **19.75%** | 15.08 | 11.71 | 10.77 | 10.43 | 10.34 | 10.36 | 15.89 | 12.92 | 12.38 | 12.45 | 12.76 | 13.19 |

Table 4.13: Fuel and outage costs ($/MWhe) for high fuel fabrication cost

| Uranium Enrichment | Outage Cost - $20 million | | | | | | Outage Cost - $50 million | | | | | |
|---|---|---|---|---|---|---|---|---|---|---|---|---|
| | Number of Batches | | | | | | Number of Batches | | | | | |
| | 1 | 2 | 3 | 4 | 5 | 6 | 1 | 2 | 3 | 4 | 5 | 6 |
| | *Packing Factor 10%* | | | | | | *Packing Factor 10%* | | | | | |
| **5.00%** | 113.2 | 89.40 | 83.45 | 81.96 | 82.26 | 83.46 | 122.2 | 102.8 | 101.4 | 104.3 | 109.1 | 114.8 |
| **10.00%** | 39.25 | 30.86 | 28.70 | 28.09 | 28.11 | 28.43 | 42.10 | 35.13 | 34.39 | 35.21 | 36.65 | 38.40 |
| **15.00%** | 26.56 | 20.81 | 19.29 | 18.82 | 18.78 | 18.95 | 28.34 | 23.48 | 22.84 | 23.27 | 24.12 | 25.18 |
| **19.75%** | 21.47 | 16.77 | 15.50 | 15.09 | 15.02 | 15.13 | 22.81 | 18.78 | 18.18 | 18.44 | 19.04 | 19.81 |
| | *Packing Factor 20%* | | | | | | *Packing Factor 20%* | | | | | |
| **5.00%** | 114.9 | 89.14 | 81.85 | 79.18 | 78.36 | 78.46 | 120.8 | 97.94 | 93.58 | 93.85 | 95.96 | 99.00 |
| **10.00%** | 45.88 | 35.48 | 32.49 | 31.36 | 30.96 | 30.94 | 48.03 | 38.70 | 36.79 | 36.72 | 37.40 | 38.45 |
| **15.00%** | 31.58 | 24.36 | 22.26 | 21.44 | 21.12 | 21.07 | 32.94 | 26.41 | 24.98 | 24.84 | 25.21 | 25.83 |
| **19.75%** | 25.66 | 19.76 | 18.02 | 17.32 | 17.04 | 16.97 | 26.69 | 21.30 | 20.08 | 19.89 | 20.13 | 20.57 |
| | *Packing Factor 30%* | | | | | | *Packing Factor 30%* | | | | | |
| **5.00%** | 137.3 | 105.68 | 96.33 | 92.55 | 91.00 | 90.56 | 142.7 | 113.7 | 107.1 | 106.0 | 107.1 | 109.4 |
| **10.00%** | 55.43 | 42.57 | 38.72 | 37.13 | 36.44 | 36.20 | 57.42 | 45.55 | 42.70 | 42.10 | 42.41 | 43.16 |
| **15.00%** | 37.80 | 28.98 | 26.31 | 25.19 | 24.68 | 24.48 | 39.05 | 30.85 | 28.81 | 28.31 | 28.43 | 28.85 |
| **19.75%** | 30.24 | 23.15 | 20.99 | 20.06 | 19.63 | 19.45 | 31.17 | 24.54 | 22.84 | 22.38 | 22.42 | 22.70 |
| | *Packing Factor 40%* | | | | | | *Packing Factor 40%* | | | | | |
| **5.00%** | 161.6 | 123.8 | 112.4 | 107.5 | 105.3 | 104.5 | 166.8 | 131.7 | 122.9 | 120.7 | 121.1 | 122.8 |
| **10.00%** | 64.80 | 49.56 | 44.91 | 42.91 | 41.97 | 41.55 | 66.73 | 52.46 | 48.77 | 47.73 | 47.75 | 48.30 |
| **15.00%** | 43.03 | 32.86 | 29.73 | 28.36 | 27.70 | 27.39 | 44.20 | 34.63 | 32.09 | 31.31 | 31.24 | 31.51 |
| **19.75%** | 33.84 | 25.81 | 23.33 | 22.23 | 21.68 | 21.42 | 34.70 | 27.10 | 25.05 | 24.38 | 24.27 | 24.43 |
| | *Packing Factor 50%* | | | | | | *Packing Factor 50%* | | | | | |
| **5.00%** | 185.2 | 141.5 | 128.1 | 122.3 | 119.5 | 118.2 | 190.4 | 149.3 | 138.5 | 135.3 | 135.1 | 136.4 |
| **10.00%** | 71.99 | 54.92 | 49.64 | 47.31 | 46.15 | 45.59 | 73.84 | 57.69 | 53.34 | 51.93 | 51.70 | 52.07 |
| **15.00%** | 47.18 | 35.94 | 32.45 | 30.88 | 30.09 | 29.69 | 48.30 | 37.62 | 34.68 | 33.67 | 33.44 | 33.60 |
| **19.75%** | 36.68 | 27.91 | 25.17 | 23.93 | 23.30 | 22.97 | 37.49 | 29.12 | 26.78 | 25.95 | 25.72 | 25.79 |

Table 4.11, Table 4.12, and Table 4.13 can be used to look at how the different costs compare to one another. In order to better show how the costs vary relative to the number of batches, figures have been made showing cost versus batch number. Each of the different figures represents a certain fuel fabrication cost and packing factor. The $20 million outage costs are plotted with a solid line while the $50 million outage costs are plotted with a dashed line. The figures are shown on the following pages.

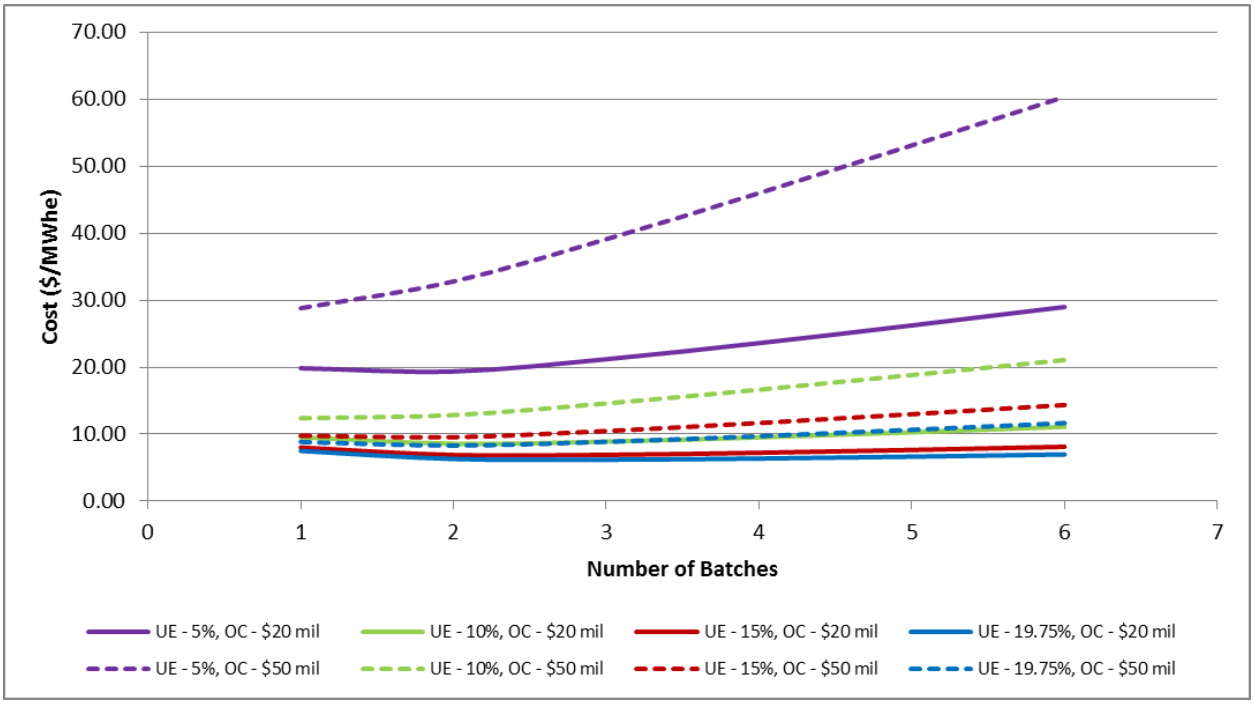


Figure 4-11: Packing factor 10%, low fuel fabrication cost

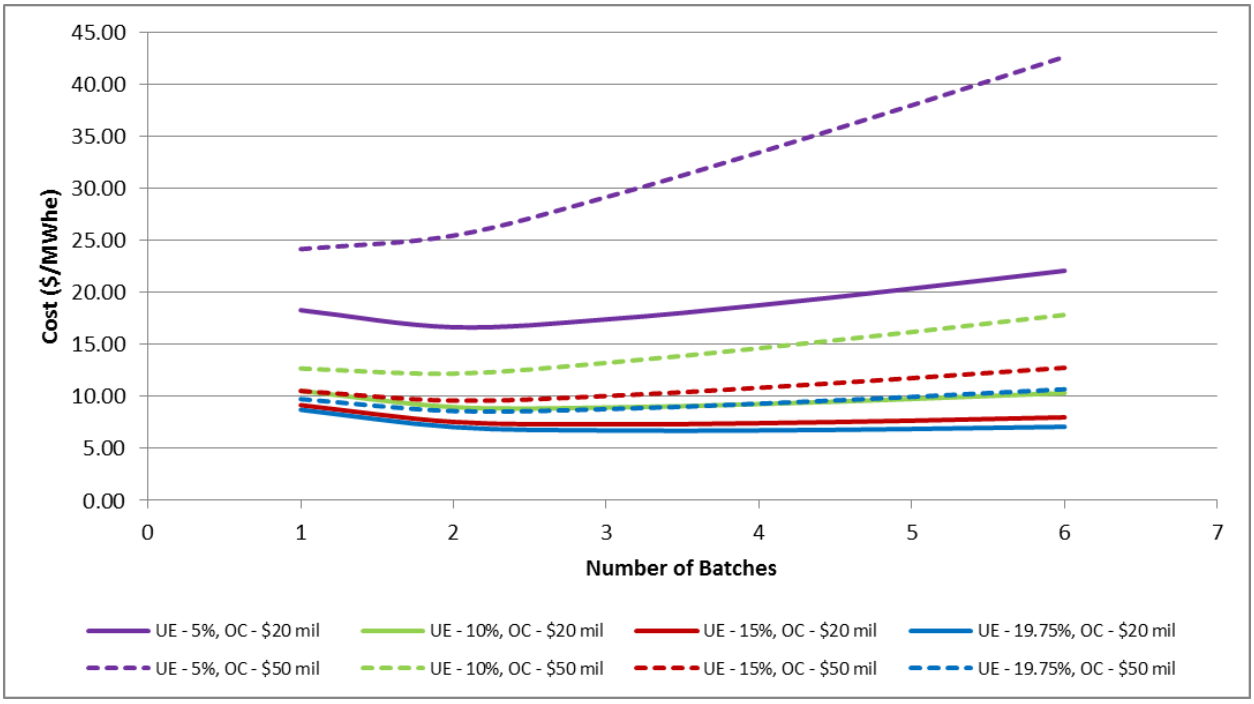


Figure 4-12: Packing factor 20%, low fuel fabrication cost

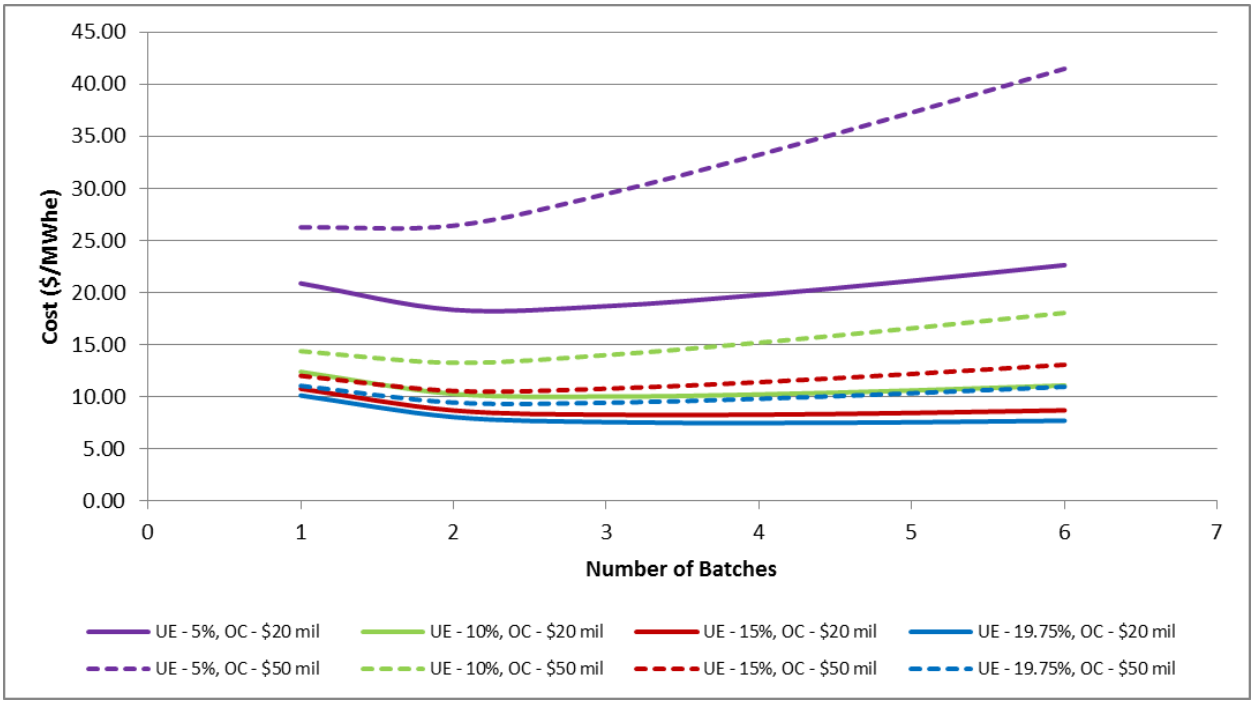


Figure 4-13: Packing factor 30%, low fuel fabrication cost

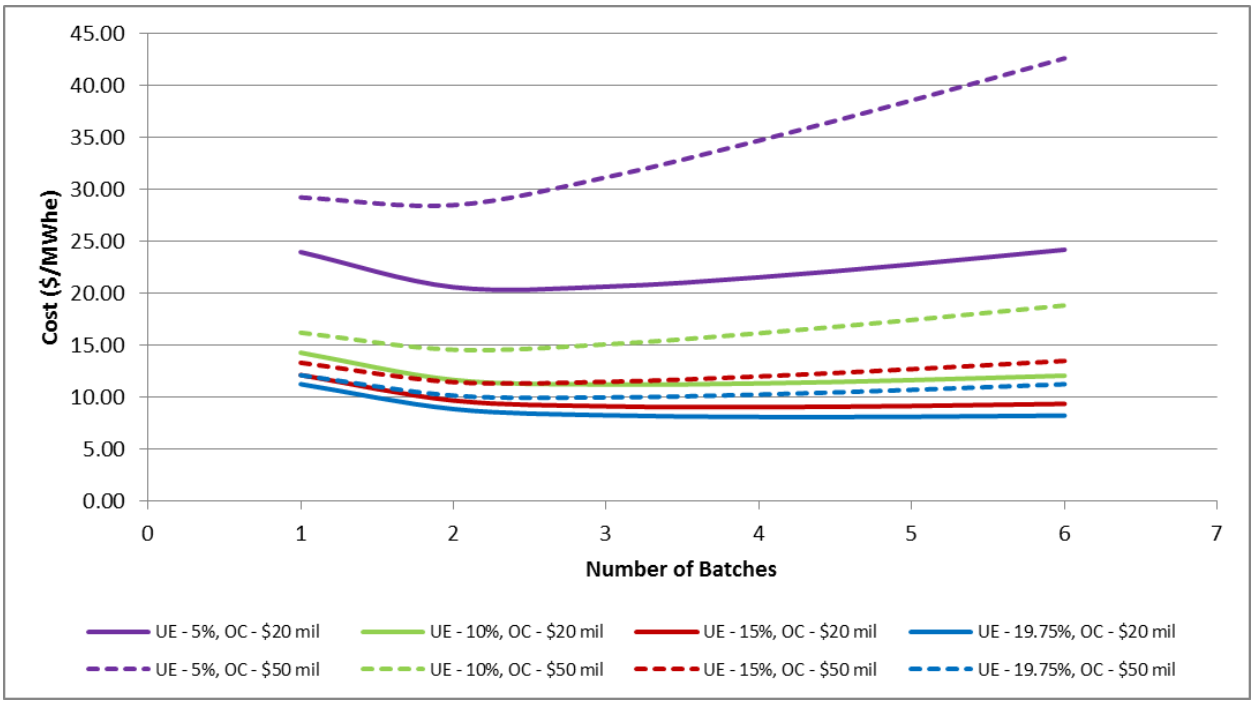


Figure 4-14: Packing factor 40%, low fuel fabrication cost

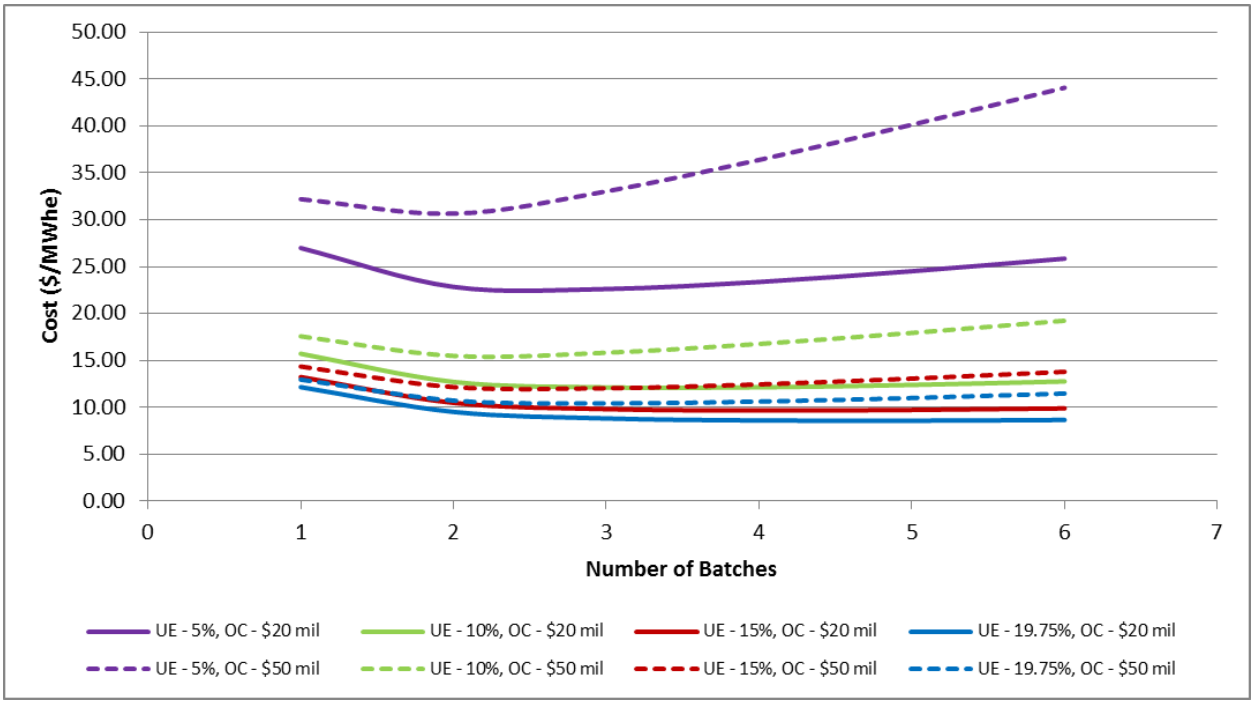


Figure 4-15: Packing factor 50%, low fuel fabrication cost

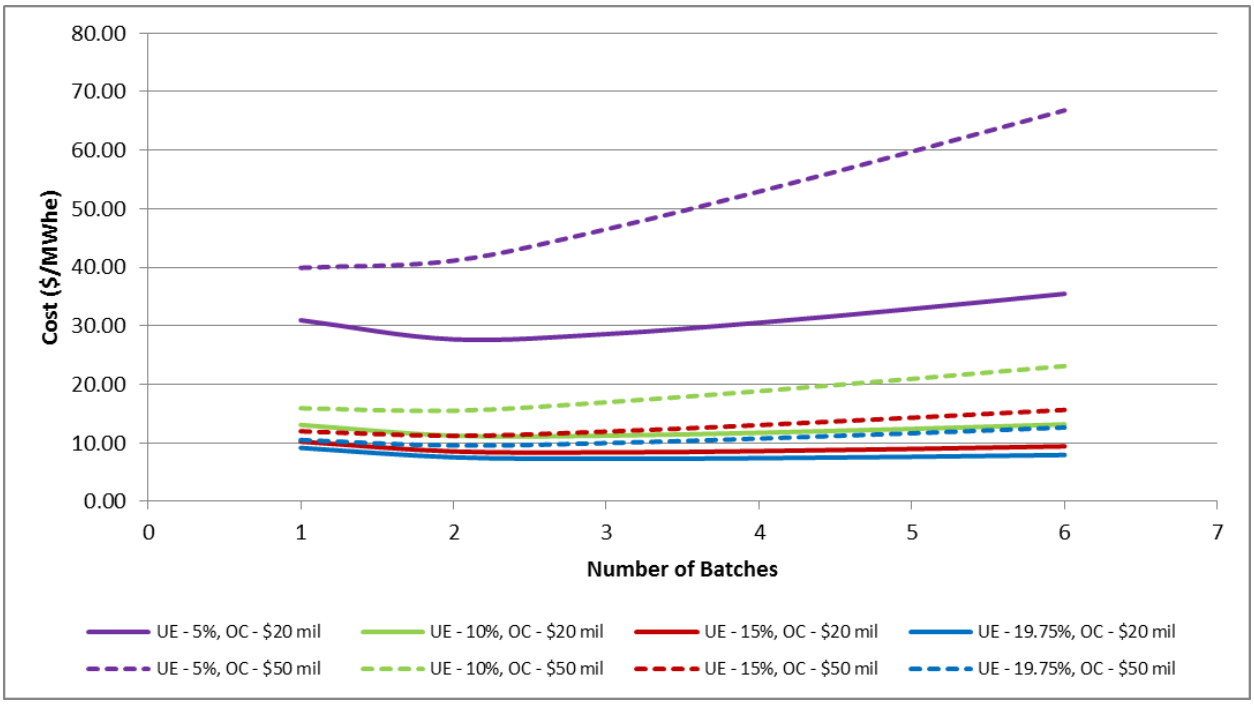


Figure 4-16: Packing factor 10%, base fuel fabrication cost

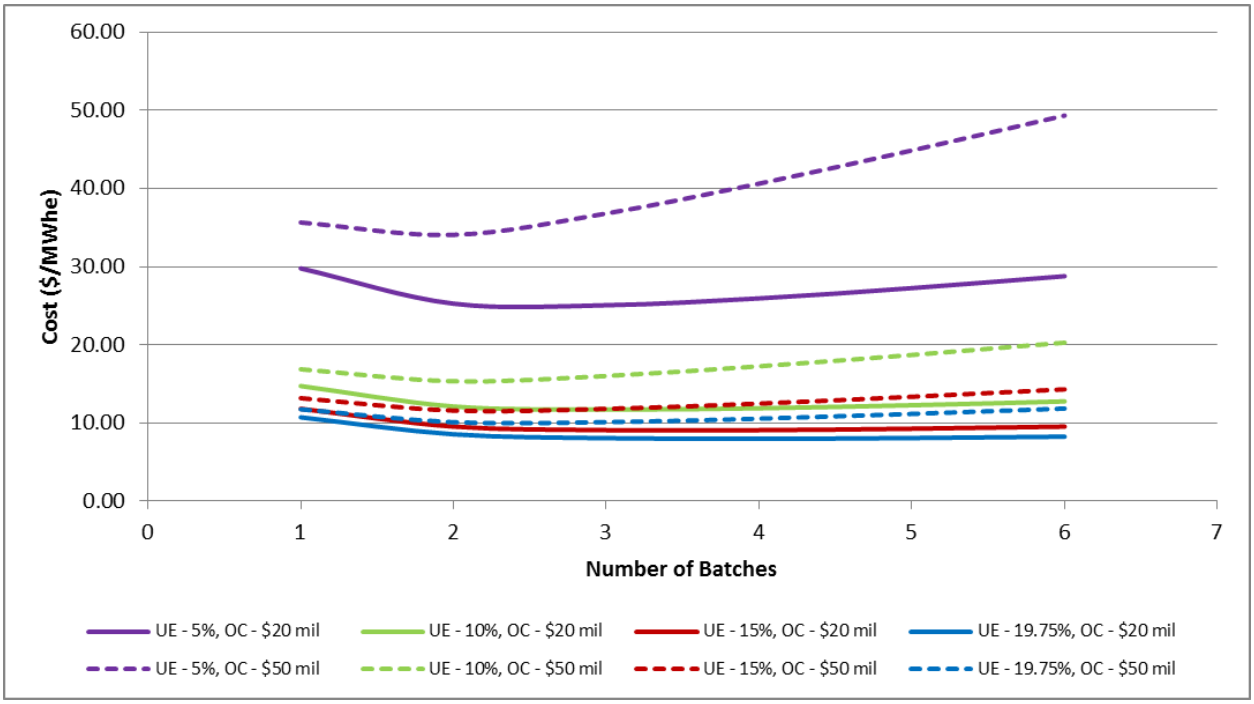


Figure 4-17: Packing factor 20%, base fuel fabrication cost

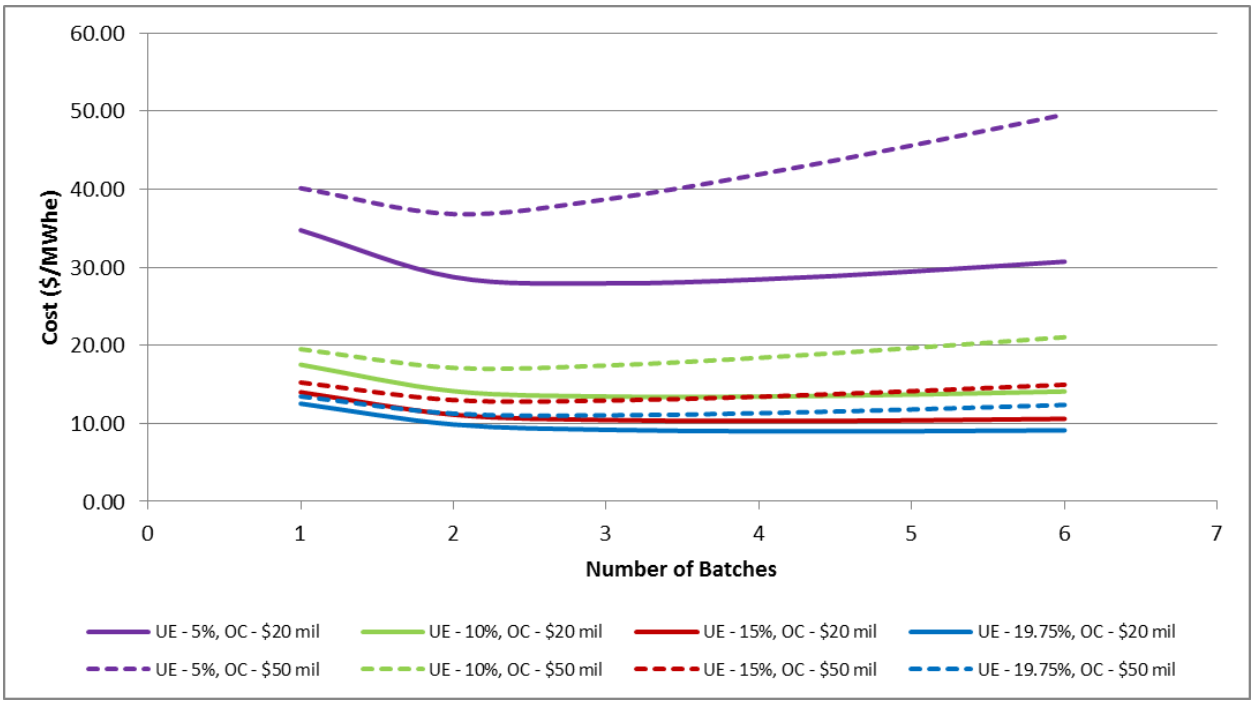


Figure 4-18: Packing factor 30%, base fuel fabrication cost

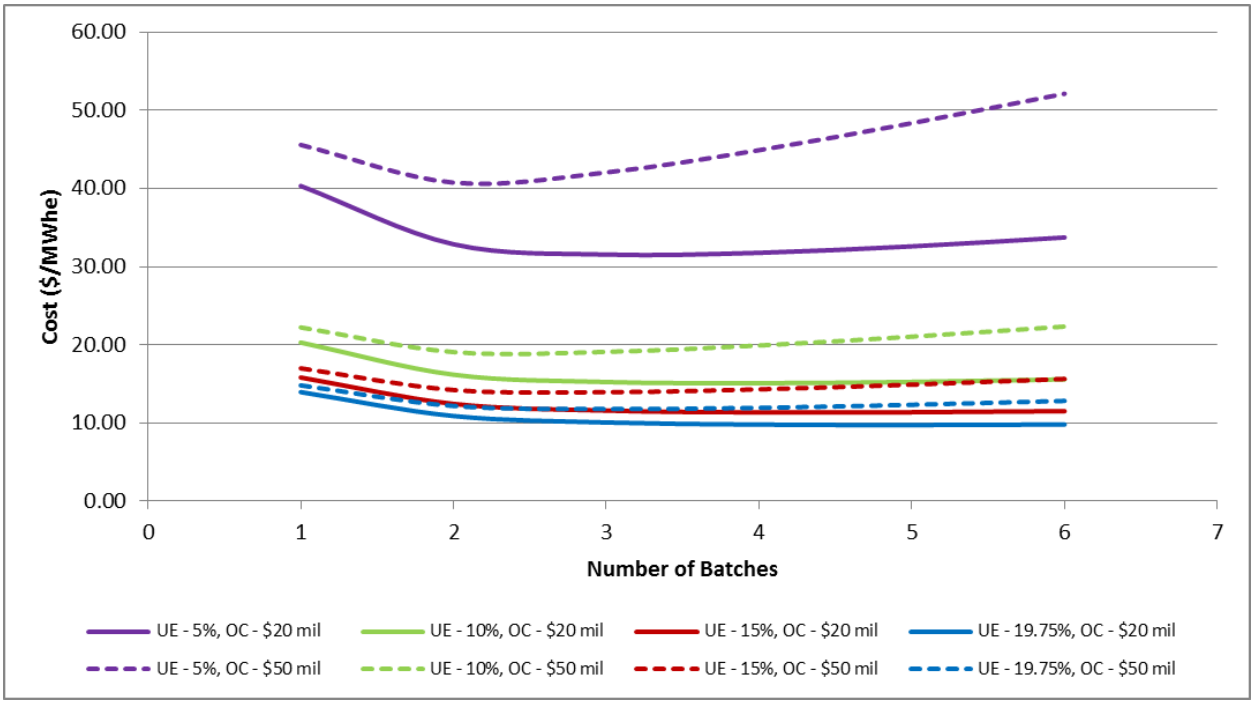


Figure 4-19: Packing factor 40%, base fuel fabrication cost

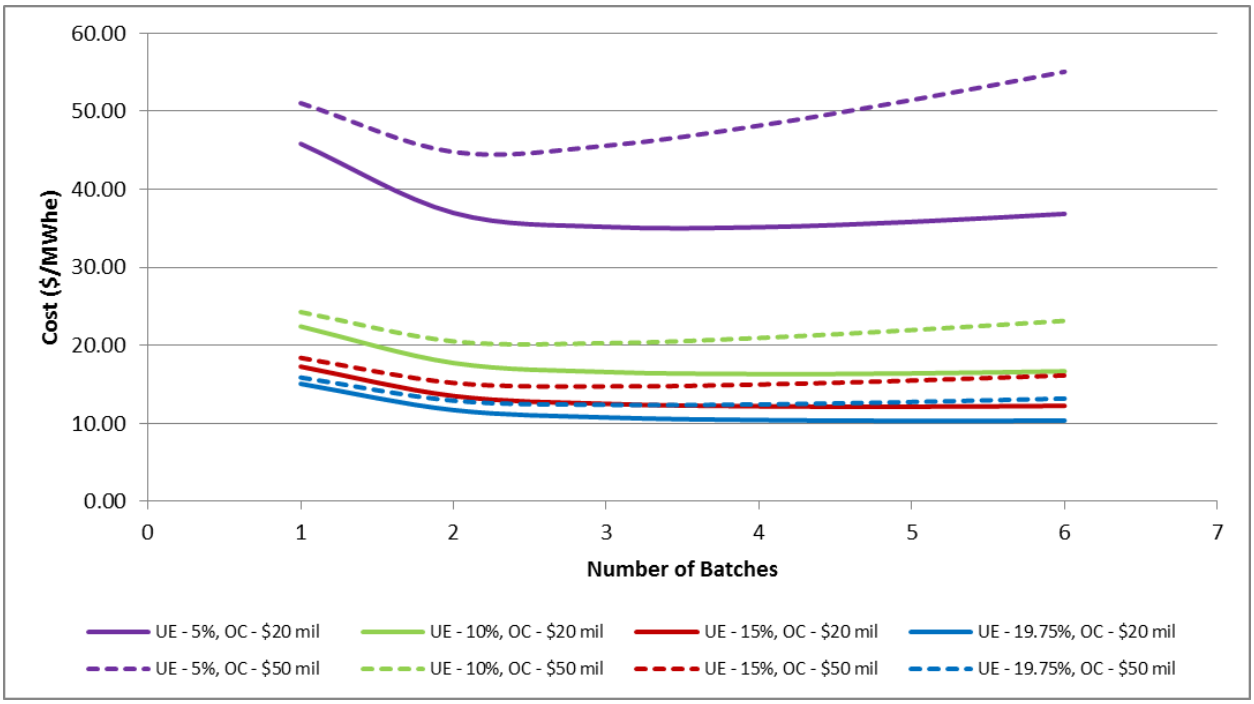


Figure 4-20: Packing factor 50%, base fuel fabrication cost

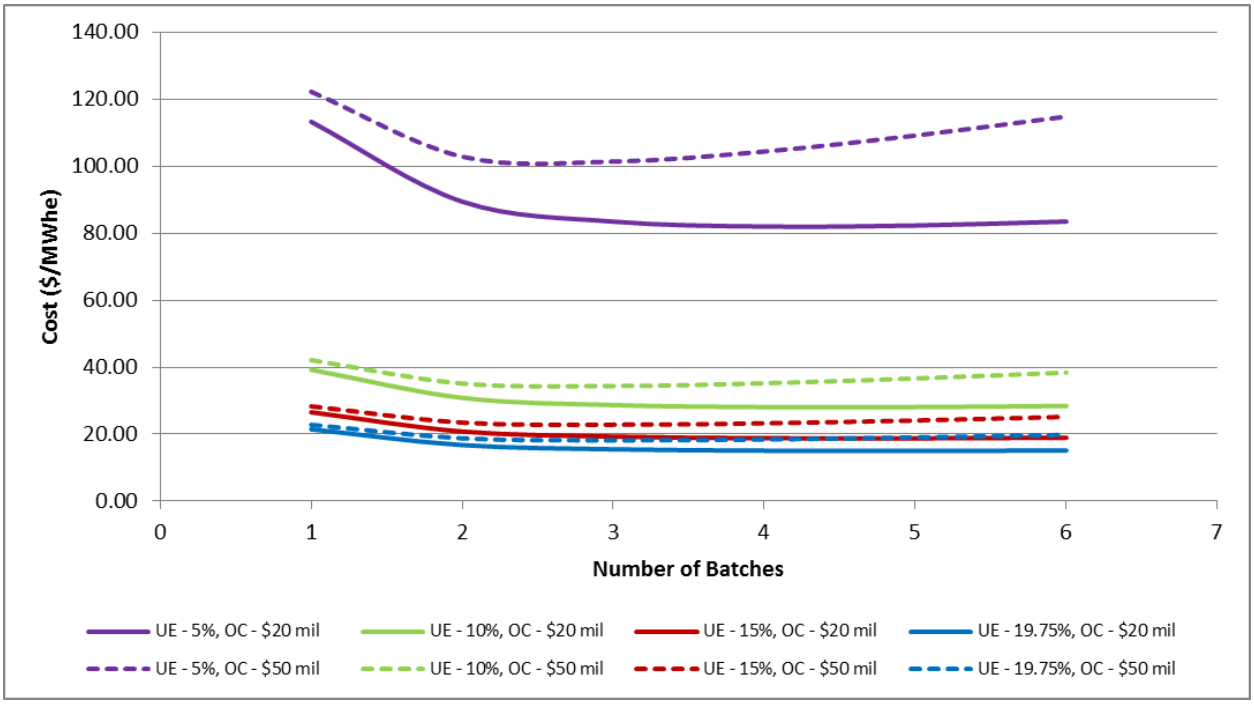


Figure 4-21: Packing factor 10%, high fuel fabrication cost

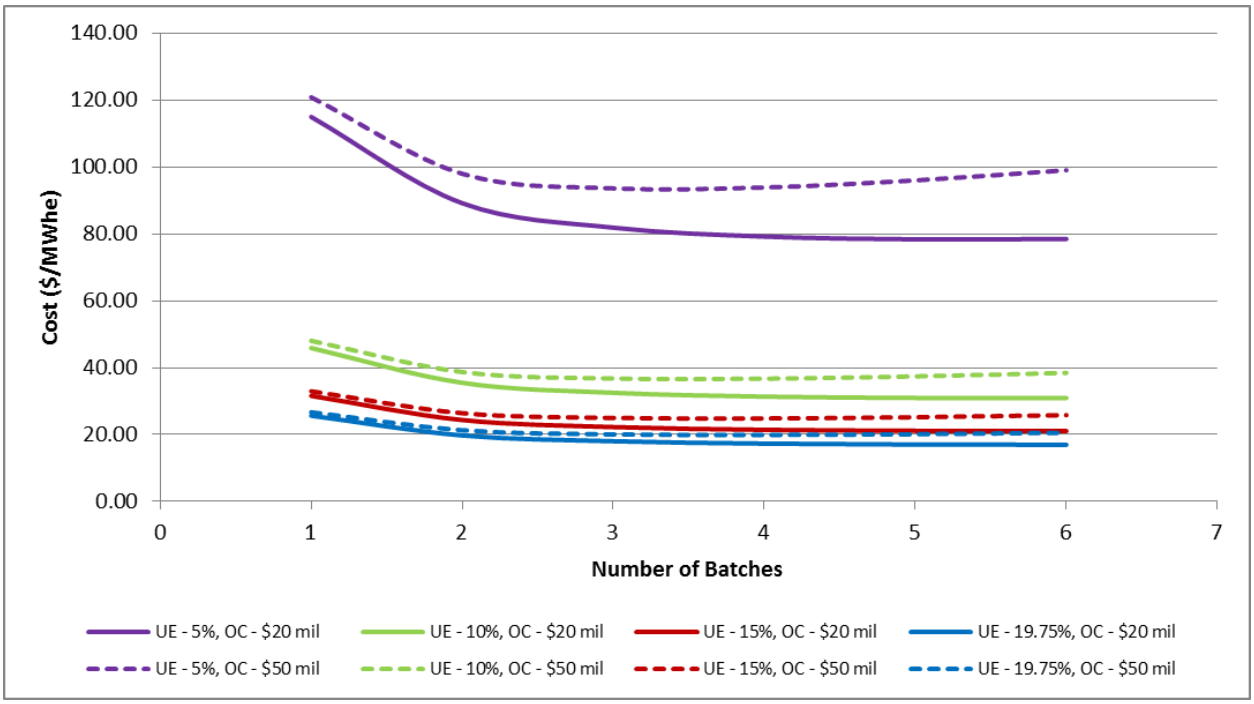


Figure 4-22: Packing factor 20%, high fuel fabrication cost

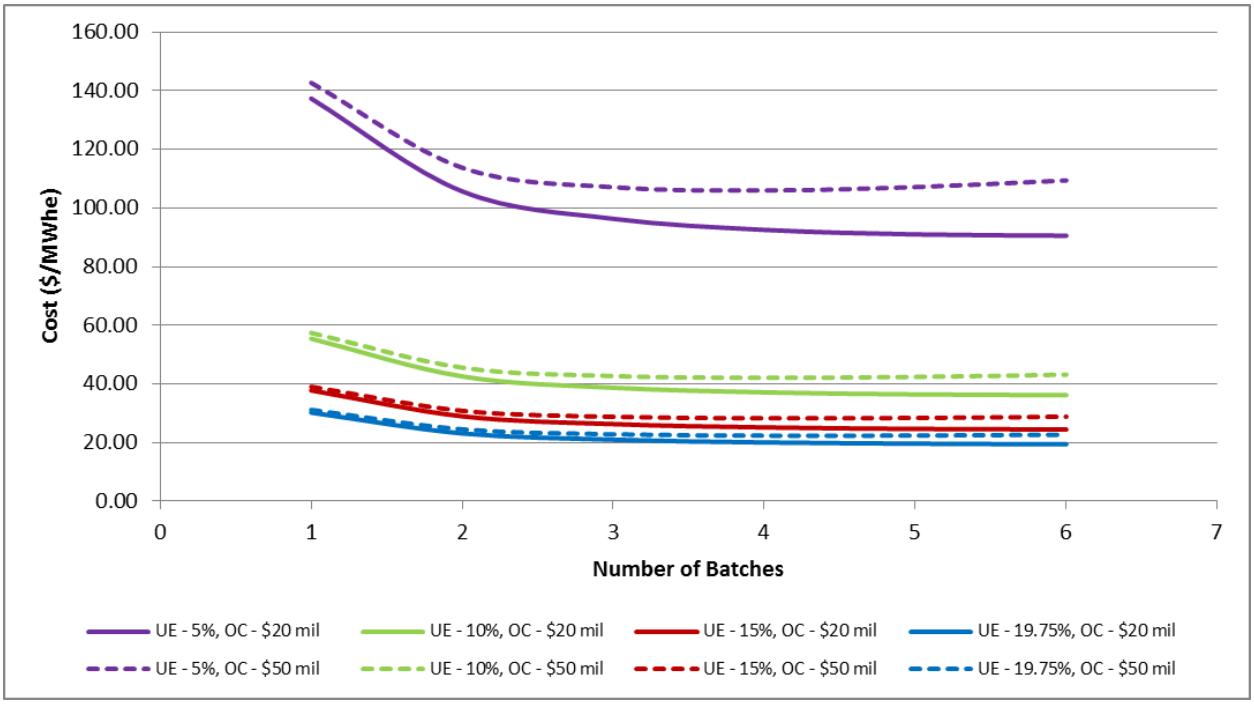


Figure 4-23: Packing factor 30%, high fuel fabrication cost

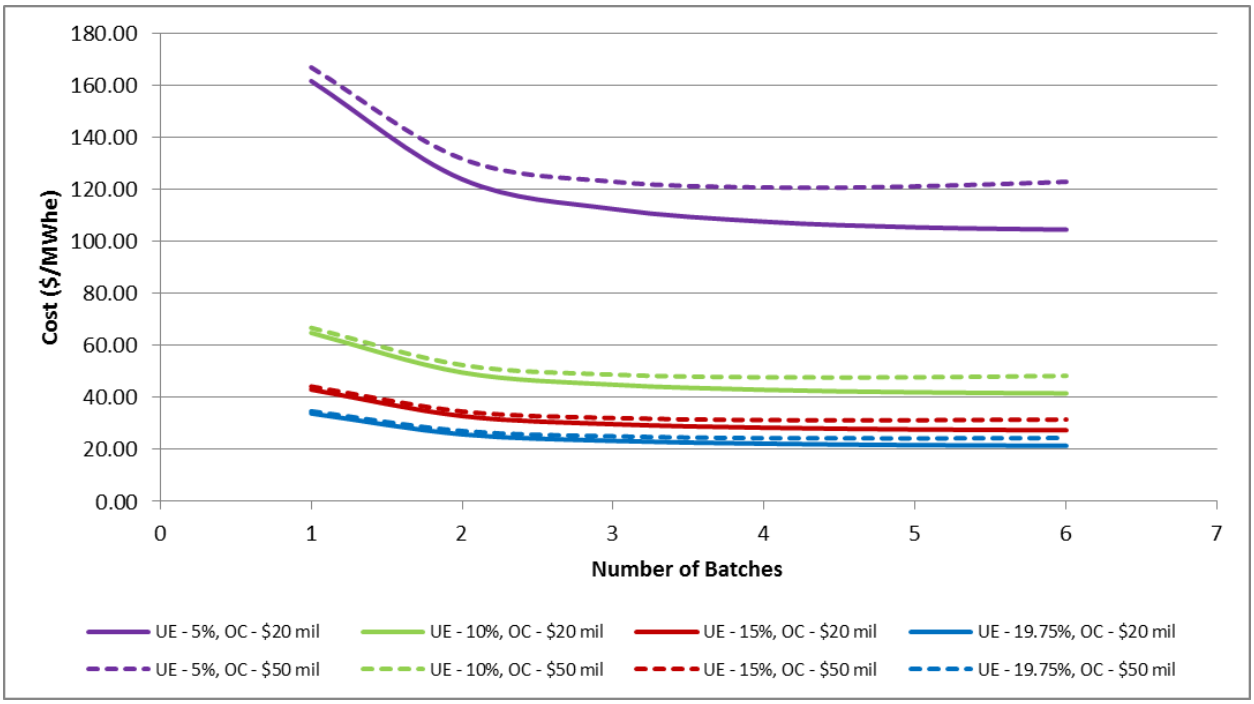


Figure 4-24: Packing factor 40%, high fuel fabrication cost

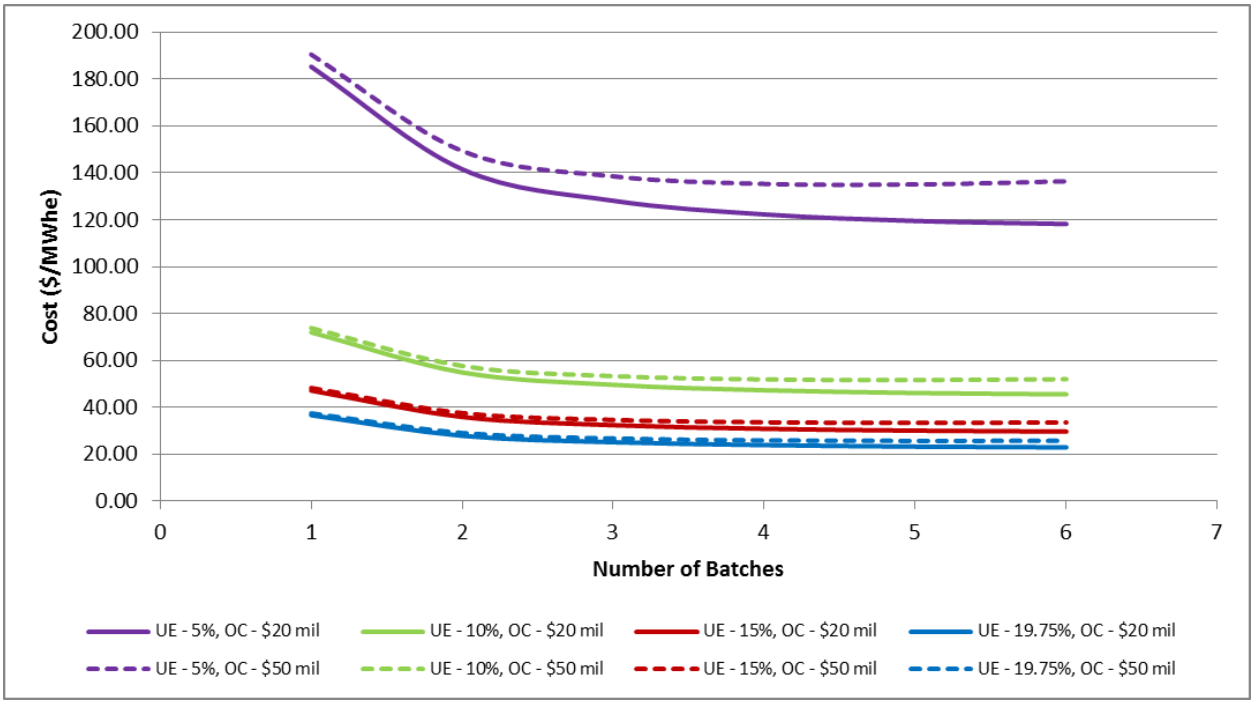


Figure 4-25: Packing factor 50%, high fuel fabrication cost

Based on the previously shown figures, it is clear that a uranium enrichment of 5% is much more expensive than the other options in all considered configurations. As a result, the use of an enrichment of 5% is probably not feasible for this particular design. However, the other uranium enrichments are often pretty competitive against one another, but in general the 19.75% enrichment appears to be most economical in all the different cases.

Therefore, we focus on the 19.75% fuel enrichment. The following figures for 19.75% enrichment show combinations of low/base/high fabrication costs and low/high outage costs at the different packing factors.

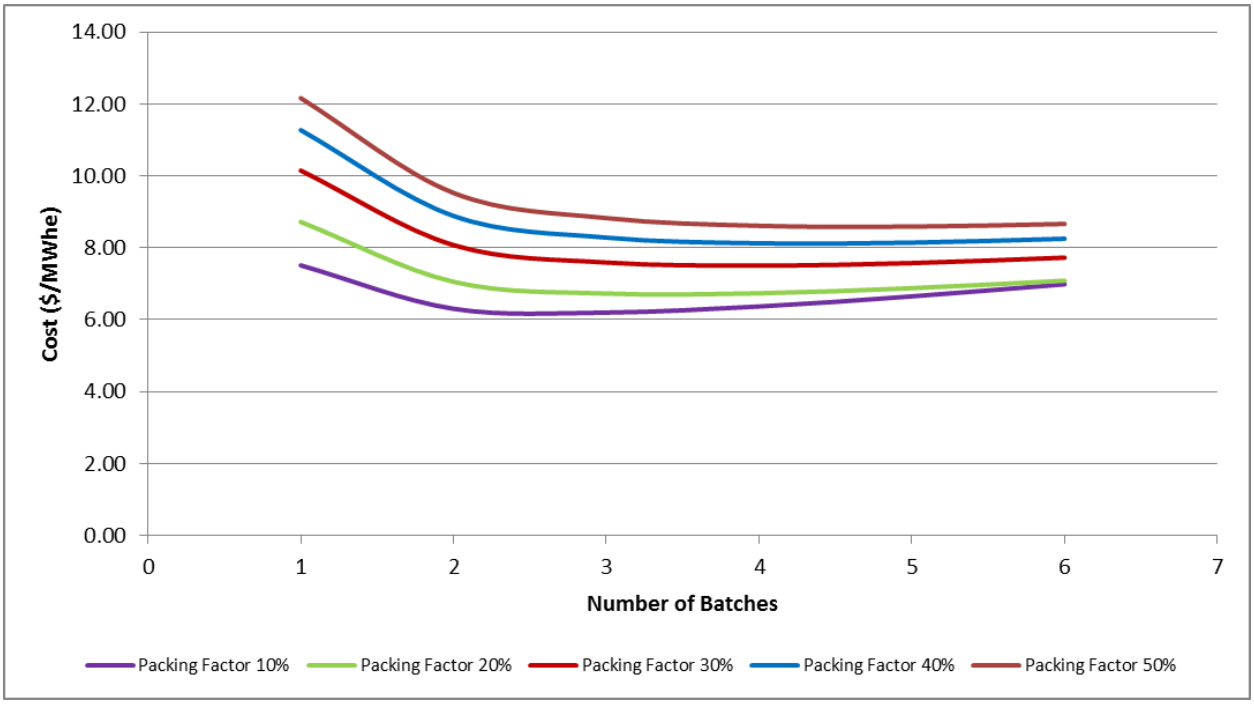


Figure 4-26: Low fabrication cost, low outage cost, 19.75% enrichment

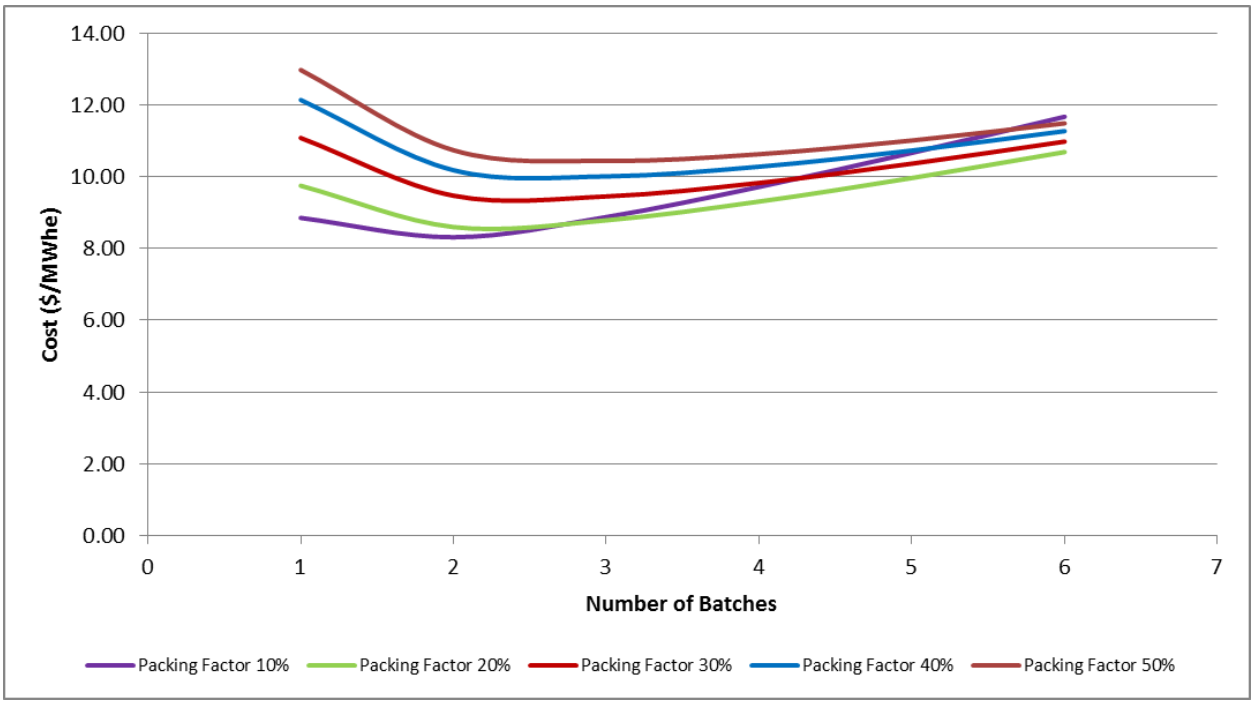


Figure 4-27: Low fabrication cost, high outage cost, 19.75% enrichment

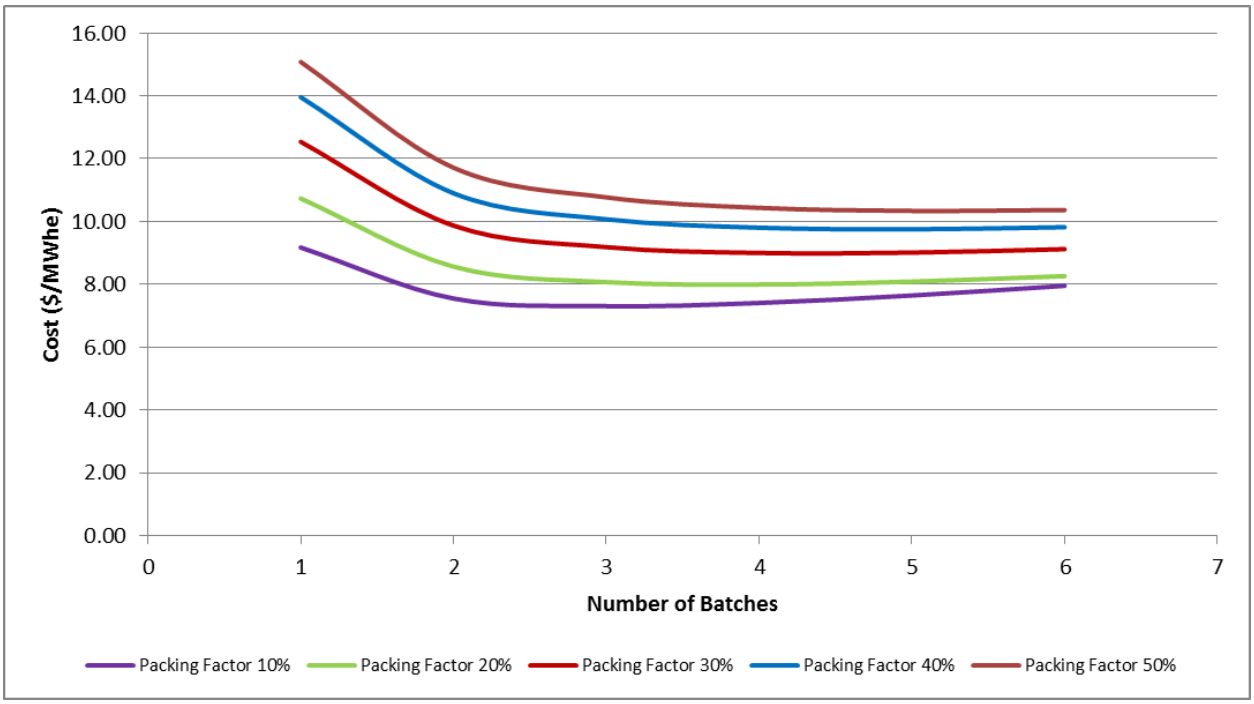


Figure 4-28: Base fabrication cost, low outage cost, 19.75% enrichment

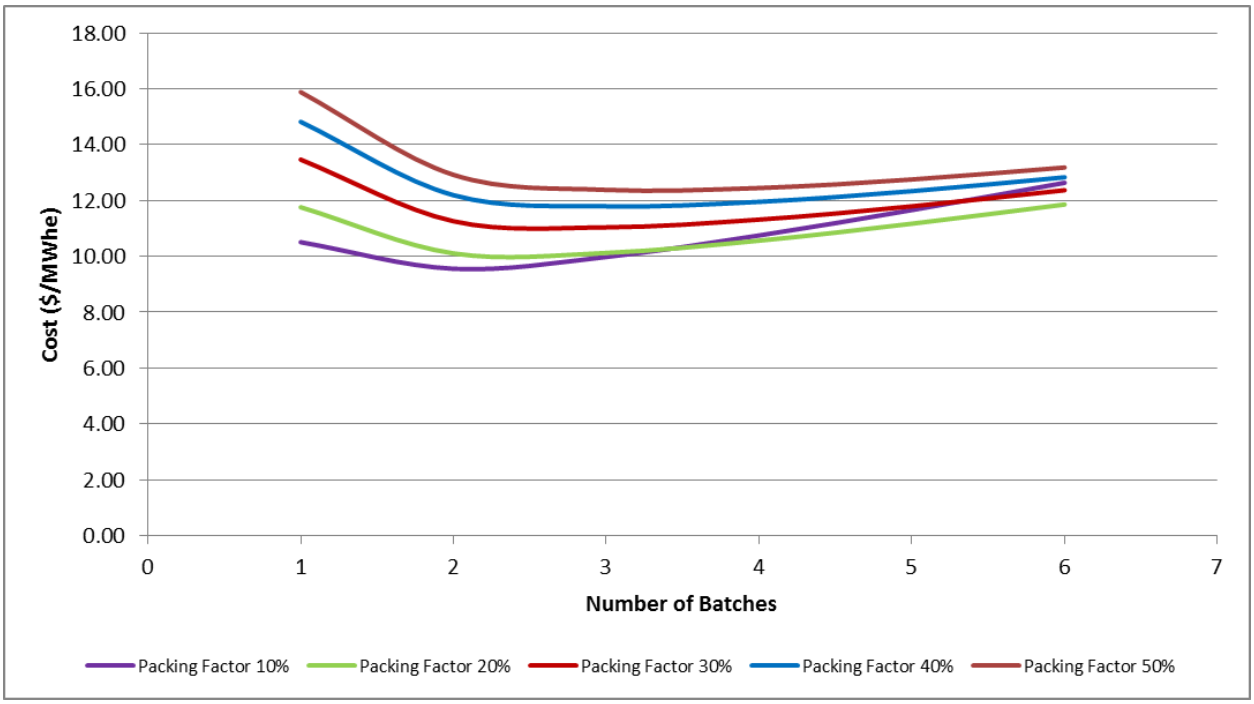


Figure 4-29: Base fabrication cost, high outage cost, 19.75% enrichment

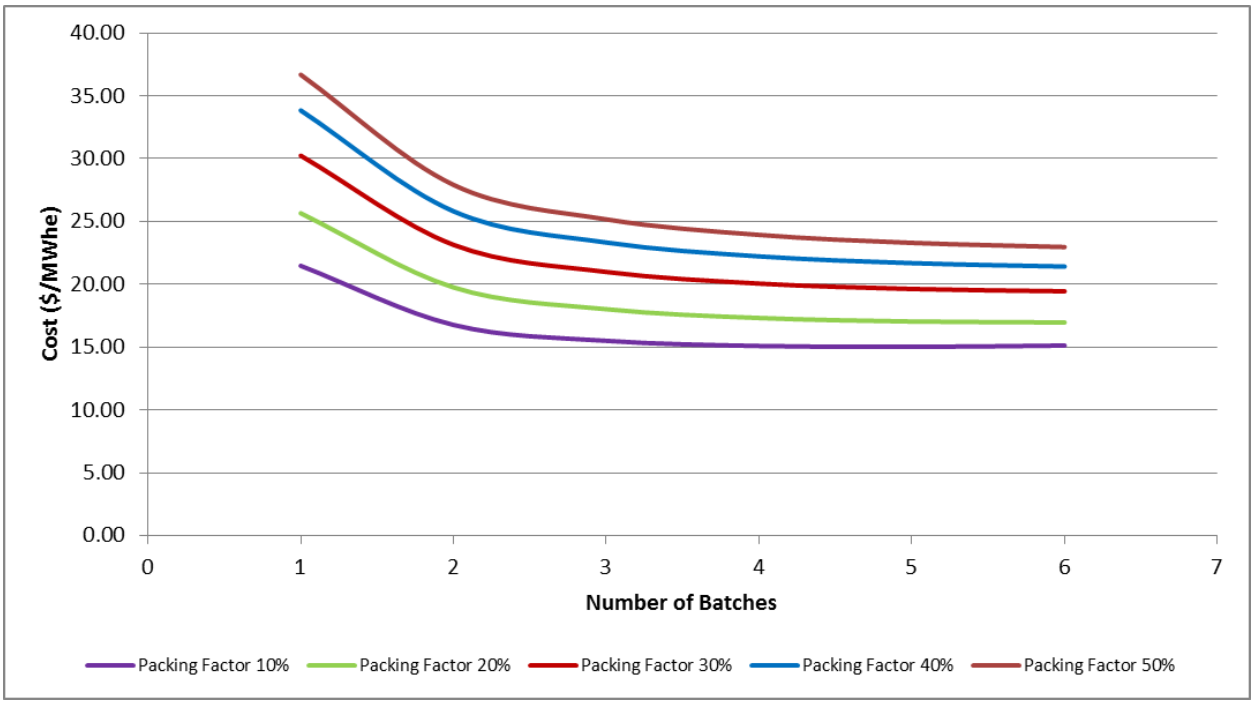


Figure 4-30: High fabrication cost, low outage cost, 19.75% enrichment

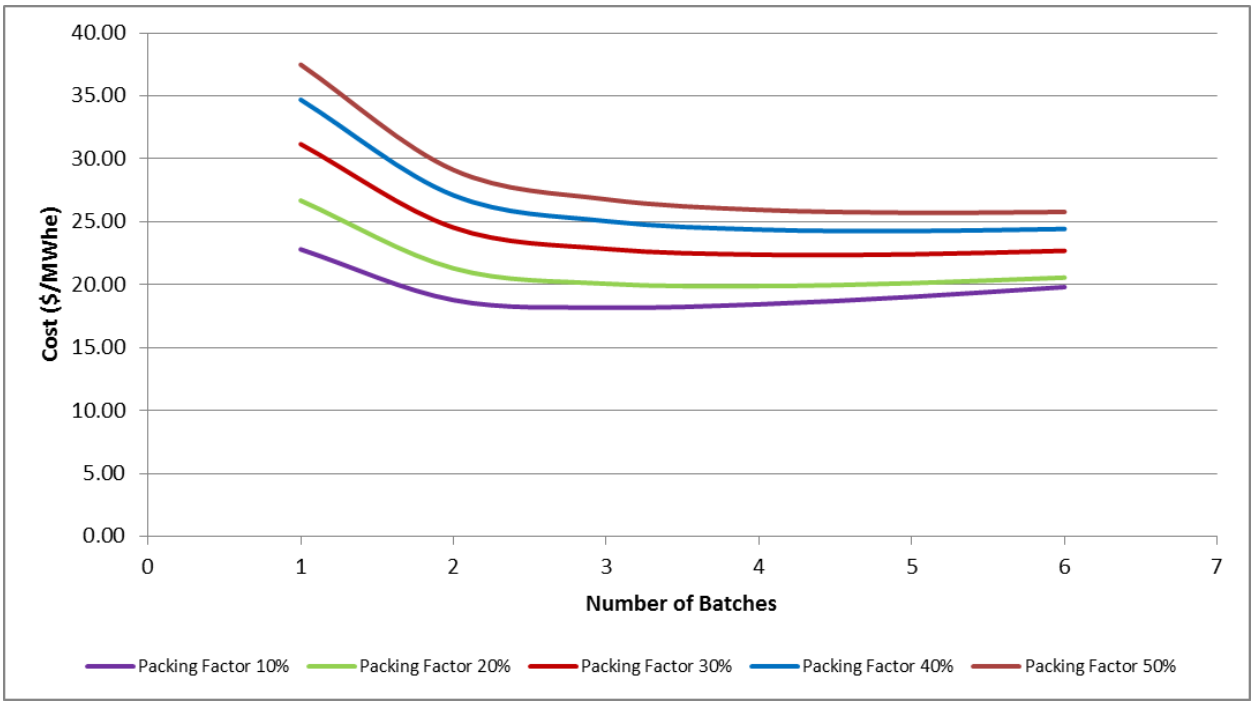


Figure 4-31: High fabrication cost, high outage cost, 19.75% enrichment

Based on the above figures, it can be observed that in most cases the lower packing factors have lower costs. The only exception to this observation is in the case of a larger number of batches (3 or more) and a high outage cost.

These results are useful for determining the limitations of the reactor in addition to providing an estimate of cost based on a variety of parameters. The results may not be perfect but they still can be used to narrow down future research by ruling out impractical and prohibitively expensive configurations.

## 4.4. Lithium Enrichment

The natural isotopic concentrations for lithium are 7.5% Li-6 and 92.5% Li-7. The lithium used in the FLiBe coolant of the LSCR is enriched because of the properties associated with Li-6. A main issue is related to the large absorption cross section inherent to Li-6. The high cross section reduces the neutrons available for fission and greatly affects the system keff. For the studies performed, the Li-7 enrichment was varied to include an enrichment of 99.995% which is specified by ORNL, several lower enrichments, and a higher enrichment [10]. The main focus was to understand the practical limitations associated with the Li-7 enrichment and whether it can be used for beneficial purposes. The main idea was to determine whether a lower enrichment can be used at reactor start up so that the Li-6 isotope acts as a burnable absorber. In order for this to work, the Li-7 enrichment must converge to a higher enrichment than what was initially used to start the reactor and the time frame for convergence must be similar to the cycle length. Based on this, the main effort was focused on finding the value that the enrichment converges to and the time frame required for this convergence.

Initially, the studies on lithium enrichment were completed using the plank model and Li-7 enrichments of 92.500% (natural enrichment), 95.000%, 97.000%, 99.000%, and 99.990%, 99.995%, and 99.999%. These preliminary studies provided information on the practical limits of Li-7 enrichment and what types of effects different enrichments had on the system. Table 4.14 provides the values for the system $k_{inf}$ at each of the enrichments. These studies were performed using a 40% packing factor and 19.75% fuel enrichment.

Table 4.14: Lithium enrichment and $k_{inf}$

| Enrichment | $k_{inf}$ | Uncertainty | Run Time (min) |
|---|---|---|---|
| 92.500% | 0.41049 | 0.00014 | 663.77582 |
| 95.000% | 0.47122 | 0.00017 | 692.20251 |
| 97.000% | 0.58095 | 0.00019 | 701.63184 |
| 99.000% | 0.76577 | 0.00021 | 738.70917 |
| 99.990% | 1.15505 | 0.00021 | 796.97052 |
| 99.995% | 1.15891 | 0.00023 | 839.91449 |
| 99.999% | 1.16206 | 0.00020 | 802.74115 |

As seen in the table, there is a substantial decrease in the $k_{inf}$ at enrichments below 99.990%. Even at an enrichment of 99.000%, the system is significantly subcritical. The higher enrichments are much closer but a large difference can be observed in the $k_{inf}$ even by a variation as small as 0.005%. The following plots show $k_{inf}$ as a function of enrichment. The plot in Figure 4-32 shows data from all the enrichments while the plot shown in Figure 4-33 only shows the three highest enrichments.

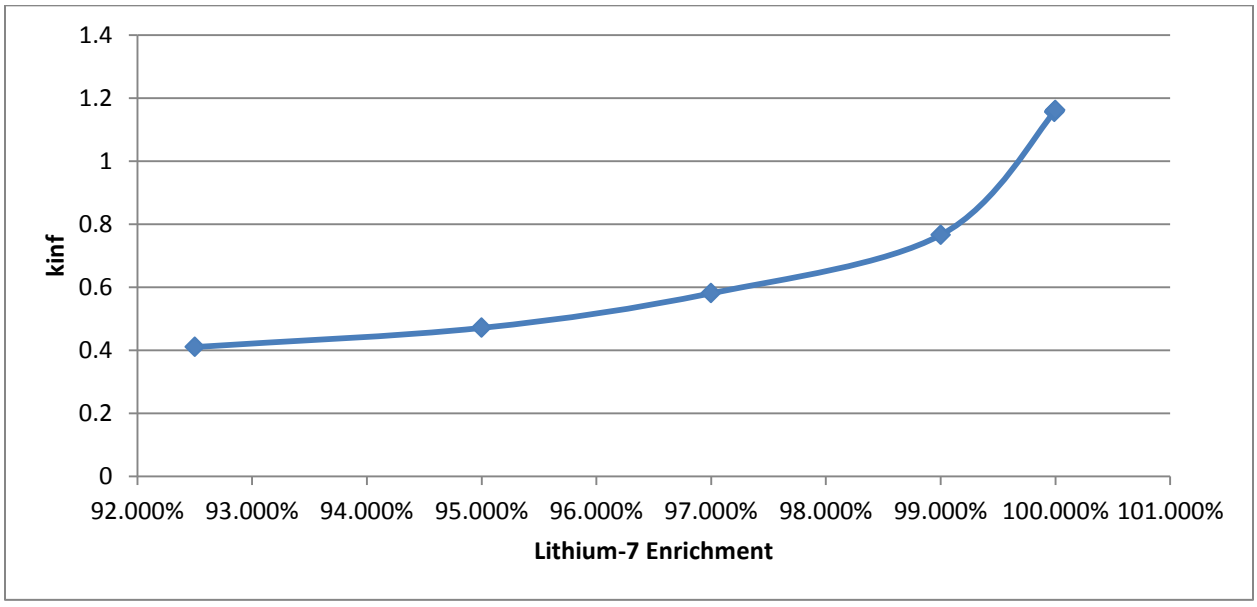


Figure 4-32: System $k_{inf}$ versus enrichment

From Figure 4-32 the $k_{inf}$ appears to follow an exponential curve as a function of the Li-7 enrichment. Based on this, a small increase in enrichment can contribute significantly to the $k_{inf}$ as long as the enrichment is already high.

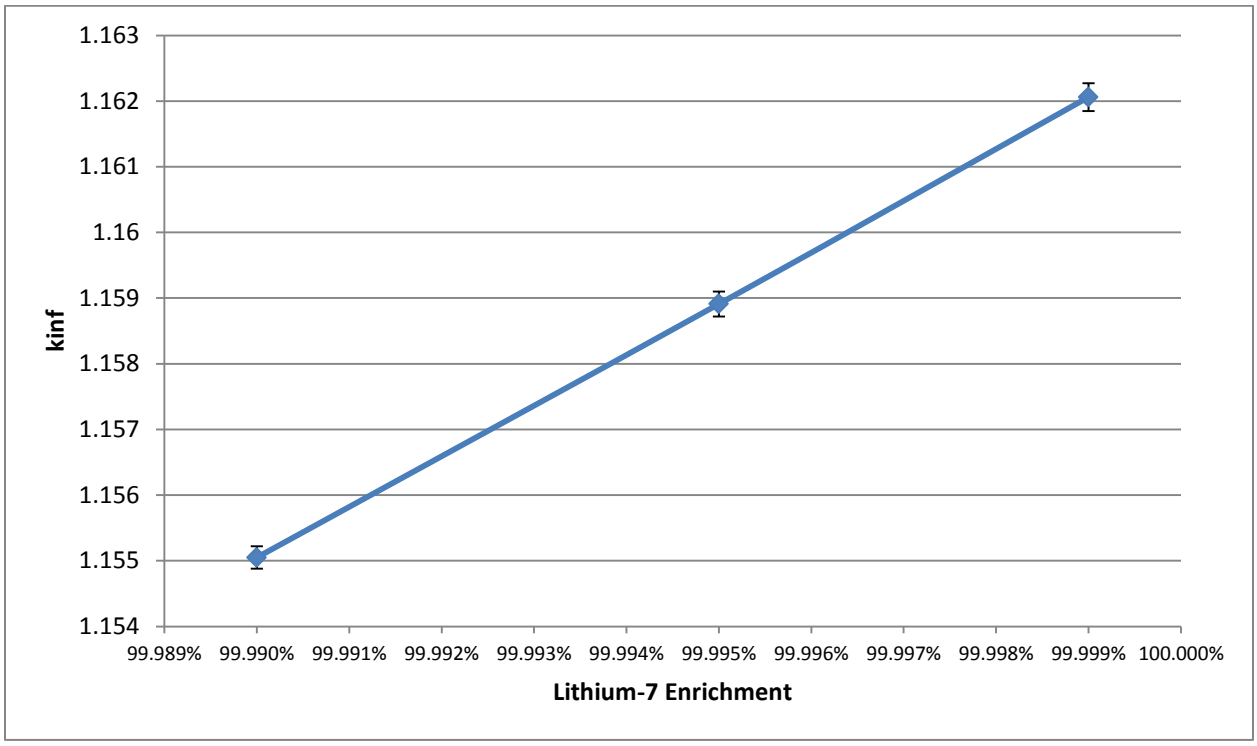


Figure 4-33: System $k_{inf}$ vs higher enrichments

The amount of absorption and fission within the systems also varies as a function of lithium enrichment. The most obvious differences can be seen between the natural enrichment and the 99.999% enrichment. However, there are noticeable differences between the highest three enrichments as well. Figure 4-34 and Figure 4-35 show the amount of neutron absorption in the FLiBe coolant when the Lithium is enriched to 99.999% in Li-7 and when natural enrichment is used. The amount of absorption is significantly higher at the lower enrichment and also encompasses a much larger range of energies.

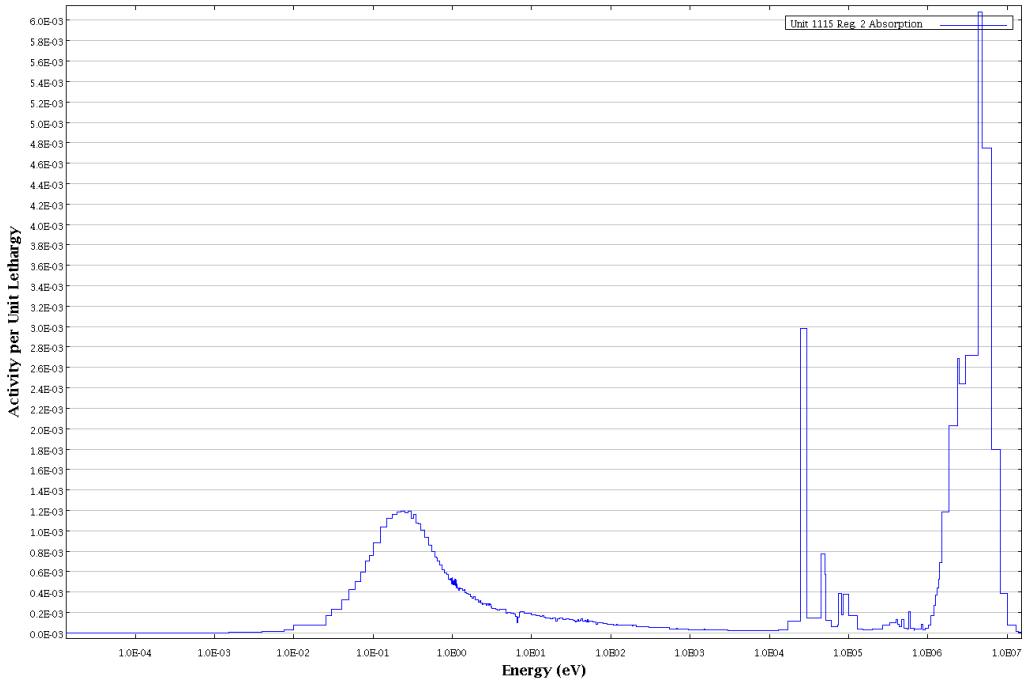


Figure 4-34: FLiBe absorption for 99.999% enrichment in Li-7

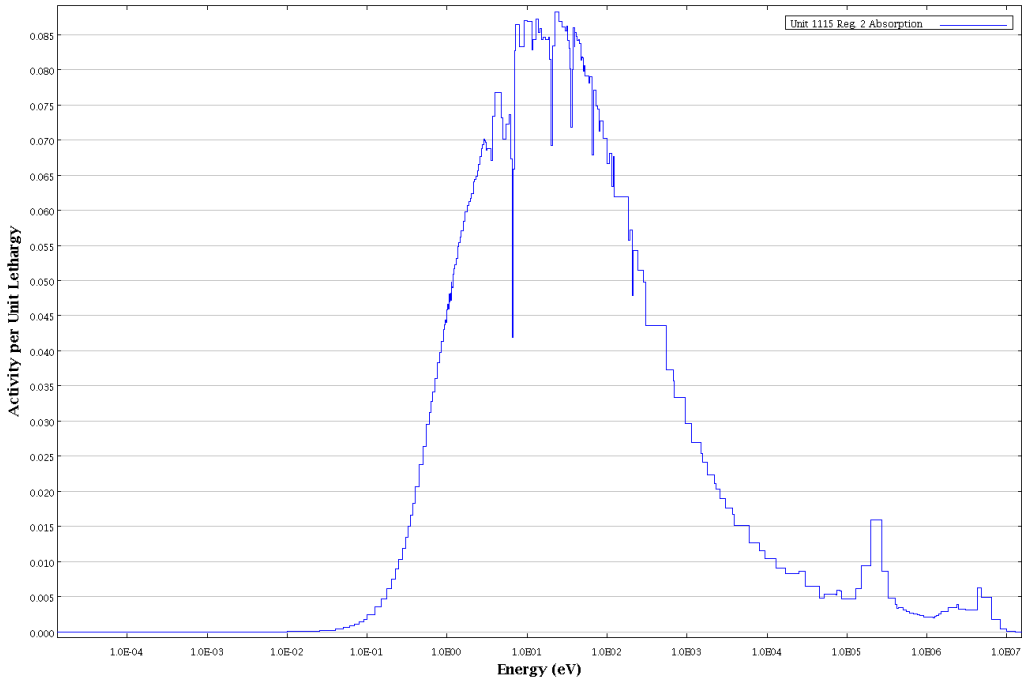


Figure 4-35: FLiBe absorption for natural isotopic abundance

Based on the initial results obtained using the plank model, a combination of two different methods were used to focus on finding the value that the enrichment converges to and the time frame required for convergence. The first method involved using the LSCR assembly model developed in SCALE and performing depletion on the fuel as well as the coolant at the different Li-7 enrichments. From the plank model studies, it had already been concluded that the enrichment must stay well above 99% for criticality, so the chosen enrichments were 99.500%, 99.900%, 99.990%, 99.995%, and 99.999%. Figure 4-36 below provides the results for the different enrichments in terms of change in $k_{inf}$ over time. It can be seen that a starting enrichment of 99.500% is much too low and that there is even a large change between 99.900% and 99.990%.

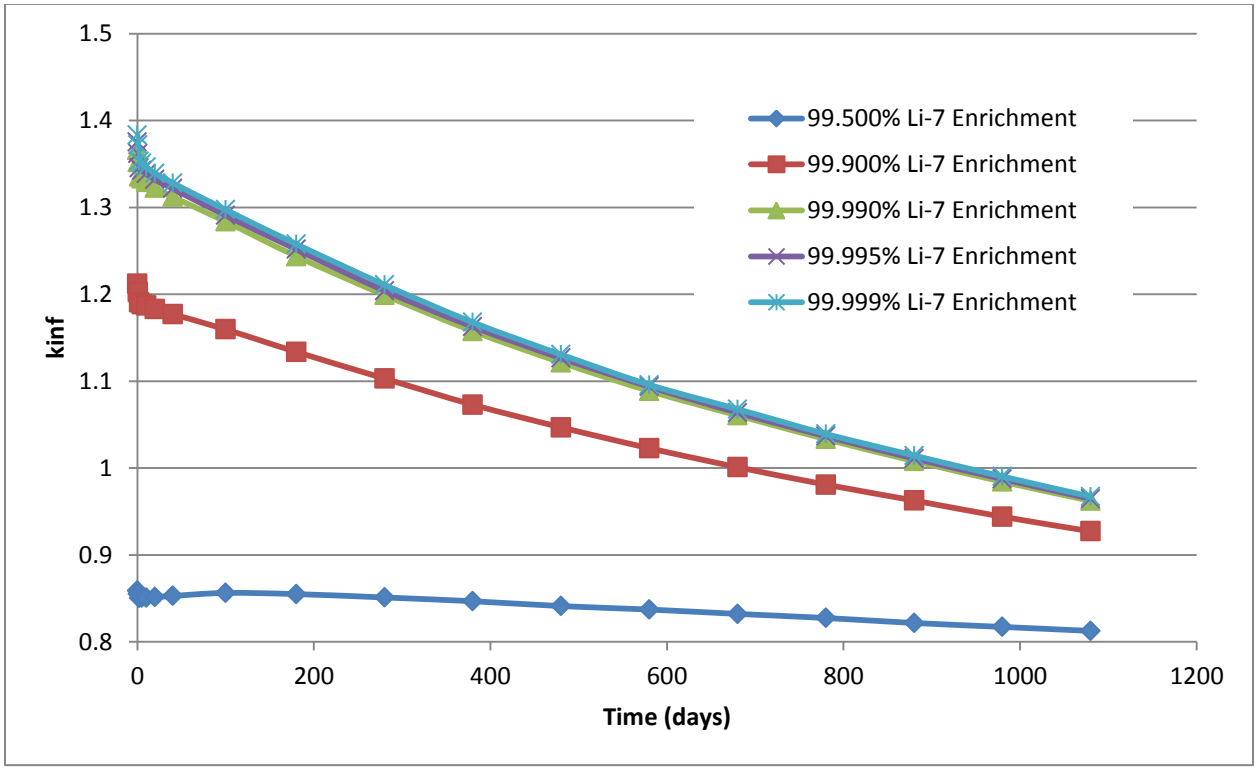


Figure 4-36: Depletion results for various enrichments

In order to determine the change in Li-7 enrichment, SCALE was set to output the masses of the Li-6 and Li-7 isotopes. From these numbers, calculating the enrichment involved performing a simple calculation of dividing the Li-7 mass by total mass of lithium. From this point the change in enrichment over time could be shown for the different starting enrichments. This is shown below in Figure 4-37 and only includes the starting enrichments that allow an initial critical state. The data shown indicates there is a value that the enrichments eventually converge to and it is near an enrichment of 99.995%.

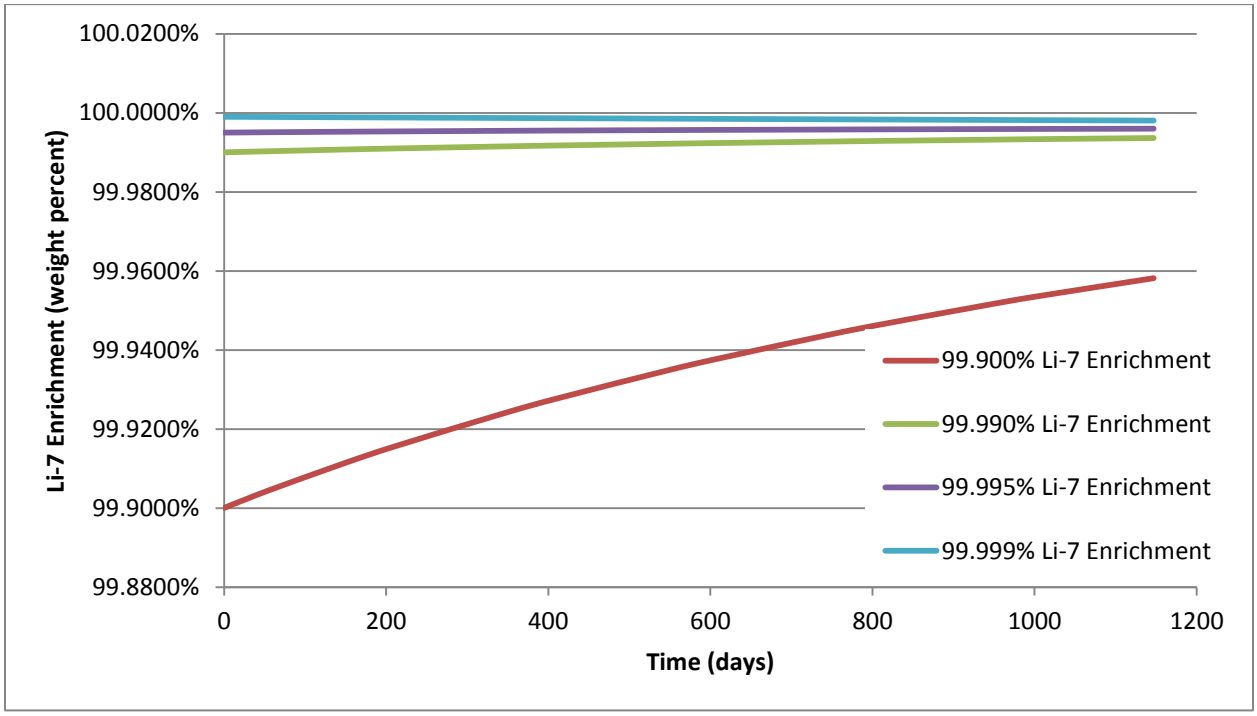


Figure 4-37: Change in Li-7 enrichment over time

In order to give more credibility to these results, an analytic model was developed in FORTRAN to calculate the change in enrichment over time. The program was made after developing a set of coupled rate equations to represent the atom densities associated with both Li-6 and Li-7. The equations only used the reactions that caused changes in atom densities by either addition or removal of atoms. The reactions cross sections used for Li-6 were (n,2n), (n,p),

(n,t), and (n,γ). For Li-7 the reactions cross sections were (n,2n), (n,2nα), (n,3nα), (n,d), and (n,γ). A two group cross section set was developed by performing a group collapse on the 238 group cross section library used for the SCALE depletions. A consistent set of cross sections was desired so that the results would be more likely to match up between the analytic model and SCALE. The benefit of the model is that it only takes seconds to run and the starting enrichment along with the amount of time to run can be readily changed. The two coupled rate equations used in the model are shown below.

$$\frac{dN_6}{dt} = -\emptyset_{th} * \sigma_{th,6} * N_6 - \emptyset_f * \sigma_{f,6} * N_6 + \emptyset_f * N_7 * \sigma_{(n,2n),7f}$$

$$\frac{dN_7}{dt} = -\emptyset_{th} * \sigma_{th7} * N_7 - \emptyset_f * \sigma_{f,7} * N_7 + \emptyset_{th} * N_6 * \sigma_{(n,\gamma),6th} + \emptyset_f * N_6 * \sigma_{(n,\gamma),6f}$$

After completing the analytic model, it was verified to strongly agree with the SCALE results. In order to show a comparison of the two methods, they have been both plotted in Figure 4-38 and it can be clearly seen that both methods provide similar results in terms of converged enrichment and the depletion time necessary to reach convergence.

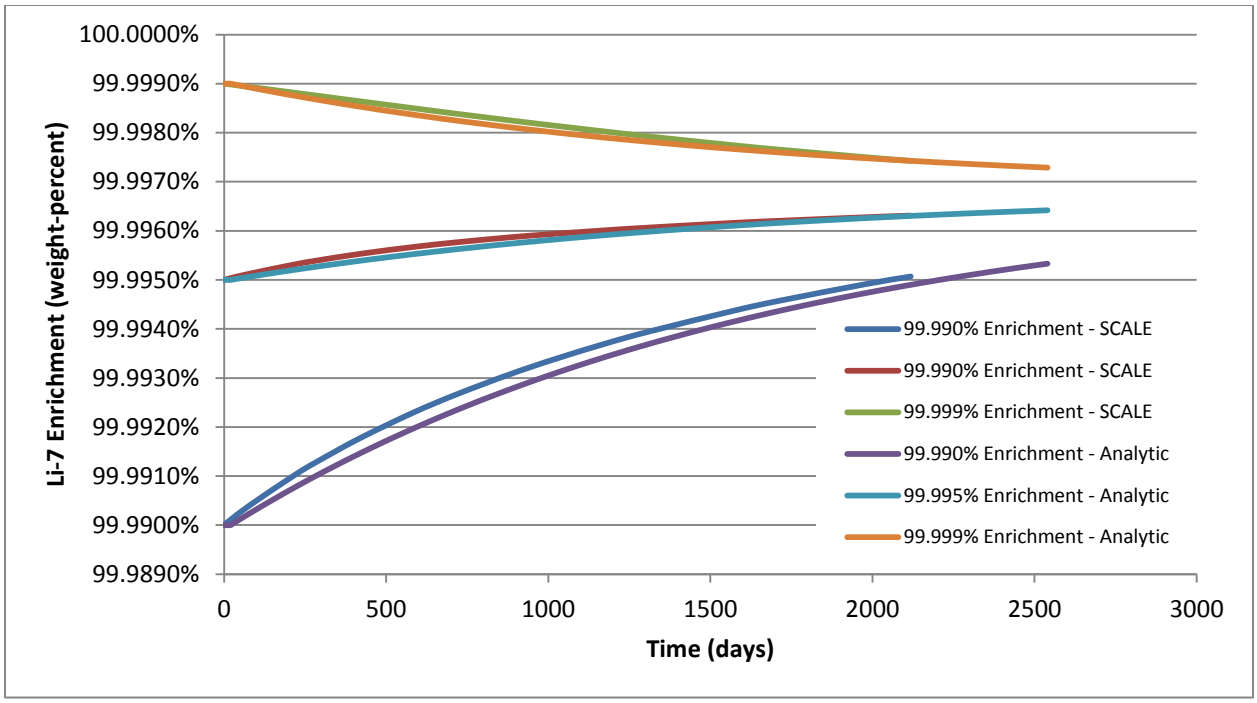


Figure 4-38: SCALE results and analytic model results

The plot from Figure 4-38 does not go out far enough to determine the exact converged enrichment but the data was extended using the analytic model and a final enrichment of 99.9969% was found. A simple extrapolation was done on the SCALE results versus performing the many depletion steps necessary and a similar enrichment was calculated. However, another characteristic shown by the previous figure is the large amount of time necessary for the enrichments to converge. The use of a lower enrichment of FLiBe as a burnable absorber would only be practical if the convergence was on the same time scale as the cycle length. From these results, it takes close to three years before any significant change occurs in the enrichment and even with this change it is not nearly enough to provide control over the reactor at startup.

Even though the results show that there is a value that the enrichment converges to, the amount of time required to reach steady state is much too long and the FLiBe coolant could not be utilized for reactivity control as a burnable absorber. Additionally, the results shown are a best

case scenario because only the coolant in the core has been considered. The actual design would have about 50% of the coolant in the core and 50% out of the core at all times. Assuming that the total amount of coolant would only receive an effective flux of about half of what was used to find the previous results, the time for convergence would take approximately twice as long.

Another issue related to having larger amounts of Li-6 in the coolant is the increased production of tritium by the absorption of thermal neutrons. Although Li-7 can undergo a similar reaction with high energy neutrons, this should be insignificant when dealing with a thermal reactor system. Tritium production is a problem due to its relatively long half-life and ability to permeate through many materials. Large amounts of tritium would create a safety risk because it would contaminate not only the coolant but also the systems used for circulation. The smallest amount of tritium production can be achieved through increasing the Li-7 enrichment as high as possible. However, when considering this option, other factors must be taken into consideration. The first thing to evaluate is enrichment cost. High enrichments may be possible but they may not be economically feasible. Furthermore, even if one begins with pure Li-7 in the coolant, (n, 2n) reactions will result in the creation of Li-6 over the lifetime of the reactor. The best choice of enrichment will be one that takes both economics and reactor safety into consideration and finds a balance between the two.

# CHAPTER 5: CONCLUSIONS

The Liquid Salt Cooled Reactor (LSCR) provides several potential benefits compared to pressurized water-cooled reactor systems. These include low operating pressure of the liquid salt coolant, the high burnup tolerance of the fuel, and the high operating temperatures which leads to increases in efficiency. However, due to inherently low heavy metal loading, the fuel cycle design presents specific challenges. The results found through this research done on the LSCR fuel design provide reasonable guidelines for expected costs and the type of configurations that should be avoided entirely. Additionally, knowledge was gained on methods for modeling the system not only accurately but also efficiently to reduce the required computing power.

The initial steps taken for this research showed how the TRISO fuel particles could be modeled more simply through a simple homogenization of the layers surrounding the fuel kernel. Since the layers surrounding the kernel are largely carbon based, the homogenization has limited effects neutronically. The result is a similar level of accuracy but a large reduction in run time when compared to an unaltered model. By determining this modeling simplification it was able to be applied to all additional models used to test other parameters.

A second simplification was performed by evaluating the equivalent 2D single assembly $k_{inf}$ values representing a 3D whole core $k_{eff}$ for different combinations of enrichment and packing factors in LSCR plank fuel. Whereas in an LWR this mainly accounts for the leakage of a finite core and typically may range between 1.02 and 1.03, this range is considerably different for the LSCR and reveals more interesting reactor physics. Due to undermoderation, the reflector is not only reflecting back some of the neutrons, but also thermalizing them and thus improving their thermal utilization, and the overall effect may even be positive, as indicated by the

equivalent value being less than unity in some cases. Specifically, the highest value reaches 1.02 and the lowest value corresponding to a 50% packing factor and 19.75% uranium enrichment is 0.990, indicating that the reflector blocks surrounding the core significantly affect the moderation of the system to the degree that they partly or fully compensate for the leakage. By performing this particular study, it allowed for the evaluation of 2D single assembly models to more accurately reflect the type of results that would be expected from a full core.

The primary parameters that were considered when looking at the fuel design included packing factor and fuel enrichment. The packing factor strongly influences moderation in the LSCR because it is graphite moderated system, so a decrease in packing factor leads to a proportional increase in the amount of moderating material available. However, a decrease in packing factor also reduces the total amount of fuel in the assembly. In order to compensate for this decrease in fuel, the fuel enrichment can be varied so that the most optimal design is achieved. The study of these two parameters provided greater insight into some practical limits on the fuel in terms of enrichment and packing factor. The most obvious point that can be made is that a uranium enrichment of 5% is not competitive in terms of performance when compared to other options.

Although these results help narrow down the possible fuel options, more detailed studies were performed using these results by developing a simple fuel cycle cost (FCC) model that could be used to compare the different options from an economic standpoint. In order to keep the cost model simplified, certain assumptions were made. First, the time value of money was neglected. Additionally, while the cost of outages was considered, the costs related to the outage duration were ignored.

The analysis based on the FCC model shows that a uranium enrichment of 5% is much more expensive than the other options in the majority of the different configurations. As a result, the use of an enrichment of 5% or lower is probably not feasible for this particular design. However, the other uranium enrichments are often pretty competitive against one another, but in general the 19.75% enrichment appears to be most economical in the different cases.

These results are useful for determining the limitations of the reactor in addition to providing an estimate of cost based on a variety of parameters. The results should not be considered definitive but are adequate enough to narrow down the types of configurations that should be considered as fuel design options for the LSCR. Additionally, knowledge was gained on methods for modeling the system not only accurately but also efficiently to reduce the required computing power and time.

The final parameter of interest for this thesis was the lithium enrichment of the FLiBe coolant. In general, the reactor design requires for the enrichment of lithium due to the high absorption cross section of Li-6. For the study performed, the Li-7 enrichment was varied to include an enrichment of 99.995%, several lower enrichments, and a higher enrichment. The main focus was to understand the practical limitations associated with the Li-7 enrichment and whether it can be used for beneficial purposes. The main idea was to determine whether a lower enrichment can be used at reactor start up so that the Li-6 isotope acts as a burnable absorber. The use of a lower enrichment of FLiBe as a burnable absorber would only be practical if the convergence was on the same time scale as the cycle length. From the results, it takes close to three years before any significant change occurs in the enrichment and even with this change it is not nearly enough to provide control over the reactor at startup.

Even though the results show that there is a value that the enrichment converges, the amount of time required to reach steady state is much too long and the FLiBe coolant could not be utilized for reactivity control as a burnable absorber. Additionally, the results shown are a best case scenario because only the coolant in the core has been considered. The actual design would have about 50% of the coolant in the core and 50% out of the core at all times. Assuming that the total amount of coolant would only receive an effective flux of about half of what was used to find the previous results, the time for convergence would take approximately twice as long.

Another issue related to having larger amounts of Li-6 in the coolant is the increased production of tritium by the absorption of thermal neutrons. Although Li-7 can undergo a similar reaction with high energy neutrons, this should be insignificant when dealing with a thermal reactor system. Tritium production is a problem due to its relatively long half-life and ability to permeate through many materials. Large amounts of tritium would create a safety risk because it would contaminate not only the coolant but also the systems used for circulation. The best choice of enrichment will be one that takes both economics and reactor safety into consideration and finds a balance between the two.

Several different questions have been answered through this research, but there is additional future work that could be conducted based on the knowledge that has been obtained. Specifically, more focus could be placed on determining an optimum fuel design based on the narrowed range of options for packing factor and fuel enrichment. The first step to this approach would involve creating additional and more detailed models to better understand the physics associated with different scenarios. One manner in which this could be accomplished is by using a method to allow for continuous energy (CE) depletion. The models used for this research used multigroup depletion because CE depletion is not an option in SCALE6.1. There is most likely

some bias between multigroup and CE depletion that could be adjusted for by applying either a reactivity-equivalent transform (RPT) or appropriate Dancoff factors.

Additionally, further emphasis could be placed on producing a more detailed fuel cycle cost model. This could be accomplished by applying a non-linear reactivity method in addition to reducing the uncertainties related to the costs for plank TRISO fuel fabrication and outages through additional research.

# APPENDIX A: MATERIAL COMPOSITIONS

Table A.1: Fuel composition

| Fuel Kernel - 19.75% Enrichment | | | |
|---|---|---|---|
| **Material** | **Number Density (atoms/cm³)** | **Temperature (K)** | **Density (g/cc)** |
| U-234 | 3.7861E+19 | 1200 | 1.47E-02 |
| U-235 | 4.9346E+21 | 1200 | 1.93E+00 |
| U-238 | 1.9760E+22 | 1200 | 7.81E+00 |
| O-16 | 3.5283E+22 | 1200 | 9.37E-01 |
| C-graphite | 1.0576E+22 | 1200 | 2.11E-01 |
| | | Total Density | 10.90 |

Table A.2: Porous buffer composition

| Porous Buffer | | | |
|---|---|---|---|
| **Material** | **Number Density (atoms/cm³)** | **Temperature (K)** | **Density (g/cc)** |
| C-graphite | 5.0140E+22 | 1200 | 1.00E+00 |
| | | Total Density | 1.00 |

Table A.3: Inner pyrolitic carbon composition

| Inner Pyrolytic Matrix | | | |
|---|---|---|---|
| **Material** | **Number Density (atoms/cm³)** | **Temperature (K)** | **Density (g/cc)** |
| C-graphite | 9.5265E+22 | 1200 | 1.90E+00 |
| | | Total Density | 1.90 |

Table A.4: SiC composition

| Silicon Carbide | | | |
|---|---|---|---|
| **Material** | **Number Density (atoms/cm³)** | **Temperature (K)** | **Density (g/cc)** |
| C-graphite | 4.8062E+22 | 1200 | 9.59E-01 |
| Si | 4.8062E+22 | 1200 | 2.24E+00 |
| | | Total Density | 3.20 |

Table A.5: Outer pyrolitic composition

| Outer Pyrolytic Matrix | | | |
|---|---|---|---|
| **Material** | **Number Density (atoms/cm³)** | **Temperature (K)** | **Density (g/cc)** |
| C-graphite | 9.3761E+22 | 1200 | 1.87E+00 |
| | | Total Density | 1.87 |

Table A.6: Matrix material compostion

| Matrix Material | | | |
|---|---|---|---|
| **Material** | **Number Density (atoms/cm³)** | **Temperature (K)** | **Density (g/cc)** |
| C-graphite | 7.9722E+22 | 1200 | 1.59E+00 |
| | | Total Density | 1.59 |

Table A.7: Sleeve/Cladding composition

| Sleeve/Cladding | | | |
|---|---|---|---|
| **Material** | **Number Density (atoms/cm³)** | **Temperature (K)** | **Density (g/cc)** |
| C-graphite | 7.9722E+22 | 1000 | 1.59E+00 |
| | | Total Density | 1.59 |

Table A.8: FLiBe coolant composition

| Coolant 2LiF-BeF2 - 99.995% Li-7 Enriched | | | |
|---|---|---|---|
| **Material** | **Number Density (atoms/cm³)** | **Temperature (K)** | **Density (g/cc)** |
| Li-6 | 1.3834E+18 | 948.15 | 1.38E-05 |
| Li-7 | 2.3721E+22 | 948.15 | 2.76E-01 |
| Be | 1.1861E+22 | 948.15 | 1.77E-01 |
| F | 4.7444E+22 | 948.15 | 1.50E+00 |
| | | Total Density | 1.95 |

# APPENDIX B: LITHIUM ENRICHMENT CHARTS AND FIGURES FOR PLANK STUDY

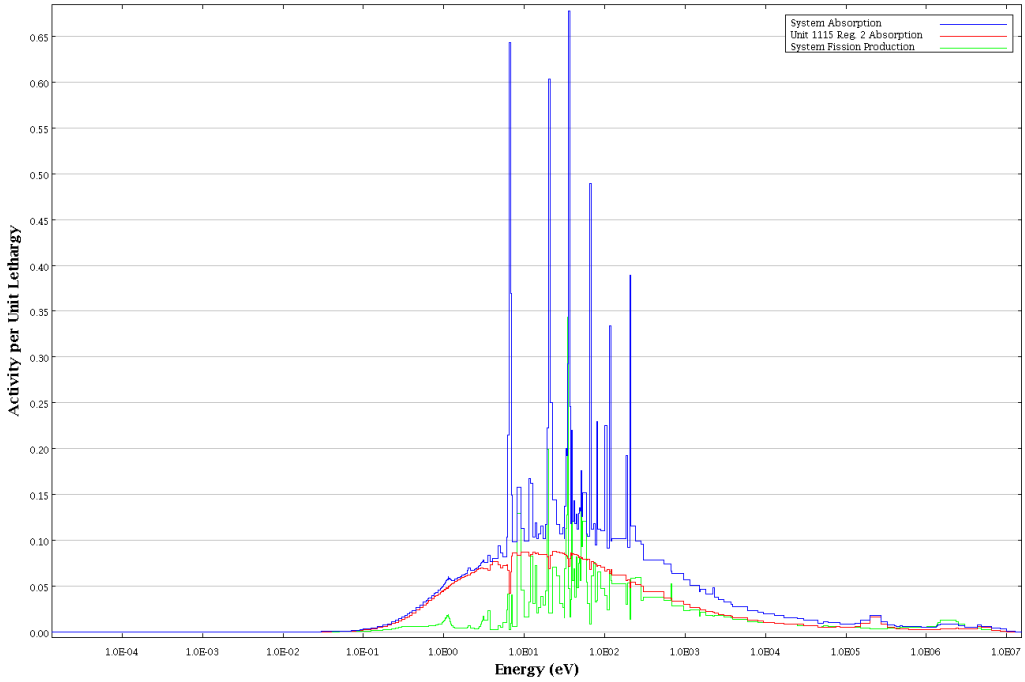


Figure B-1: Fission and absorption for natural enrichment

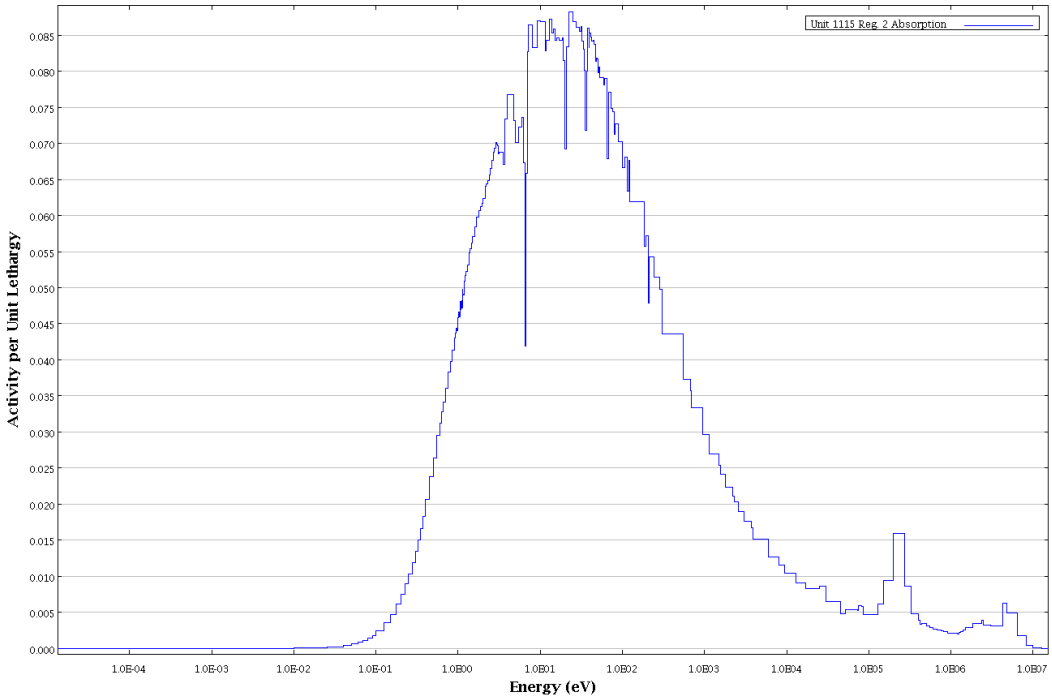


Figure B-2: FLiBe absorption for natural enrichment

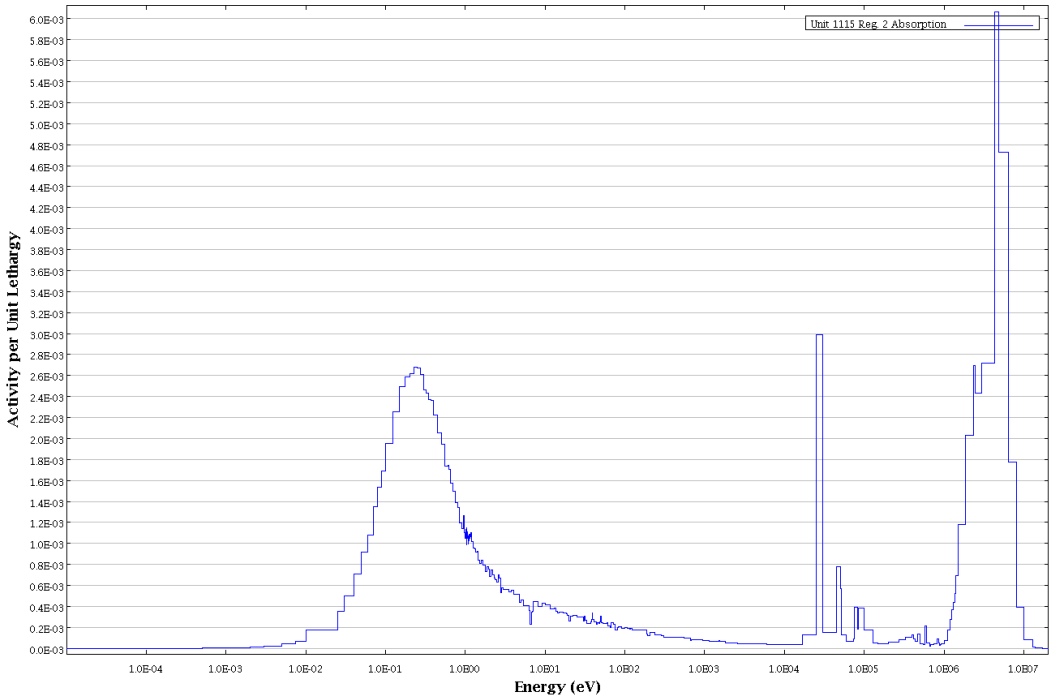


Figure B-3: FLiBe absorption for 99.990% enrichment

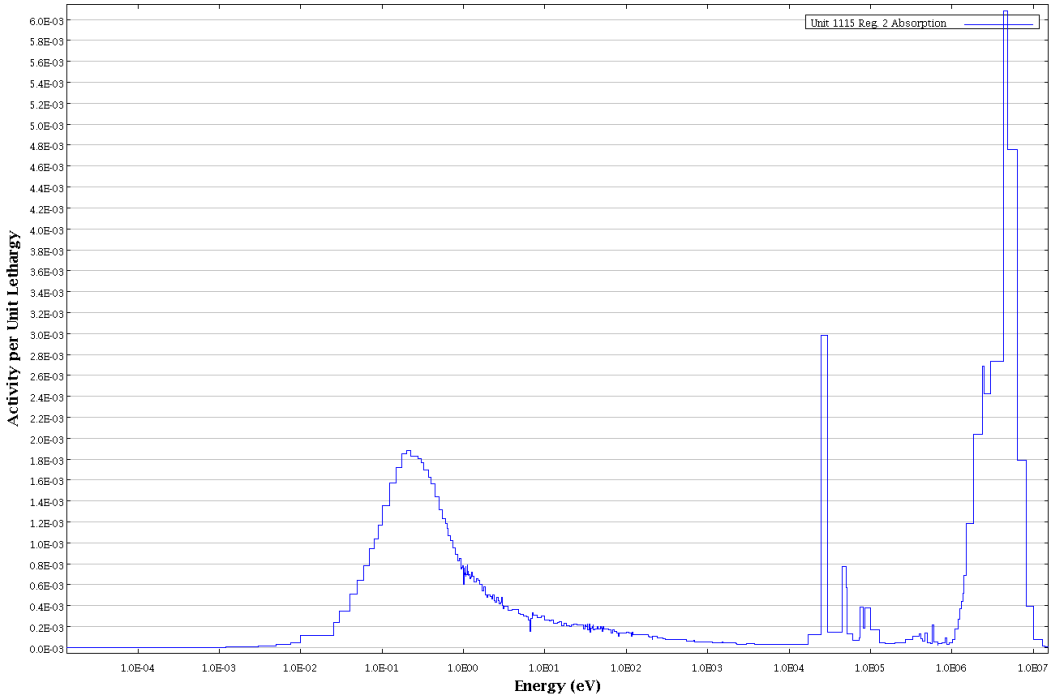


Figure B-4: FLiBe absorption for 99.995% enrichment

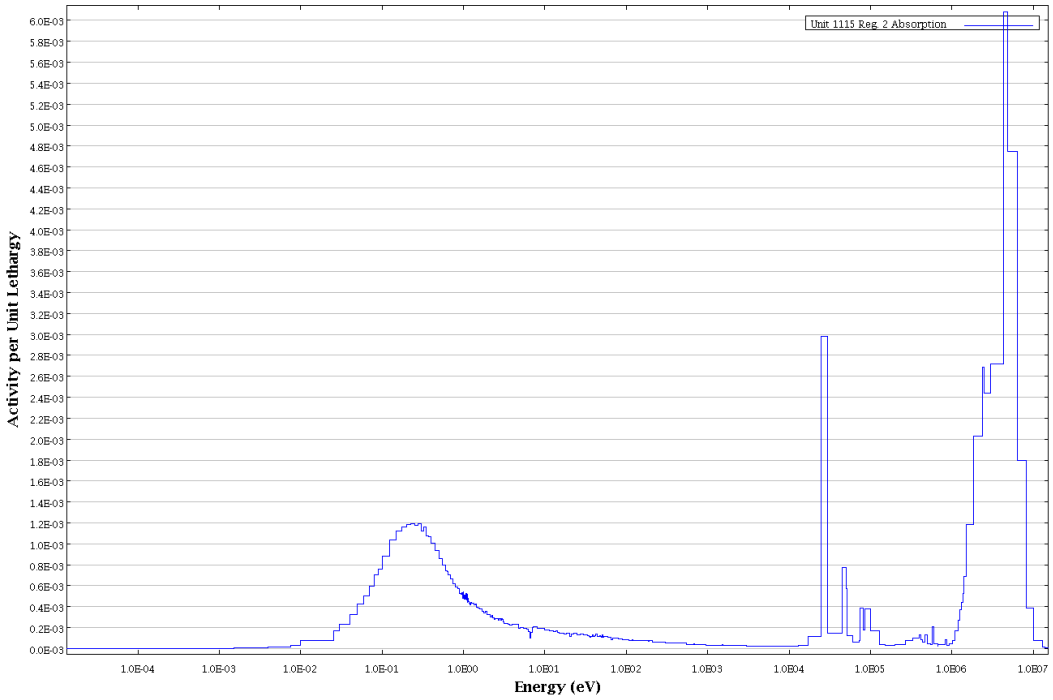


Figure B-5: FLiBe absorption for 99.999% enrichment

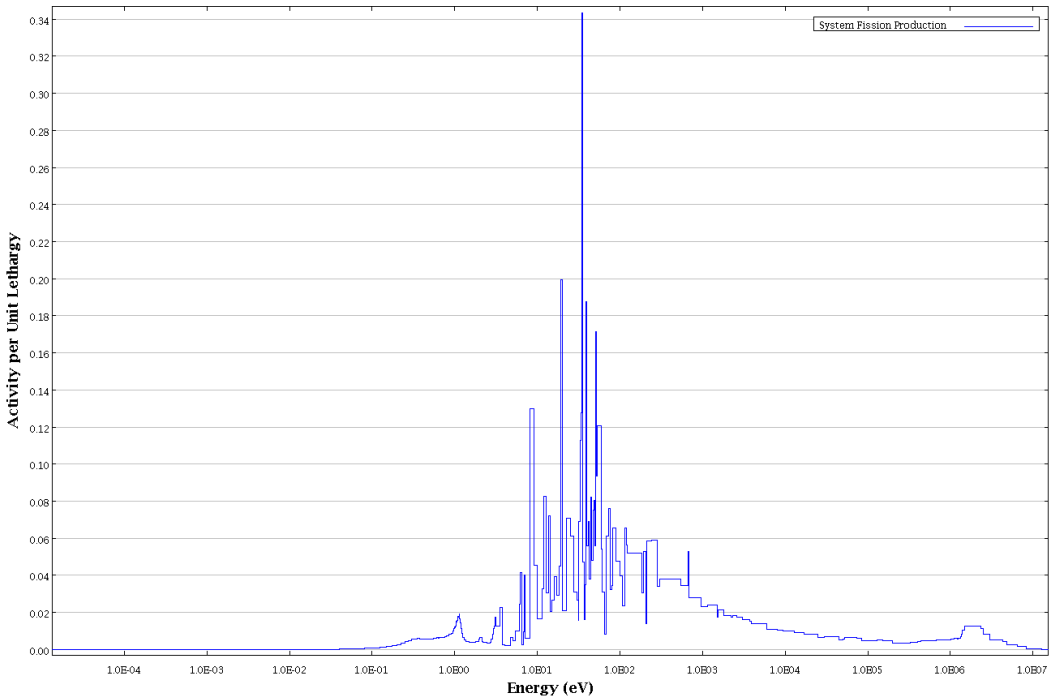


Figure B-6: System fission for natural enrichment

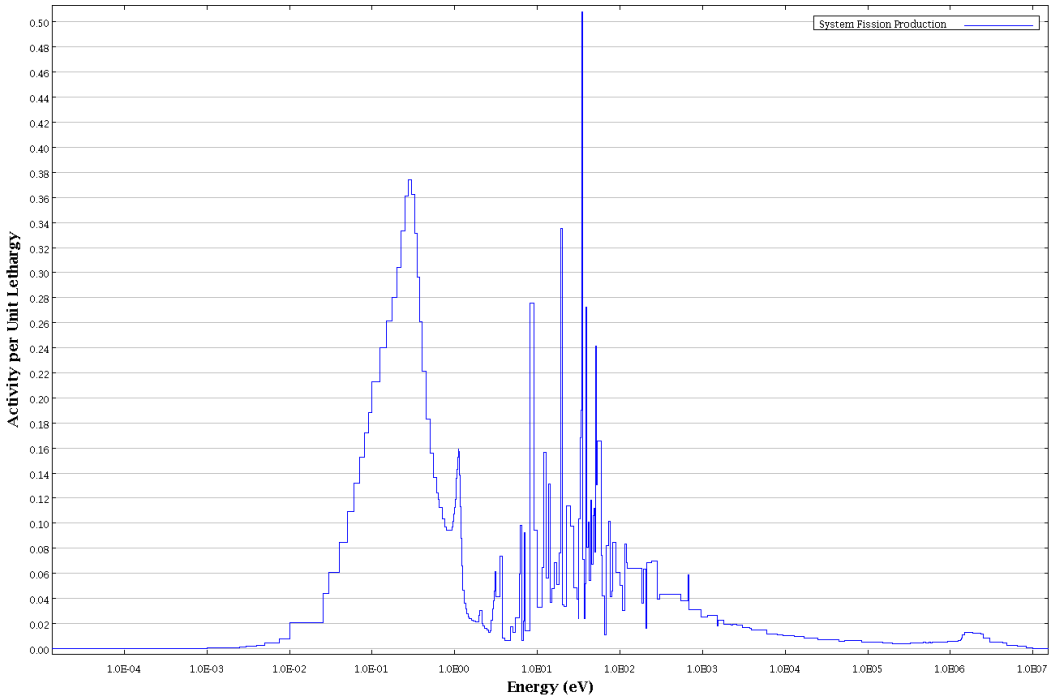


Figure B-7: System fission for 99.990% enrichment

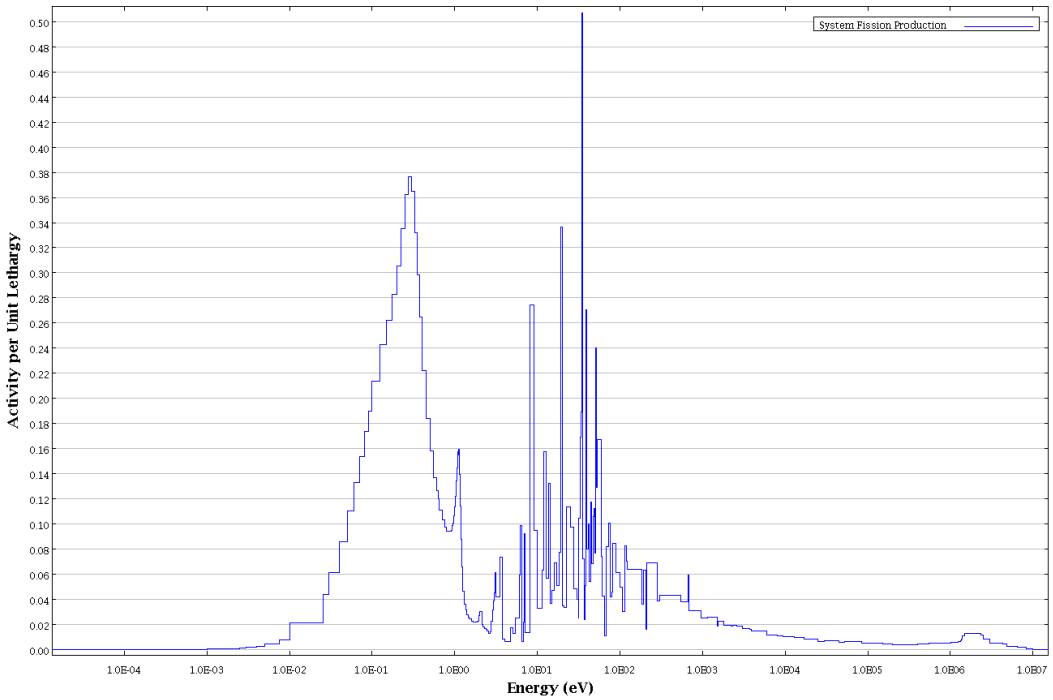


Figure B-8: System fission for 99.995% enrichment

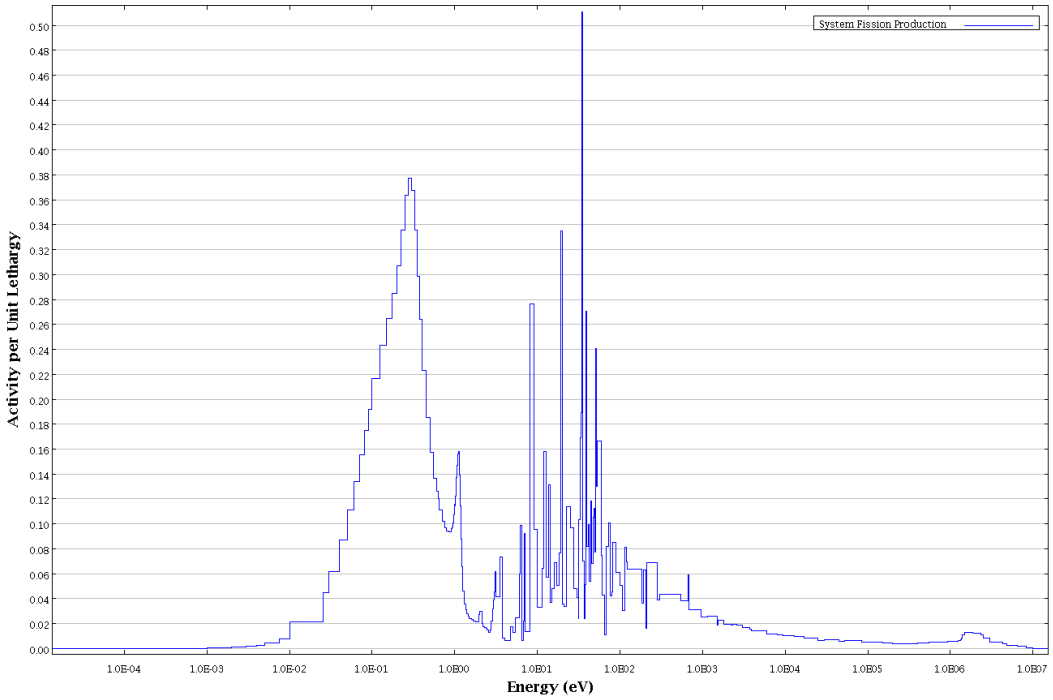


Figure B-9: System fission for 99.999% enrichment

Table B.1: Fission and absorption data for natural

| Unit | Region | Fissions | n2n | n3n | Absorptions |
|---|---|---|---|---|---|
| | | 3.605E-01 | 1.050E-02 | 1.369E-06 | 1.005E+00 |
| | UCO | 3.605E-01 | 2.122E-04 | 1.369E-06 | 4.249E-01 |
| **TRISO** | Buffer and IPyC | 0.000E+00 | 0.000E+00 | 0.000E+00 | 8.643E-05 |
| **Particle** | SiC | 0.000E+00 | 3.094E-07 | 0.000E+00 | 9.920E-04 |
| | IPyC and Matrix | 0.000E+00 | 0.000E+00 | 0.000E+00 | 4.297E-04 |
| **FLiBe** | - | 0.000E+00 | 1.029E-02 | 0.000E+00 | 5.779E-01 |

Table B.2: Fission and absorption data for 99.990%

| Unit | Region | Fissions | n2n | n3n | Absorptions |
|---|---|---|---|---|---|
| | | 1.215E+00 | 1.051E-02 | 1.133E-06 | 1.005E+00 |
| | UCO | 1.215E+00 | 2.102E-04 | 1.133E-06 | 9.839E-01 |
| **TRISO** | Buffer and IPyC | 0.000E+00 | 0.000E+00 | 0.000E+00 | 2.338E-04 |
| **Particle** | SiC | 0.000E+00 | 2.902E-07 | 0.000E+00 | 2.748E-03 |
| | IPyC and Matrix | 0.000E+00 | 0.000E+00 | 0.000E+00 | 1.098E-03 |
| **FLiBe** | - | 0.000E+00 | 1.030E-02 | 0.000E+00 | 1.497E-02 |

Table B.3: Fission and absorption data for 99.995%

| Unit | Region | Fissions | n2n | n3n | Absorptions |
|---|---|---|---|---|---|
| | | 1.220E+00 | 1.057E-02 | 1.230E-06 | 1.005E+00 |
| | UCO | 1.220E+00 | 2.119E-04 | 1.230E-06 | 9.867E-01 |
| **TRISO** | Buffer and IPyC | 0.000E+00 | 0.000E+00 | 0.000E+00 | 2.323E-04 |
| **Particle** | SiC | 0.000E+00 | 2.976E-07 | 0.000E+00 | 2.757E-03 |
| | IPyC and Matrix | 0.000E+00 | 0.000E+00 | 0.000E+00 | 1.097E-03 |
| **FLiBe** | - | 0.000E+00 | 1.036E-02 | 0.000E+00 | 1.229E-02 |

Table B.4: Fission and absorption data for 99.999%

| Unit | Region | Fissions | n2n | n3n | Absorptions |
|---|---|---|---|---|---|
| | | 1.224E+00 | 1.054E-02 | 1.335E-06 | 1.005E+00 |
| | UCO | 1.224E+00 | 2.107E-04 | 1.335E-06 | 9.888E-01 |
| **TRISO** | Buffer and IPyC | 0.000E+00 | 0.000E+00 | 0.000E+00 | 2.403E-04 |
| **Particle** | SiC | 0.000E+00 | 2.894E-07 | 0.000E+00 | 2.756E-03 |
| | IPyC and Matrix | 0.000E+00 | 0.000E+00 | 0.000E+00 | 1.109E-03 |
| **FLiBe** | - | 0.000E+00 | 1.033E-02 | 0.000E+00 | 1.010E-02 |

# APPENDIX C: SAMPLE SCALE INPUT FILE FOR ASSEMBLY MODEL

```
=t6-depl parm=(centrm,addnux=4)
LSCR - Burnup of LSCR Assembly Model
v7-238
' ---------- Materials ----------
' ------------------------------
read composition
' ---- Fuel, 19.75% Enrichment ----
'
U-234       1  0  3.7861e-05  1200    end
U-235       1  0  0.00493458  1200    end
U-238       1  0  0.0197601   1200    end
O-16        1  0  0.0352829   1200    end
C-graphite  1  0  0.0105760   1200    end
'
' ---- Buffer, IPyC, Silicon Carbide, OPyC, Matrix Material ----
'
C-graphite  2  0  0.076304410   1200    end
Si          2  0  0.003755145   1200    end
'
' ---- Graphite Meat ----
'
C-graphite  7  0  7.97223e-02 1200    end
'
' ---- Sleeve/Cladding on Plate ----
C-graphite  8  0  7.97223e-02 1000    end
'
' ---- FLiBe Coolant (99.995% enriched Li-7) ----
Li-6        9  0  1.383440E-06 948.15  end
Li-7        9  0  2.372050E-02 948.15  end
Be          9  0  0.0118609   948.15  end
F           9  0  0.0474437   948.15  end
'
' ---- Graphite in Fuel Block ----
C-graphite  10  0  9.82741e-02 948.15  end
'
end composition

' ---- Cell data ----
' -------------------
read celldata
latticecell sphsquarep
fuelr=0.02135 1  pitch=0.0926537 2 end
end celldata

' ---- Depletion and Burndata ----
' --------------------------------
read depletion 1 9 end depletion
read burndata
```

```
49    power=98.2068  burn=1    down=0  nlib=1  end
50    power=98.2068  burn=2    down=0  nlib=1  end
51    power=98.2068  burn=4    down=0  nlib=1  end
52    power=98.2068  burn=6    down=0  nlib=1  end
53    power=98.2068  burn=14   down=0  nlib=1  end
54    power=98.2068  burn=26   down=0  nlib=1  end
55    power=98.2068  burn=94   down=0  nlib=1  end
56    power=98.2068  burn=66   down=0  nlib=1  end
57    power=98.2068  burn=134  down=0  nlib=1  end
58    power=98.2068  burn=66   down=0  nlib=1  end
59    power=98.2068  burn=134  down=0  nlib=1  end
60    power=98.2068  burn=66   down=0  nlib=1  end
61    power=98.2068  burn=134  down=0  nlib=1  end
62    power=98.2068  burn=66   down=0  nlib=1  end
63    power=98.2068  burn=134  down=0  nlib=1  end
64    power=98.2068  burn=66   down=0  nlib=1  end
65    power=98.2068  burn=134  down=0  nlib=1  end
66    end burndata
67
68    ' ---- Opus ----
69    ' --------------
70    read opus
71    matl=1 9 end
72    time=days
73    typarms=nucl
74    units=gram
75    title=Masses of Actinides and Fission Products
76    symnuc=u-234 u-235 u-236 u-237 u-238 pu-238 pu-239
77    pu-240 pu-241 pu-242 pu-243 np-237 am-241 am-242m am-243
78    cm-242 cm-243 cm-244 cm-245 cm-246
79    sr-90 i-131
80    cs-133 cs-134 cs-135 cs-137 nd-143 nd-144 nd-145 nd-146
81    nd-148 nd-150 pm-147 sm-147 sm-148 sm-149 sm-150 sm-151
82    sm-152 eu-153 sm-154 eu-154 gd-154 eu-155 gd-155 end
83    new case
84    time=days
85    typarms=elements
86    units=curies
87    symnuc= Ac Ag Al Am Ar As At Au B  Ba Be Bi Bk Br C  Ca Cd Ce Cf Cl
88    Cm Co Cr Cs Cu Dy Er Es Eu F  Fe Fr Ga Gd Ge H  He Hf Hg Ho
89    I  In Ir K  Kr La Li Lu Mg Mn Mo N  Na Nb Nd Ne Ni Np O  Os
90    P  Pa Pb Pd Pm Po Pr Pt Pu Ra Rb Re Rh Rn Ru S  Sb Sc Se Si
91    Sm Sn Sr Ta Tb Tc Te Th Ti Tl Tm U  V  W  Xe Y  Yb Zn Zr end
92    new case
93    time=days
94    typarms=elements
95    units=watts
96    symnuc= Ac Ag Al Am Ar As At Au B  Ba Be Bi Bk Br C  Ca Cd Ce Cf Cl
97    Cm Co Cr Cs Cu Dy Er Es Eu F  Fe Fr Ga Gd Ge H  He Hf Hg Ho
98    I  In Ir K  Kr La Li Lu Mg Mn Mo N  Na Nb Nd Ne Ni Np O  Os
99    P  Pa Pb Pd Pm Po Pr Pt Pu Ra Rb Re Rh Rn Ru S  Sb Sc Se Si
```

```
Sm Sn Sr Ta Tb Tc Te Th Ti Tl Tm U  V  W  Xe Y  Yb Zn Zr end
new case
time=days
typarms=nucl
units=gram
title=Mass of Tritium and Lithium Isotopes
symnuc= h-3 li-6 li-7 end
new case
time=days
typarms=nucl
units=curies
title=Radioactivity of Tritium
symnuc= h-3 end
end opus

read model
read parameter
cfx=yes
flx=yes
gen=250
nsk=25
npg=10000
sig=0.0001
tba=100
htm=no
plt=yes
end parameter

' ---------- Geometry ----------
' ----------------------------
read geometry
unit 1110
com="Graphite Spacer Cube"
cuboid 1  0.0463269  -0.0463269  0.0463269  -0.0463269  0.0463269  -0.0463269
media 2 1 1
boundary 1
'
unit 1111
com="TRISO Fuel Particle"
sphere 1  0.02135
cuboid 2  0.0463269  -0.0463269  0.0463269  -0.0463269  0.0463269  -0.0463269
media 1 1 1
media 2 1 2 -1
boundary 2
'
unit 1112
com="Fuel Portion of Fuel Plate"
parallelepiped 1  21.47743  0.748911263  9.26538       30        0        0
array 1112 1  place 1 1 1 0.0463269 0.0463269 0.0463269
boundary 1
'
```

```
unit 1113
com="Graphite center with fuel plates"
parallelepiped 1  21.47743  2.71354626519  9.26538       30        0        0
hole 1112  origin  x=0 y=0 z=0
hole 1112  origin  x=0.982317501 y=1.7014238209 z=0
media 7 1 1
boundary 1
'
unit 1114
com="Complete Fuel Plate"
parallelepiped 1  21.70837  2.944486  9.26538       30        0        0
hole 1113  origin  x=0.173205 y=0.1 z=0
media 8 1 1
boundary 1
'
unit 1115
com="Group of Six Fuel Plates"
parallelepiped 1  22.51666  22.51666      9.26538       30        0        0
hole 1114   origin  x=0.606218 y=0.35  z=0
hole 1114   origin  x=2.482606 y=3.6   z=0
hole 1114   origin  x=4.358995 y=6.85  z=0
hole 1114   origin  x=6.23583  y=10.1  z=0
hole 1114   origin  x=8.111771 y=13.35 z=0
hole 1114   origin  x=9.98816  y=16.6  z=0
media 9 1 1
boundary 1
'
'
global unit 1116
com="Fuel Assembly, 18 Fuel Plates, and Control Blade Slot"
hexprism    10 23.375 9.26538 0
hexprism    1  22.5   9.26538 0
hole  1115 rotate a1=210 origin x=-2.000000   y=23.67136103   z=0.
hole  1115 rotate a1=90  origin x=21.5        y=-10.10362971  z=0.
hole  1115 rotate a1=330 origin x=-19.500000  y=-13.56773132  z=0.
cuboid      2  10.  0.  0.5 -0.5 9.26538 0  rotate a1=-30.
cuboid      3  10.  0.  0.5 -0.5 9.26538 0  rotate a1=90.
cuboid      4  10.  0.  0.5 -0.5 9.26538 0  rotate a1=210.
cylinder    5  1.2  9.26538  0
media 0 1 2 -5
media 0 1 3 -5
media 0 1 4 -5
media 0 1 5
media 10 1 1 -2 -3 -4 -5
media 9 1 10 -1
boundary 10
end geometry

' ---------- Array Specification ----------
' -----------------------------------------
read array
```

```
ara=1112 nux=250 nuy=7 nuz=100 typ=square
com='Fuel Arrangement in Plate'
fill
250r1111
250r1111
250r1111
250r1111
250r1111
250r1111
250r1111
99q1750
end fill
end array

' ---------- Plot Cross Sections ----------
' -----------------------------------------
read plot

ttl='Fuel Block'
XUL=-28.0 YUL=28.0  ZUL=0.0463269
XLR=28.0  YLR=-28.0 ZLR=0.0463269
UAX=1 VDN=-1 NAX=12800 END

end plot
' ---------- Boundary Conditions ----------
' -----------------------------------------
read bnds
body=10
all=mirror
end bnds

end data
end model
end
```

# APPENDIX D: SAMPLE SCALE INPUT FILE FOR CORE MODEL

```
=t6-depl parm=(centrm,addnux=4)
LSCR - Burnup of LSCR Full Core Model
v7-238
' ---------- Materials ----------
' ------------------------------
read composition
' ---- Fuel, 19.75% Enrichment ----
U-234       1  0  3.7861e-05  1200    end
U-235       1  0  0.00493458  1200    end
U-238       1  0  0.0197601   1200    end
O-16        1  0  0.0352829   1200    end
C-graphite  1  0  0.0105760   1200    end
'
' ---- Buffer, IPyC, Silicon Carbide, OPyC, Matrix Material ----
C-graphite  2  0  0.076304410   1200    end
Si          2  0  0.003755145   1200    end
'
' ---- Graphite Meat ----
C-graphite  7  0  7.97223e-02 1200    end
'
' ---- Sleeve/Cladding on Plate ----
C-graphite  8  0  7.97223e-02 1000    end
'
' ---- FLiBe Coolant (99.995% enriched Li-7) ----
Li-6        9  0  1.38344e-06 948.15  end
Li-7        9  0  0.0237205   948.15  end
Be          9  0  0.0118609   948.15  end
F           9  0  0.0474437   948.15  end
'
' ---- Graphite in Fuel Block ----
C-graphite  10  0  9.82741e-02 948.15  end
'
' ---- Graphite Reflector Block ----
C-graphite  11  0  8.72433e-02 948.15  end
'
' ---- Alloy 800H Clad in CR ----
C-graphite 12 0  3.2210e-04  923.15  end
Al          12 0  6.7209e-04  923.15  end
Si          12 0  6.0263e-04  923.15  end
P           12 0  3.1225e-05  923.15  end
S           12 0  1.5081e-05  923.15  end
Ti          12 0  3.7884e-04  923.15  end
Cr          12 0  1.9530e-02  923.15  end
Mn          12 0  8.8022e-04  923.15  end
Fe          12 0  3.8092e-02  923.15  end
Ni          12 0  2.6777e-02  923.15  end
Cu          12 0  2.2830e-04  923.15  end
'
```

```
end composition

' ---- Cell data ----
' -------------------
read celldata
latticecell sphsquarep
fuelr=0.02135 1  pitch=0.0926537 2 end
end celldata

' ---- Depletion and Burndata ----
' --------------------------------
read depletion 1 9 end depletion
read burndata
power=98.2068  burn=1    down=0  nlib=1  end
power=98.2068  burn=2    down=0  nlib=1  end
power=98.2068  burn=4    down=0  nlib=1  end
power=98.2068  burn=6    down=0  nlib=1  end
power=98.2068  burn=14   down=0  nlib=1  end
power=98.2068  burn=26   down=0  nlib=1  end
power=98.2068  burn=94   down=0  nlib=1  end
power=98.2068  burn=66   down=0  nlib=1  end
power=98.2068  burn=134  down=0  nlib=1  end
power=98.2068  burn=66   down=0  nlib=1  end
power=98.2068  burn=134  down=0  nlib=1  end
power=98.2068  burn=66   down=0  nlib=1  end
power=98.2068  burn=134  down=0  nlib=1  end
power=98.2068  burn=66   down=0  nlib=1  end
power=98.2068  burn=134  down=0  nlib=1  end
power=98.2068  burn=66   down=0  nlib=1  end
power=98.2068  burn=134  down=0  nlib=1  end
end burndata

' ---- Opus ----
' --------------
read opus
matl=1 9 end
time=days
typarms=nucl
units=gram
title=Masses of Actinides and Fission Products
symnuc=u-234 u-235 u-236 u-237 u-238 pu-238 pu-239
pu-240 pu-241 pu-242 pu-243 np-237 am-241 am-242m am-243
cm-242 cm-243 cm-244 cm-245 cm-246
sr-90 i-131
cs-133 cs-134 cs-135 cs-137 nd-143 nd-144 nd-145 nd-146
nd-148 nd-150 pm-147 sm-147 sm-148 sm-149 sm-150 sm-151
sm-152 eu-153 sm-154 eu-154 gd-154 eu-155 gd-155 end
new case
time=days
typarms=elements
units=curies
```

```
100   symnuc= Ac Ag Al Am Ar As At Au B  Ba Be Bi Bk Br C  Ca Cd Ce Cf Cl
101   Cm Co Cr Cs Cu Dy Er Es Eu F  Fe Fr Ga Gd Ge H  He Hf Hg Ho
102   I  In Ir K  Kr La Li Lu Mg Mn Mo N  Na Nb Nd Ne Ni Np O  Os
103   P  Pa Pb Pd Pm Po Pr Pt Pu Ra Rb Re Rh Rn Ru S  Sb Sc Se Si
104   Sm Sn Sr Ta Tb Tc Te Th Ti Tl Tm U  V  W  Xe Y  Yb Zn Zr end
105   new case
106   time=days
107   typarms=elements
108   units=watts
109   symnuc= Ac Ag Al Am Ar As At Au B  Ba Be Bi Bk Br C  Ca Cd Ce Cf Cl
110   Cm Co Cr Cs Cu Dy Er Es Eu F  Fe Fr Ga Gd Ge H  He Hf Hg Ho
111   I  In Ir K  Kr La Li Lu Mg Mn Mo N  Na Nb Nd Ne Ni Np O  Os
112   P  Pa Pb Pd Pm Po Pr Pt Pu Ra Rb Re Rh Rn Ru S  Sb Sc Se Si
113   Sm Sn Sr Ta Tb Tc Te Th Ti Tl Tm U  V  W  Xe Y  Yb Zn Zr end
114   new case
115   time=days
116   typarms=nucl
117   units=gram
118   title=Mass of Tritium and Lithium Isotopes
119   symnuc= h-3 li-6 li-7 end
120   new case
121   time=days
122   typarms=nucl
123   units=curies
124   title=Radioactivity of Tritium
125   symnuc= h-3 end
126   end opus
127
128   read model
129   read parameter
130   cfx=yes
131   flx=yes
132   gen=250
133   nsk=25
134   npg=10000
135   sig=0.0001
136   tba=100
137   htm=no
138   plt=yes
139   end parameter
140
141   ' ---------- Geometry ----------
142   ' ------------------------------
143   read geometry
144   unit 1111
145   com="TRISO Fuel Particle"
146   sphere 1  0.02135
147   cuboid 2  0.0463269  -0.0463269  0.0463269  -0.0463269  0.0463269  -0.0463269
148   media 1 1 1
149   media 2 1 2 -1
150   boundary 2
```

```
'
unit 1112
com="Fuel Portion of Fuel Plate"
parallelepiped 1  21.47743  0.7489117492  9.26538       30        0        0
array 1112 1  place 1 1 1 0.0463269 0.0463269 0.0463269
boundary 1
'
unit 1113
com="Graphite center with fuel plates"
parallelepiped 1  21.47743  2.71354626519  9.26538       30        0        0
hole 1112  origin  x=0 y=0 z=0
hole 1112  origin  x=0.9823175008 y=1.7014238206 z=0
media 7 1 1
boundary 1
'
unit 1114
com="Complete Fuel Plate"
parallelepiped 1  21.70837  2.944486  9.26538       30        0        0
hole 1113  origin  x=0.173205 y=0.1 z=0
media 8 1 1
boundary 1
'
unit 1115
com="Group of Six Fuel Plates"
parallelepiped 1  22.51666  22.51666      9.26538       30        0        0
hole 1114   origin  x=0.606218 y=0.35  z=0
hole 1114   origin  x=2.482606 y=3.6   z=0
hole 1114   origin  x=4.358995 y=6.85  z=0
hole 1114   origin  x=6.23583  y=10.1  z=0
hole 1114   origin  x=8.111771 y=13.35 z=0
hole 1114   origin  x=9.98816  y=16.6  z=0
media 9 1 1
boundary 1
'
'
unit 20
com="Fuel Assembly, 18 Fuel Plates, and Control Blade Slot"
hexprism    10 23.375 9.26538 0
hexprism    1  22.5   9.26538 0
hole  1115 rotate a1=210 origin x=-2.000000   y=23.67136103   z=0.
hole  1115 rotate a1=90  origin x=21.5        y=-10.10362971  z=0.
hole  1115 rotate a1=330 origin x=-19.500000  y=-13.56773132  z=0.
cuboid      2  10.  0.  0.5 -0.5 9.26538 0  rotate a1=-30.
cuboid      3  10.  0.  0.5 -0.5 9.26538 0  rotate a1=90.
cuboid      4  10.  0.  0.5 -0.5 9.26538 0  rotate a1=210.
cylinder    5  1.2  9.26538  0
media 0 1 2 -5
media 0 1 3 -5
media 0 1 4 -5
media 0 1 5
media 10 1 1 -2 -3 -4 -5
```

```
202     media 9 1 10 -1
203     boundary 10
204     '
205     '
206     unit 10
207     com="Graphite Reflector Block"
208     cylinder    1  2.0    9.26538 0
209     hexprism    2  23.375 9.26538 0
210     media 9 1 1
211     media 11 1 2 -1
212     boundary 2
213     '
214     '
215     global unit 1
216     com="Reactor Core"
217     cylinder   1 478 9.26538 0
218     array 1 1 place 13 13 1 0 0 0
219     cylinder   2 480 9.26538 0
220     cylinder   3 513 9.26538 0
221     cylinder   4 518 9.26538 0
222     media 12 1 2 -1
223     media 9  1 3 -2
224     media 12 1 4 -3
225     boundary 4
226
227     end geometry
228
229     ' ---------- Array Specification ----------
230     ' ----------------------------------------
231     read array
232
233     ara=1  nux=25 nuy=25 nuz=1 typ=hexagonal
234     fill
235     10  10  10  10  10  10  10  10  10  10  10  10  10  10  10  10  10  10  10  10  10  10  10  10  10
236     10  10  10  10  10  10  10  10  10  10  10  10  10  10  10  10  10  10  10  10  10  10  10  10  10
237     10  10  10  10  10  10  10  10  10  10  10  10  10  10  10  10  10  10  10  10  10  10  10  10  10
238     10  10  10  10  10  10  10  10  10  10  10  10  10  10  20  20  20  20  20  20  10  10  10  10  10
239     10  10  10  10  10  10  10  10  10  10  10  10  20  20  20  20  20  20  20  20  20  10  10  10  10
240     10  10  10  10  10  10  10  10  10  10  20  20  20  20  20  20  20  20  20  20  20  20  10  10  10
241     10  10  10  10  10  10  10  10  10  20  20  20  20  20  20  20  20  20  20  20  20  20  10  10  10
242     10  10  10  10  10  10  10  10  20  20  20  20  20  20  20  20  20  20  20  20  20  20  10  10  10
243     10  10  10  10  10  10  10  20  20  20  20  20  20  20  20  20  20  20  20  20  20  20  10  10  10
244     10  10  10  10  10  10  20  20  20  20  20  20  20  20  20  20  20  20  20  20  20  20  10  10  10
245     10  10  10  10  10  20  20  20  20  20  20  20  20  20  20  20  20  20  20  20  20  20  10  10  10
246     10  10  10  10  10  20  20  20  20  20  20  20  20  20  20  20  20  20  20  20  20  20  10  10  10  10
247     10  10  10  10  20  20  20  20  20  20  20  20  20  20  20  20  20  20  20  20  20  20  10  10  10  10
248     10  10  10  10  20  20  20  20  20  20  20  20  20  20  20  20  20  20  20  20  20  10  10  10  10  10
249     10  10  10  20  20  20  20  20  20  20  20  20  20  20  20  20  20  20  20  20  20  10  10  10  10  10
250     10  10  10  20  20  20  20  20  20  20  20  20  20  20  20  20  20  20  20  20  10  10  10  10  10  10
251     10  10  10  20  20  20  20  20  20  20  20  20  20  20  20  20  20  20  20  10  10  10  10  10  10  10
252     10  10  10  20  20  20  20  20  20  20  20  20  20  20  20  20  20  20  10  10  10  10  10  10  10  10
```

```
253     10 10 10 20 20 20 20 20 20 20 20 20 20 20 20 20 10 10 10 10 10 10 10 10 10
254     10 10 10 20 20 20 20 20 20 20 20 20 20 20 20 20 10 10 10 10 10 10 10 10 10
255     10 10 10 10 20 20 20 20 20 20 20 20 20 20 10 10 10 10 10 10 10 10 10 10 10
256     10 10 10 10 10 20 20 20 20 20 20 10 10 10 10 10 10 10 10 10 10 10 10 10 10
257     10 10 10 10 10 10 10 10 10 10 10 10 10 10 10 10 10 10 10 10 10 10 10 10 10
258     10 10 10 10 10 10 10 10 10 10 10 10 10 10 10 10 10 10 10 10 10 10 10 10 10
259     10 10 10 10 10 10 10 10 10 10 10 10 10 10 10 10 10 10 10 10 10 10 10 10 10
260     end fill
261
262     ara=1112 nux=250 nuy=7 nuz=100 typ=square
263     com='Fuel Arrangement in Plate'
264     fill
265     250r1111
266     250r1111
267     250r1111
268     250r1111
269     250r1111
270     250r1111
271     250r1111
272     99q1750
273     end fill
274
275     end array
276
277     ' ---------- Plot Cross Sections ----------
278     ' -----------------------------------------
279     read plot
280
281     ttl='Full Reactor Core'
282     XUL=-550.0 YUL=550.0  ZUL=0.0463269
283     XLR=550.0  YLR=-550.0 ZLR=0.0463269
284     UAX=1 VDN=-1 NAX=12800 END
285
286     end plot
287
288     ' ---------- Boundary Conditions ----------
289     ' -----------------------------------------
290     read bounds
291       surface(1)=vacuum
292       surface(2)=mirror
293       surface(3)=mirror
294     end bounds
295
296     end data
297     end model
298     end
```

# APPENDIX E: FORTRAN ANALYTIC MODEL FOR LITHIUM

```
1   PROGRAM LithiumEnrichment
2   !-------------------------------------------------------------!
3   !! Variables for Problem !!
4   DOUBLE PRECISION, DIMENSION(:), ALLOCATABLE :: N6T, N7T, TT, AP, WP,time
5   !Values for Number Density
6   DOUBLE PRECISION :: dT, dN6, dN7, T, Y, phit, phif, phitot
7   !Parameters for equations
8   DOUBLE PRECISION :: N6o, N7o, E, Avg, mm6, mm7
9   !Parameters for finding initial Number Density
10  DOUBLE PRECISION :: sth6, sft6, sth7, sft7, sy6t, sy6f, sn7          !Cross Sections
11  INTEGER :: N, I
12
13  !! Defining Cross Sections for Problem !!
14  sth6 = (258.4060896 + 0.010560199)/1.E24
15  !Thermal Cross Section for Li-6 ((n,t) + (Rad Cap))
16  sft6 = (0.000111272 + 0.000362336 + 9.197779372 + 0.000372827)/1.E24
17  !Fast Cross Section for Li-6 ((n,2n) + (n,p) + (n,t) + (Rad Cap))
18  sth7 = (0.012467899)/1.E24
19  !Thermal Cross Section for Li-7 (Radiative Capture)
20  sft7 = (325*3.60359E-06 + 7.89709E-07 + 3.24092E-09 + 5.48862E-07 + 0.000439651)/1.E24
21  !Fast Cross Section for Li-7 ((n,2n) + (n,2na) + (n,3na) + (n,d) + (Rad Capt))
22  sy6t = (0.010560199)/1.E24
23  !(n,gamma) Cross Section for Li-6 Thermal
24  sy6f = (0.000372827)/1.E24                    !(n,gamma) Cross Section for Li-6 Fast
25  sn7  = 325*(3.60359E-06)/1.E24                !(n,2n) Cross Section for Li-7
26
27  !! Time Length and Time Differential !!
28  Y  = 20                       !Number of years
29  T  = Y*(365)*24*3600          !Number of seconds
30  dT = 86400*10                 !Number of seconds per interval
31  N  = T/dT                     !Number of intervals
32  ALLOCATE(N6T(N), N7T(N), TT(N),time(N))   !Size of Number Density vectors
33  ALLOCATE(AP(N), WP(N))
34
35  !! Initial Number Densities for Li-6 and Li-7 !!
36  write(*,*) "Please Enter an Li-7 Enrichment:"
37  read(*,*) E                   !Enrichment of Li-7
38  Avg = 6.0221415E+23           !Avogadro's Number
39  mm6 = 6.015122795             !Molar Mass of Li-6
40  mm7 = 7.016004550             !Molar Mass of Li-7
41  N6o = 2.76365903E-01*(1-E)*Avg/mm6   !Initial Number Density of Li-6
42  N7o = 2.76365903E-01*E*Avg/mm7       !Initial Number Density of Li-7
43  N6T(1) = N6o
44  N7T(1) = N7o
45  TT(1)  = 0
46  time(1)= 0

47  !! Atom and Weight Percents !!
```

```
48      AP(1) = N7T(1)/(N7T(1)+N6T(1))
49      WP(1) = AP(1)*mm7/(AP(1)*mm7 + (1-AP(1))*mm6)
50
51      DO I = 1,N-1
52
53      !! Flux Values for the problem !!
54      phit   = 1.91373E+13
55      phif   = 2.21755E+14 !phitot-phit
56
57      dN6 = (-1*phit*N6T(I)*sth6 - phif*N6T(I)*sft6 + phif*N7T(I)*sn7)*dT
58      dN7 = (-1*phit*N7T(I)*sth7 - phif*N7T(I)*sft7 + phit*N6T(I)*sy6t + phif*N6T(I)*sy6f)*dT
59
60      N6T(I+1) = N6T(I) + dN6
61      N7T(I+1) = N7T(I) + dN7
62      TT(I+1)  = I*dT
63      time(I+1) = TT(I+1)/86400
64
65      AP(I+1) = N7T(I)/(N7T(I)+N6T(I))
66      WP(I+1) = AP(I)*mm7/(AP(I)*mm7 + (1-AP(I))*mm6)
67
68      END DO
69
70      open(unit = 1, file="NumDens.txt")
71      write(1,*) ' Time = 1st Column'
72      write(1,*) ' Li-6 Number Densities = 2nd Column'
73      write(1,*) ' Li-7 Number Densities = 3rd Column'
74      write(1,*) ' Weight Percent = 4th Column'
75      write(1,*) ' '
76      DO I=1,N
77      write(1,'(F10.2, A, E12.6, A, E12.6, A, F10.8)') time(I), '   ', N6T(I), '   ', N7T(I), '   ',  WP(I)
78      END DO
79      close(1)
80
81      END PROGRAM LithiumEnrichment
```

# REFERENCES


[1] D. E. Holcomb, et al., "Current Status of the Advanced High Temperature Reactor", ICAPP 2012, ANS, *Chicago, IL, 2012.*

[2] D. Ilas, D. E. Holcomb, and V. K. Varma, "Advanced High-Temperature Reactor Neutronic Core Design", PHYSOR - Advances in Reactor Physics - Linking Research, Industry, and Education, *Knoxville, TN, 2012.*

[3] M. W. Rosenthal, P. R. Kasten, and R. B. Briggs, "Molten-Salt Reactors--History, Status, and Potential", (1969).

[4] H. G. Macpherson, *The Molten Salt Reactor Adventure.* Nuclear Science and Engineering, 1985. **90**: p. 374-380.

[5] *A Technology Roadmap for Generation IV Nuclear Energy Systems*, 2002, DOE Nuclear Energy Reserach Advisory Committee. p. 1-97.

[6] Y. Kim and M. Baek, "Elimination of Double-Heterogeneity through a Reactivity-Equivalent Physical Transformation", GLOBAL, *Tsukuba, Japan, 2005.*

[7] T. K. Kim, T. A. Taiwo, and W. S. Yang, "Preliminary Neutronic Studies for the Liquid-Salt-Cooled Very High Temperature Reactor ( LS-VHTR ) prepared by Nuclear Engineering Division", (2005).

[8] D. T. Ingersoll, et al., "Status of Preconceptual Design of the Advanced High-Temperature Reactor ( AHTR )", 1800553684, (2004).

[9] D. T. Ingersoll, et al., "Core Physics Characteristics and Issues for the Advanced High-Temperature Reactor", (2004).

[10] D. E. Holcomb, et al., "Core and Refueling Design Studies for the Advanced High Temperature Reactor", ORNL/TM-2011/365, Oak Ridge National Laboratory (2011).

[11] J. C. Gehin, et al., "Pre-Conceptual Design of a Fluoride- Salt-Cooled Small Modular Advanced High-Temperature Reactor ( SmAHTR )", 1800553684, (2010).

[12] S. Goluoglu and M. L. Williams, "Modeling Doubly Heterogeneous Systems in SCALE", (2005).

[13] J. M. Noh, et al., *Development of a computer code system for the analysis of prism and pebble type VHTR cores.* Annals of Nuclear Energy, 2008. **35**(10): p. 1919-1928.

[14] A. T. Cisneros and D. Ilas, "Neutronics and Depletion Methods for Parametric Sutdies of Fluoride-Salt-Cooled High-Temperature Reactors with Slab Fuel Geometry and Multi-Batch Fuel Management Schemes", PHYSOR - Advances in Reactor Physics - Linking Research, Industry, and Education, *Knoxville, TN, 2012.*

[15] R. Kelly and D. Ilas, "Verification of a Depletion Method in SCALE for the Advanced High Temperature Reactor", PHYSOR - Advances in Reactor Physics - Linking Research, Industry, and Education, *Knoxville, TN, 2012.*

[16] S. Greene, "FHRs and the Future of Nuclear Energy", (2010).

[17] R. G. Cochran and N. Tsoulfanidis, *The Nuclear Fuel Cycle: Analysis and Management*. 1990, La Grange Park, Illinois: American Nuclear Society.

[18] D. E. Shropshire, et al., *Advanced Fuel Cycle Cost Basis*, DOE, Editor 2008: Idaho National Laboratory.